Medizinische Fakultät der
Martin-Luther-Universität Halle-Wittenberg

Subpopulation-specific regulation of migration and integration in the postnatal olfactory bulb

Dissertation zur Erlangung des akademischen Grades
Doktor der Medizin (Dr. med.)

von Clara Haubold
geboren am 02.02.1994 in Berlin

Betreuer: Prof. Dr. Rüdiger Horstkorte

Gutachter*innen:
- Prof. Dr. Arne Viestenz
- Dr. Simone Diestel, Universität Bonn

18.01.2022
29.06.2022

Referat

Neurogenese persistiert bei einigen Säugetierspezies über die embryonale Phase hinaus nur in bestimmten adulten Gehirnarealen: in der subgranulären Zone der Hippocampusformation sowie in der subventrikulären Zone (SVZ). Neuroblasten, die von neuronalen Stammzellen der SVZ generiert werden, migrieren zunächst tangential entlang des rostralen migratorischen Stroms (engl. RMS: rostral migratory stream) bis zum *Bulbus olfactorius* (engl. OB: olfactory bulb). Dort verlassen sie den RMS und wechseln in einen radialen Migrationsmodus, der langsamer und weniger zielgerichtet ist. Sobald die verschiedenen Neuroblastenpopulationen ihre jeweilige finale Schicht im OB erreicht haben, entwickeln sie sich entweder zu periglomerulären (engl. PGCs: periglomerular cells) oder zu granulären Interneuronen (engl. GCs: granule cells) weiter. Anschließend bilden sie funktionelle, meist inhibitorische Synapsen mit den bereits existierenden Neuronen vor Ort aus.
Anhand der postnatalen Neurogenese des OBs lassen sich bestimmte Schritte der neurogenetischen Sequenz (Stammzellamplifikation, Migration, finale Differenzierung) räumlich getrennt verfolgen, weshalb dieses System einzigartige Möglichkeiten für die Stammzellforschung bietet. Zur Entwicklung erfolgreicher Therapien für jene Patienten, die u.a. unter einem Verlust neuronaler Zellstrukturen leiden, muss künftig mehr über die spezifische Regulation verschiedener zellulärer Populationen in Erfahrung gebracht werden. Von besonderem Interesse ist dabei eine detaillierte Beschreibung von Integration und Migration unterschiedlicher neuronaler Subtypen.

Bei unseren Experimenten wurde die postnatale Elektroporation sowohl für eine klare Markierung als auch für gezielte Manipulationen periglomerulärer und granulärer Interneuronen genutzt. In Kombination mit *in vivo* Bildgebungstechniken konnte so gezeigt werden, dass PGCs und GCs während der tangentialen und radialen Migration einem sehr ähnlichen Bewegungsmuster folgen. Sobald die Neuroblasten allerdings den RMS verlassen hatten, zeigten sie typbedingte Unterschiede in ihrer Kalziumaktivität. Dies könnte darauf hindeuten, dass das Membranpotential eine wichtige Rolle in Segregationsprozessen spielt. Unseren Beobachtungen zufolge ist die Ca^{2+}-Aktivität der OB-Neuroblasten von deren Depolarisation durch spannungsgesteuerte Kalziumkanäle abhängig. Modernste chemogenetische Tools ermöglichten es, in die intrinsische Aktivität künftiger Interneuronen einzugreifen und Effekte auf ihr migratorisches Verhalten und schlussendliche Positionierung zu erforschen. Obgleich eine verminderte Ca^{2+}-Aktivität bei keiner der Zellpopulationen einen Einfluss auf Migrationsparameter hatte, waren veränderte Verteilungsmuster während der Differenzierungsphase klar erkennbar. Dieser Effekt war interessanterweise zelltypspezifisch, da eine verminderte Zellzahl ausschließlich für die GC-Population festgestellt wurde, während die Anzahl an PGCs in der glomerulären Schicht (engl. GL: glomerular layer) unverändert blieb. Aufgrund dessen, dass signifikante Verteilungsunterschiede bei aktivitätsgeminderten Zellen zu verschiedenen Zeitpunkten (8/10/12 dpe) auftraten, kann ausgeschlossen werden, dass es sich hierbei lediglich um eine transiente Observation handelt. Zusätzlich wurden unsere Annahmen von einer histochemischen Caspase-3-Immunfärbung gestärkt: die Überlebensrate aktivitätsgeblockter GCs sank eindeutig lokalisiert in der granulären Schicht (engl. GCL: granule cell layer). Chemogenetisch herbeigeführte Aktivitätssteigerungen lieferten weitere wichtige Beweise für subtypenspezifische Regulationsmechanismen. Selbst wenn diese Herangehensweise nur bedingt physiologisch ist, illustriert sie dennoch flagrant die verschiedenen Reaktionsweisen beider Arten von Interneuronen: mit steigender Ca^{2+}-Aktivität beschleunigen GCs ihre Migration während PGCs ihre Geschwindigkeit drosseln.
Insgesamt tragen unsere Erkenntnisse wesentlich zu einem besseren Verständnis diverser Kontrollmechanismen von neuronalen Stammzellen während ihrer Migrations- und Integrationsphase im postnatalen OB bei. In der Zukunft könnte dies helfen, neurologische Ersatztherapien zu entwickeln und nachhaltig zu verbessern.

Haubold, Clara: Subpopulation-specific regulation of migration and integration in the postnatal olfactory bulb, Halle (Saale), Univ., Med. Fak., Diss., 74 Seiten, 2021

TABLE OF CONTENT

List of Abbreviations

AMPA	α-amino-3-hydroxy-5-methyl-4-isoxazolepropionic acid
aNPCs	adult neural progenitor cells
Bcl-2	B-cell lymphoma 2
BrdU	5-bromodeoxyuridine
Ca^{2+}	calcium
CalB	calbindin
CalM	calmodulin
CalR	calretinin
cAMP	cyclisches adenosinmonophosphat
CNO	clozapine-N-oxide
CNS	central nervous system
CREB	cAMP response element-binding protein
DG	dentate gyrus
DMSO	dimethylsulfoxyde
dpi	days post-injection
DREADD	designer receptor exclusively activated by a designer drug
EPL	external plexiform layer
ER	endoplasmic reticulum
eTCs	external tufted cells
GABA	γ-aminobutyric acid
GCL	granule cell layer
GFAP	glial fibrillary acidic protein
GFP	green fluorescent protein
GL	glomerular layer
GluR	glutamate receptor
hM3Dq	human M3 muscarinic cholinergic Gq-coupled receptor
hrs	hours
iPSCs	induced pluripotent stem cells
IZ	intermediate zone
KO	knocked out
LOT	lateral olfactory tract
MCL	mitral cell layer
MCs	mitral cells

MIA	migration-inducing activity
mTCs	middle tufted cells
NMDA	N-Methyl-D-aspartate
NSCs	neural stem cells
OB	olfactory bulb
ORs	odourant receptors
OSNs	olfactory sensory neurones
Pax6	paired box 6
PBS	phosphate buffered saline
PCR	polymerase chain reaction
pCREB	phosphorylated cAMP response element-binding protein
PD	Parkinson's disease
PGCs	periglomerular cells
PSA–NCAM	polysialylated-neural cell adhesion molecule
RMS	rostral migratory stream
SGZ	subgranular zone
TH	tyrosine hydroxylase
Tshz1	teashirt zinc finger family member 1
V-SVZ	ventricular- subventricular zone
VGCC	voltage gated Ca^{2+} channels
VZ	ventricular zone

1. INTRODUCTION

1.1. The medical significance of understanding neurogenesis in the OB

Neurodegenerative diseases caused by the progressive death of neurons in different regions of the nervous system are a major problem during ageing and ischemia. A large loss of nerve cells results in characteristic neurological signs and symptoms which often deeply impair patients' lives. Partly owing an extended lifespan, the prevalence of neurodegenerative disorders is increasing. This includes, for example, the decay of dopaminergic cells during Parkinson's disease as well as sudden cell death after an interruption of blood flow and deprivation of oxygen as occurring during a stroke. Since the brain is not capable by itself to replace lost neurons, efficient neuronal replacement strategies have to be developed to cure those patients. Promising treatments involve the activation of endogenous neuronal progenitor cells. Therefore, intensive research has to be done in order to retrace the formation of neuronal progenitors as well as their mechanisms to migrate and integrate.
To better understand the character and treatment of neurodegenerative disorders, I will first explain some general physiological facts about neurogenesis focusing particularly on adult human neurogenesis. Then, I take the examples of Parkinson's disease and ischemia stroke to explain causes and current treatments before I come to therapeutic strategies that might lead to better medical results in the future by using the potential of neural stem cells.

1.1.1. Neurogenesis - a physiological process that continues throughout life in certain species

During neurogenesis all cell types of the nervous system are produced by neural stem cells (NSCs). Historically, neurogenesis was viewed to occur only during embryonic and perinatal development. However, it was shown later that neurogenesis can persist throughout life for specific brain areas in some species (Eriksson et al. 1998). During adult neurogenesis, functional neurons are generated from adult NSCs possibly contributing to neural circuit plasticity (Paredes et al. 2016b).
In mammals, one can find NSCs in two distinct areas, in the ventricular subventricular zone (V-SVZ) of the striatum's lateral ventricular wall and in the hippocampus. In the V-SVZ, adult NSCs generate actively dividing intermediate cells, called progenitors. As soon as they start expressing migration marker like doublecortin they are called neuroblasts. Those immature neuroblasts migrate from the SVZ along the rostral migratory stream to the olfactory bulb (OB) and differentiate into interneurons that integrate into local circuits (Doetsch et al. 1999). In the hippocampus, NSCs are found in the subgranular zone (SGZ) of the dentate gyrus. The immature neuroblasts there generate DG glutamatergic granule neurons (Seri et al. 2004).
While the presence of those two stem cell niches in rodents is well-documented, it has been passionately debated amongst experts during the last decades, whether or not

adult neurogenesis exists in the human brain. Just recently, two papers concerning this issue have been released in the space of only a few weeks. Both of them address the same topic, their conclusions however are largely contrary: The first report claims that human hippocampal neurogenesis ends after childhood, assuming therefore that the function of the dentate gyrus must differ between humans and other species in which cell renewal is preserved though-out life (Sorrells et al. 2018). On the other hand, the second study concludes the exact opposite publishing that the prevalence of proliferating progenitor and immature neurons pools is stable even at a high age (Boldrini et al. 2018). By comparing the two approaches and taking into account additional data, the state of the field was summarized by Kempermann who comes to the conclusion that there is currently no reason to abandon the idea of neurogenesis across the human lifespan (Kempermann et al. 2018).

Meanwhile, the status of an intact rostral migratory stream in the human olfactory system is even more doubted (Gould 2007). While cells with a migratory phenotype seem to be present, no traces for the formation of the RMS are found. Nevertheless, there appears a wider consensus upon the prevalence of a proliferative cell population both in the SVZ and OB, even among the elderly (Sanai et al. 2004). For example, Doublecortin^{+}cells with morphological features of migratory and immature granule cells appear all over the human OB (Maresh et al. 2008). In accordance, signs of cellular division colocalizing with neuronal markers were found in the layers of the adult human olfactory system (Paredes et al. 2016a).
It is important to keep species-based differences of neurogenesis in mind when doing research and applying the acquired knowledge to patients.

1.1.2. Exemplary diseases

Parkinson's disease

Parkinson's Disease (PD) results from a chronic progressive degeneration of dopaminergic neurons in the substantia nigra. These cells are responsible for producing the chemical messenger dopamine which is crucial for motor control. Consequently, the cardinal symptoms of PD are movement disorders such as tremor, bradykinesia, rigidity and postural instability. Additionally, patients suffer from cognitive and behavioral changes, and show symptoms related to autonomic nervous system failure. However, those symptoms appear often very late, when already about 80% of the nigrostriatal dopaminergic innervation is lost, because network restructuring and synaptic plasticity reduce the functional deficits or even mask the disease entirely (Zigmond et al. 1990). PD is the second most common neurodegenerative disease (Stoker and Barker 2018) associated with risk factors including high age, family history and exposure to pesticides or certain chemicals (Beitz 2014). The ultimate cause of PD is still unknown which makes it difficult to find a

definitive disease-modifying therapy. Thus, symptomatic strategies which involve dopaminergic medications such as Levopoda are currently the mainstay in treating PD patients. However, side effects that can develop after long-term use or high-dose treatment include dyskinesias and motor fluctuations (Rizek et al. 2016). Hence, it is necessary to develop better options in the treatment of PD.

Ischemia stroke

During an ischemic stroke, a cerebral artery occlusion causes an acute loss of neurons, astroglia, and oligodendroglia leading to the disruption of synaptic architecture. The classical clinical treatment aims to prevent a recurrent hit using thrombolytic therapy and percutaneous intravascular interventions as well as medication such as aspirin. However, the application of thrombolytic therapy must take place within the narrow time window of 3–4.5hrs after acute stroke onset and can lead to serious hemorrhagic complications. Even with modern therapeutical approaches, morbidity and mortality after an ischemic stroke are high — leaving surviving patients often with severe disabilities (Hao et al. 2014).

1.1.3. Novel therapeutic strategies for neuronal replacement

Since physiological human adult neurogenesis is a rare process that is not designed to automatically replace impaired or lost cells within the entire brain, externally controlled stem cell therapy is considered as the future state-of-art treatment of neurodegenerative diseases aiming to regain brain function. It represents a promising approach because it works not only as pure replacement but also through additional mechanisms like the secretion of neurotrophic factors, immune modulation, and stimulation of endogenous neurogenesis.

Until now, three distinct strategies for neuronal replacement are considered: (1) endogenous recruitment from neurogenic niches or local cells (Nakatomi et al. 2002); (2) exogenous cell transplantation (Taupin 2006); and (3) forced conversion of local glia to a neuronal fate (Karow et al. 2012). While the first approach has not yet shown significant and long-lasting success, the second strategy has already achieved both clinically and experimentally remarkable outcomes. The third approach is tested *in vivo* for repair tasks at the moment, but is still far away from clinical application since cell handling and immunological rejection remain tough challenges (Grade and Gotz 2017).

The observation that a stroke itself activates murine SVZ neurogenesis (Abrahams et al. 2009) provides evidence that nature has already developed an endogenous recruitment strategy. Following the rescuing pathway started by ischemia, endogenous progenitors proliferate and subsequently migrate into the severely damaged area in order to differentiate into the phenotype of those neurons that have been mostly destroyed by the insult. However, despite induced neurogenesis by

endogenous NSCs, the number and survival rate of new neurons derived from endogenous neurogenesis are rather low and new neurons are unable to replace the lost neurons in stroke victims sufficiently for full recovery (Arvidsson et al. 2002). Nevertheless, if it was ensured that those endogenous adult-born neurons are functional after migration to the damaged site, a novel therapeutic approach could

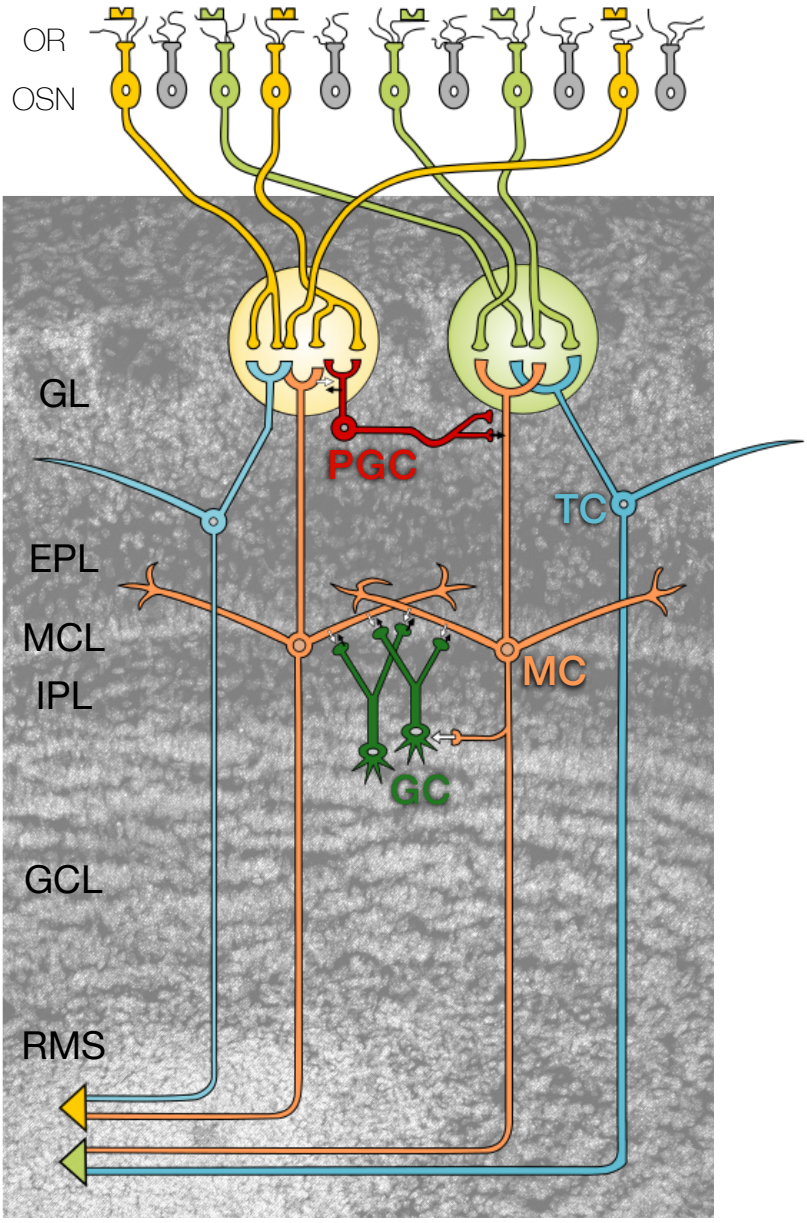

Figure 1: ***Basic circuit overview of the synaptic organization in the rodent olfactory bulb***
Different odor molecules bind to odorant receptors (OR) which are expressed on the cilial membrane surface of olfactory sensory neurons (OSN) in the epithelium. OSNs with an equal type of receptor send their axons to the same glomerular module (yellow and light green). The OR-specific signal is then transmitted to either mitral cells (MC, orange) or tufted cells (TC, blue) both innervating glomeruli. Subsequently, those two types of projection neurons send their axons to the olfactory cortex. To sharpen the tuning specificity of the output neurons, granule cells (GC, dark green) and periglomerular cells (PGC, red) modulate local circuits through lateral inhibition. Since PGCs lay more superficially they modulate the signal at an earlier time point acting as primary filter, while the GCs that are located in a deeper layer interfere later on. Modified from *Mori et al., 1999.* Short white arrows represent excitatory synapses, short black arrows denote inhibitory synapses. GL, glomerular layer; EPL, external plexiform layer; MCL, mitral cell layer; IPL, internal plexiform layer; GCL, granule cell layer; RMS, rostral migratory stream.

simply aim to stimulate their formation. For instance, endogenous stem cell production can be further enhanced by the intraventricular infusion of growth factors. Possibly, this endogenous recruitment (1) can be further developed to serve as future therapy for neuronal cell regeneration healing not only stroke but also other neurological diseases (Nakatomi et al. 2002).
Taking a closer look on exogenous cell transplantation (2) shows that finding an efficient donor source is the crucial step to comprehensive application. Especially, the use of undifferentiated embryonic material is currently criticized due to ethical reasons (Colman and Burley 2001). In the future, ethical problems can possibly be overcome with the help of induced pluripotent stem cells (iPSCs) and the improvement of reprogramming methods (Takahashi and Yamanaka 2006). Following the pioneering work of Björklund (Gage et al. 1983) it has already been demonstrated in brain lesion animal models that iPSCs-derived neurons are able to survive and extend long-range projections to target areas in the adult injured brain leading to improved behavior (Michelsen et al. 2015). It is even expected that clinical translation to PD patients takes place in the next years (Barker et al. 2016).
Furthermore, isolating neural stem cells from adult brains, which can be cultivated as continuous self-renewing neurospheres is tempting. As adult SVZ and hippocampal stem cells maintain their immature characteristics, such as proliferation, migration and neural differentiation, they form a promising donor source for cell-replacement strategies (Gritti et al. 2002). However, this cell population is located in deep layers of the brain and therefore difficult to harvest. For this reason induced pluripotent stem cells may be a better option for clinical needs.
In order to gain access to this remarkable potential for brain repair, we have to understand in more detail the molecular mechanisms regulating proliferation, differentiation, cell fate, migration, and survival. Furthermore, the knowledge of host tissue conditions has to be enlarged. This includes the crucial steps in survival and function of newly generated neurons (Lledo and Saghatelyan 2005). Even if there is much work ahead, iPSCs represent a promising strategy worth pursuing additionally to pharmacology. Especially, in the regard of present therapeutic side effects like the motor and non-motor fluctuations which are developed in up to 75% of PD patients after 4 to 6 years of Levodopa treatment (Tambasco et al. 2018).
For addressing these points, an appropriate research model is essential. In my studies, I take advantage of the continuous neurogenesis in the olfactory bulb that I will now introduce.

1.1.4. The olfactory bulb as research model

As explained before, it would be a revolutionary medical achievement to use endogenous neural stem cells to produce neuronal progenitor cells for replacing the cellular network in pathological regions. In the adult rodent brain, neuro- and

gliogenesis is sustained in two main areas. On the one hand in the subgranular zone, located in the dentate gyrus of the hippocampus, where neurogenesis is important for learning, memory, and mood regulation (Deng et al. 2010, Samuels and Hen 2011). On the other hand, interneurons for the olfactory system are generated throughout life in the ventricular-subventricular zone, the largest germinal zone in the adult rodent brain. The cells generated in the V-SVZ have to migrate along a precise route before they reach their final position where they integrate in a pre-existing neuronal arrangement. The mouse OB neurogenesis is an ideal model to study the mechanisms of migration guidance as well as the regulation of integration in the adult brain for several reasons: 1) It is located superficially and therefore easily accessible for direct microscopy observations. 2) We can manipulate it efficiently using modern techniques such as DNA electroporation. 3) One day, the obtained results could possibly serve as a base for medical applications since the mammal neuronal system of the mouse shows some parallels to the human one.

1.2. Postnatal neurogenesis in the olfactory bulb

Here, I will give an overview of the current knowledge concerning olfactory bulb neurogenesis. To start, I will characterize the OB neuronal diversity and briefly explain, the interactions of its cellular components. Afterwards, I will describe the source of this neuronal diversity in different regions of the subventricular zone.

1.2.1. Cells and layers of the olfactory system

I will subsequently summarize characteristics of involved cell types and their interactions. Therefore, I outline briefly the main features of the olfactory perception from the sensory epithelium to the deepest layer of the OB, the granule cell layer. Later, each cell type will be described in more detail.

The olfactory pathway

Plenty of different odors are found in the environment. To differentiate between this wide range of nasal sensory input and to rapidly recognize familiar odors, a very efficient sensory system is needed.

Olfactory sensory neurons (OSNs) located in the nasal cavity are the first body compartments to receive smelling signals. The detection of odorants is achieved by the binding of mostly lipophilic odorant molecules to olfactory receptors (ORs). Sensory neurons in the olfactory epithelium are continuously renewed every 30 to 60 days. Their somata lay in the middle of the epithelium and extend on the apical side into dendritic knobs which emanate tapering cilia. From the basal pole on the opposite side axons arise and penetrate the basal lamina. Those axons are then pooled to form bundles that are surrounded by highly specialized olfactory ensheathing glial cells. Contrasting the OSN’s uniform morphology, their molecular phenotype with cell

surface antigens and second messenger pathways is one of the most diverse in the nervous system. A single odorant can activate not only one but multiple of the thousand different OR species. ORs have a seven transmembrane domain structure. After an odorant binds to the cilia located on the OSN dendrite, a G-protein-cascade is activated. This triggers cyclic nucleotide-gated channels to open and let Na^+ and Ca^{2+} get into the cell which in turn provokes depolarization through a Cl^- efflux (Mombaerts 2004). The action potential is further transmitted via the OSN's axons that run as many small nerve fascicles (Fila olfactoria) through the cribriform plate of the ethmoid bone. The totality of all fibers is called olfactory nerve. After the penetration of the cribriform plate, the original organization of OSNs' axons as fascicles is abolished. Now, all axons expressing the same type of receptors, recognize each other and project to one or two specific target sites in the OB resulting in the formation of a spherical glomerular structure (Mombaerts et al. 1996). In the mouse OB more or less 1800 of those glomeruli can be detected. Since the same receptor species projects to only one glomerulus, it is assumed that stimuli are represented in the olfactory bulb as a topographic map which may be used for perception of odor in the olfactory cortex (Mori and Sakano 2011). Eventhough sensory neurons are continuously renewed from epithelial basal cells, they keep their specificity regarding their link to one distinct glomeruli. The primary information about odorant identity is encoded through the combination of activated glomeruli and their level of activation (Wachowiak and Shipley 2006). From the OB, this information is sent to the amygdala, the orbitofrontal cortex and the hippocampus, where they are further processed.
Following the general structure of the brain, the OB is highly laminated with specialized cell types in each layer. Unlike the cortex and its mainly excitatory projection neurons, the OB is a predominantly inhibitory circuit with diverse, locally connecting interneurons (Shepherd 2004). From a histological point of view the main olfactory bulb consists of five layers (Fig. 1), which are In order from surface to the center:

- **Glomerular layer (GL)** - periglomerular cells (PGCs), external tufted cells (eTCs), short-axon cells
- **External plexiform layer (EPL)** - tufted cells (TCs)
- **Mitral cell layer (MCL)** - mitral cells (MCs)
- **Internal plexiform layer (IPL)** - short-axon cells
- **Granule cell layer (GCL)** - granule cells (GCs), short-axon cells

Projection neurons of the OB

In the OB, there exist two types of cells that project directly to the central cortex: tufted and mitral cells. Both of them are attached to one single glomerulus with their primary dendrite. Each glomerulus is innervated by roughly twenty proximate mitral and tufted cells (Nagayama et al. 2014). At the connection site, they receive synaptic

input from the OSNs' axons. Their secondary dendrite is elongated to the external plexiform layer (EPL), where reciprocal synapses are formed with granule cell dendrites (Mori and Yoshihara 1995). Mitral and tufted cell axons reach further down in the bulb giving off recurrent collaterals before they finally form the lateral olfactory tract (LOT).

Based on their laminar positioning within the external plexiform layer, TCs are typically classified into external (also superficial), middle and internal TCs (Mori et al. 1983). Additionally, external tufted cells (eTC) surround glomeruli in the glomerular layer (GL) are part of the juxtaglomerular cells. Through monosynaptic input from the olfactory nerve, eTCs (10-15 μm) can be activated at a lower threshold than mitral cells, suggesting that they coordinate the activation of the entire glomerular microcircuit and provide feedforward excitation (De Saint Jan et al. 2009). However, it has been revealed recently, that eTCs can also suppresses both spontaneous and odour-evoked firing. Consequently, eTCs are now divided into two molecularly different groups: one purely excitatory and the second one GABAergic (Tatti et al. 2014). After leaving the LOT, TCs' axons reach projection sites in the olfactory cortex which differ from those attached to MC axons. While TCs connect to specific areas of the anterior olfactory cortex: the olfactory peduncle, olfactory tubercle, and a part of the piriform cortex, MCs connect throughout the entire olfactory cortex (Nagayama et al. 2014).

The inner zone of the EPL hosts of the second type of OB projection neurons, the mitral cells (MCs). Amongst all cells of the OB, MCs have the biggest somata (>20 μm). Just like TCs their single apical process elongates into one glomerulus while collaterals of their basal dendrites remain exclusively within the granule cell layer. Besides all similarities, the two cell types display a different axonal projection pattern and process other aspects of olfactory information (Nagayama et al. 2004).

Olfactory bulb interneurons

While only 1% of the neurons of the OB are directly connected to the olfactory cortex, the predominant cell type in the OB are inhibitory GABAergic interneurons needed as a filter. They are distributed in three zones: the glomerular, plexiform and granule cell layer. The main type in the GL are the periglomerular cells (PGCs) which connect MCs' and TCs' primary dendrites via reciprocal synapses (Fig. 1). Their small somata (diameter: 6-8μm) surround the glomeruli. PGCs have one or often two dendrites which connect one or two glomeruli. Their axons can either reach up to five glomeruli away or be completely missing (Pinching and Powell 1971). It is remarkable, that those PGCs that are added postnatally do not posses axons.

Due to the great range of their synaptic phenotypes, it is currently hypothesized that PGCs fulfill a variety of functions such as the spread of synchronization or the control of oscillatory responses of MCs (Shepherd 2004). Based on morphological

characteristics like intraglomerular dendritic arborisations and synaptic contacts, two main types of PGCs can be distinguished: type-1 cells which are Tyrosine Hydroxylase (TH) positive and connect not only principal cells but also OSNs and type-2 PGCs that form synapses exclusively with principal cells and express specific markers like Calbindin (CalB), Calretinin (CalR), Parvalbumin or the GABA α5-subunit (Kosaka and Kosaka 2008, Nagayama et al. 2014).
Within the glomerular microcircuit, it is highly probable that the PGCs act in a leading role to control the decorrelation of MC/TCs through inhibition of local primary dendrites via dendrodendritic synapses. Especially, decorrelation of MC/TC firing in an odor concentration-dependent manner leads to an efficient mechanism to code stimulus intensity (Geramita and Urban 2017).

In the beginning of the 19th century, scientists baptized the axon-less cells laying between IPL and RMS granule cells due to their very small somata (diameter: 6-8μm). GCs are the most numerous neuronal subtype in the OB. Their deep process branches within the GCL whereas their superficial one reaches up to the EPL. Similarly to TCs, GCs can be sorted into three groups depending on their positioning: superficial = GC-type 3, intermediate = GC-type 1, deep = GC-type 2. The peripheral processes of the type 1 GCs branch at the border between the MCL and the EPL, whereas the ones of type 2 cells stay in the inner half of the EPL. Superficial GCs have processes that run radially without any arborisation in the centre of the EPL. Until recently, specific molecular markers were rare for GCs. However, not long ago, it has been discovered that CaMKIIα-expression can reliably define granule cells involved in different functional circuits (Malvaut et al. 2017).
When a granule cell receives a signal, it will in turn inhibit another neighboring mitral or tufted cell (Xiong and Chen 2002). This so-called lateral inhibition is believed to be one of the major strategies to block the activity of the olfactory projection neurons and thus increase the signal-to-noise ratio of sensory stimuli.

The exceptional fact that — in contrast to most parts of the brain — the majority of OB interneurons are postnatally generated and integrated in the bulb circuits will be further explained in the following chapter.

1.2.2. Postnatal cell addition

Here, I will follow the way of adult-born neurons from their origin in the V-SVZ to their final destination in the OB.

Organization of V-SVZ neurogenesis

The V-SVZ is regionalized and composed of the following cell types (Fig. 2): neural stem cells, transit NSCs amplifying cells, neuroblasts and ependymal cells (Doetsch et

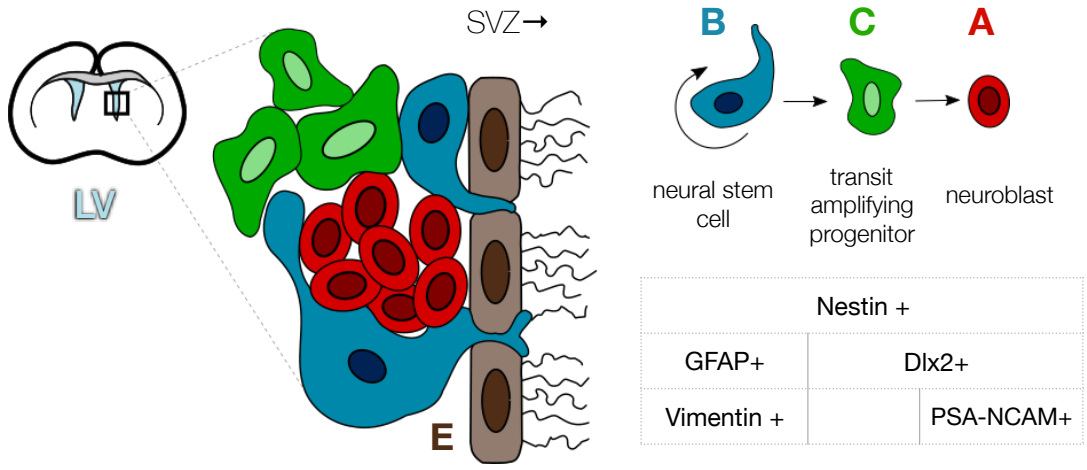

Figure 2: ***Early cell development in the neurogenic niche***
The interneurons that are added to the olfactory bulb (OB) throughout life originate from a germinal region known as the subventricular zone (SVZ), next to the walls of the lateral ventricles (LV, left). In this zone of proliferation (middle) stem cells (type B cells, blue) divide to generate transit-amplifying progenitor cells (type C cells, green), which afterwards give rise to neuroblasts (type A cells, red) that subsequently migrate towards their final position in the OB. Different markers label the cell types non-specifically (right). E, ependymal cell

al. 1999). Neural stem cells are the primary progenitors that give rise to neurons and glia not only in the embryonic but also in the neonatal and adult brain. Interestingly, it is believed that adult NSCs originate from embryonic NSCs (Fuentealba et al. 2015). Even-though, the system has been studied intensively, no specific marker was found so far to distinguish the different cell types specifically. This is why a precise classification remains difficult.

Most adult V-SVZ neural stem cells enter quiescence (qNSCs) in mid-embryogenesis and remain silent until they become activated (aNSCs) postnatally. aNSCs, also called B cells then divide to generate transit amplifying type C cells, which subsequently undergo several rounds of division themselves before finally producing the type A cells, the migrating neuroblasts (Doetsch et al. 1999). As a result of this formation process, type C cells lay in focal clusters closely associated with chains of type A cells (Fig. 2). C cells can be located all around the lateral wall of the lateral ventricle but are mostly absent in the RMS. They have smooth contours, an undifferentiated cytoplasm and are immuno-negative for GFAP (glial fibrillary acidic protein), PSA–NCAM (polysialylated-neural cell adhesion molecule) and vimentin indicating that they neither correspond to glial cells nor to migrating neuroblasts.

Recently, it has been discovered that 70%-80% of B cells divide symmetrically to generate progenitors, whereas 20%-30% remain in the niche where they self-renew for several months. Because the amplification of progeny is a consuming process, the B population depletes over time (Obernier et al. 2018).

Migrating neuronal precursors named type A cells are arranged in chains and lie parallel to the ventricle walls where they move through tunnel-like structures formed by astrocytes. They are positive for Nestin, PSA–NCAM and Dlx2.

Generating specific types of OB neurons

Approximately 95% of the new neurons in the olfactory bulb become GCs (Lledo and Saghatelyan 2005), whereas only a minority differentiates into PGCs (Whitman and Greer 2007). Interestingly, the fate of the SVZ progenitor cells seems to be determined by their positioning, as specification programs are conserved from development to adulthood in the NSCs of the different walls (Azim et al. 2015).

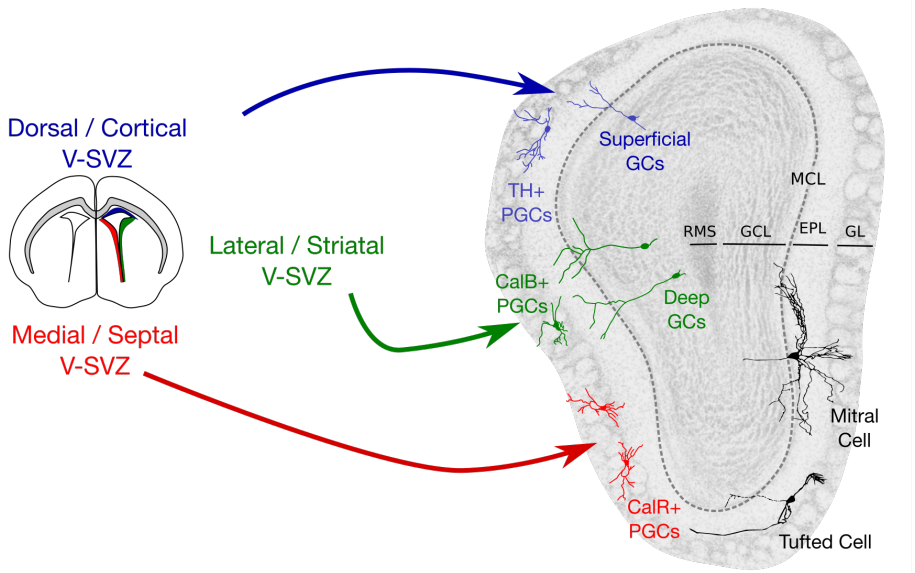

Figure 3: ***Origin-specific fate of neural progenitors***
Coronal schema of ventral- sub ventricular zone (V-SVZ, left) and coronal section of the rodent olfactory bulb (OB, right). Adult neural stem cells line all walls of the lateral ventricle. Depending on their location: lateral (green), dorsal (blue) or medial (red) they give rise to different types of OB interneurons that can be distinguished by specific markers. Mitral and Tufted cells are represented in black. Image created by Stéphane Burgeon. RMS, rostral migratory stream; GCL, granule cell layer; MCL, mitral cell layer; EPL, external plexiform layer; GL, glomerular layer; PGCs, periglomerular cells; GCs, granule cells; TH, tyrosine hydroxylase; CalB, calbindin; CalR, calretinin

In general, three different regions of the SVZ are described: the dorsal part next to the corpus callosum, the lateral part near the striatum, and the medial septum (Fig. 3). Using different techniques such as viral labelling or electroporation it was shown that each area gives rise to a specific subset of interneuron subtypes (Merkle et al. 2007). The PGC production is located mostly dorsally but also in the medial septal wall. Notably, PGC subtypes are again produced region-specifically: associating the dorsal area to TH+ and the medial part to CalR+ cells. Granule cells originate from all over the SVZ, though less from the medial septum. Dorsal regions tend to produce superficial granule cells, whereas ventral regions give rise to deep granule cells (Fernandez et al. 2011).

The SVZ subdomains that were encoded during embryogenesis are sustained postnatally by local molecular gradients that induce lineage-specific transcription factors and therefore contribute to the diversity of neuronal and glial fates. The alteration of their gradients can influence the process of neurogenesis partially or entirely. Some key molecules directing progenitor fate have been identified. The transcription factor Pax6 for example is important for the formation of dopaminergic

PG but not for granule cells (Kohwi et al. 2005, de Chevigny et al. 2012), while the zinc-finger transcription factor Sp8 is necessary during the generation of some GABAergic and CalR-expressing subtypes (Waclaw et al. 2006).
In addition, genetic fate mapping experiments with Dlx1/2 precursors showed that different interneuron subtypes are born predominantly at specific pre- and postnatal periods. Within the GL for instance, the production of TH+ interneurons is at its maximum during early embryogenesis and decreases thereafter. Differently, the generation of CalB+ cells is highest during late embryogenesis and goes down postnatally, while CR+ cell production is rare during embryogenesis and increases upon birth (Batista-Brito et al. 2008). As a result, the OB circuits are composed of interneurones with a large range of ages (days to months).

Role of postnatal and adult neurogenesis

Quantitative studies of Platel et al. (Platel et al. 2019) indicate that around 0,5% of the olfactory granule cell population is added per day, leading to the interesting question, why such an energy consuming process it is necessary and which functional impact the integration of newly added cell into mature circuits has. Investigations challenging adult bulbar neurogenesis by special SZV-treatments, such as the infusion of the antimitotic drug cytosine arabinosine, have not revealed striking sensory deficits per se (Breton-Provencher et al. 2009). This proves that olfactory perception is not mediated by adult-generated neurons on a large scale. However, some cognitive functions were clearly disturbed suggesting that adult-born neurons with their unique synaptic plasticity play an important role for (1) maintenance of the OB circuit; (2) shaping odor pattern-segregation; (3) perceptual learning, and/or (4) olfactory memory (Lazarini and Lledo 2011). Overall, past observations show that functions of OB adult neurogenesis are highly complex. Further studies will have to be designed for addressing this issue in more detail. Distinct populations of adult-born interneurons (periglomerular cells versus granule cells) could for instance be selectively targeted since the role for new periglomerular cells in olfactory information processing is still pending.

1.3. Migration from the SVZ to the OB

After neuroblasts have been generated in the SVZ, they have to cover a distance ranging from 3 to 8 mm depending on their site of birth (Doetsch and Alvarez-Buylla 1996) in order to reach their final position in the OB. Leaving the margin of the central nervous system (CNS) adjacent to the lateral ventricle, they first migrate at high speed through the rostral migratory stream, a sharply bounded pathway, before they slow down and integrate into their target layer in the OB (Fig. 4).
Rather than moving constantly forward, future OB interneuron migration appears to be saltatory, with a period of relative immobility between migratory spurts (Fig. 9). Each

migration step is marked by four phases: leading process extension then branching, swelling formation and finally nucleus translocation, which involves dynamic cytoskeleton modifications. In both radial and tangential migration, the cytoskeleton made up of actomyosin coordinates nuclear movement (Schaar and McConnell 2005). In this chapter, I will further characterize those two migration modes known as tangential and radial migration and summarize what is known of their regulatory mechanism. The route from the SVZ to the OB as well as the main RMS is sustained by various guidance mechanisms such as blood vessels, neuronal chains and astrocytes (Fig. 4).

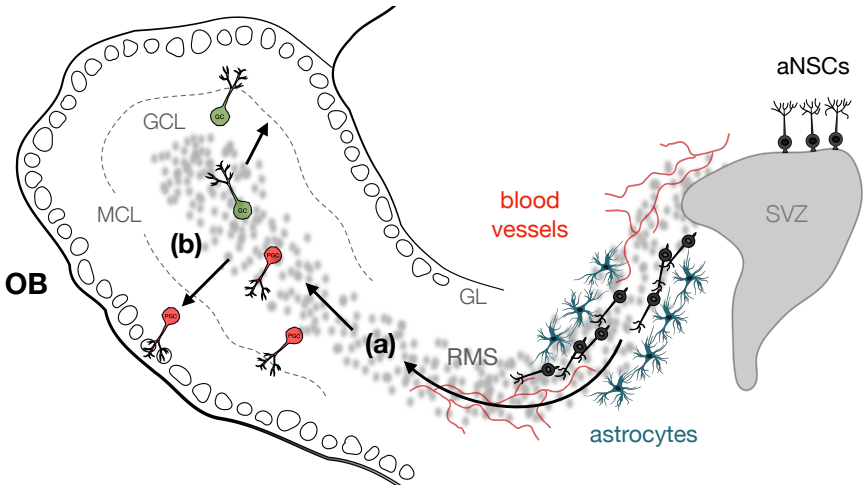

Figure 4: ***Types of migration and RMS scaffolding mechanisms***
The subventricular zone (SVZ) is one of the rare constitutive neurogenic areas in the adult CNS. There, adult neural stem cells (aNSC) lining the lateral ventricles give rise to new neurons. In this sagittal section of the rodent forebrain migration of interneuron progenitors (black) towards the olfactory bulb (OB) and some of its regulators are schematically shown. Within the rostral migratory stream (RMS), the future interneurons form chains through homophilic interactions and are guided by blood vessels (red) as well as by astrocytes (turquoise) that surround the borders of the RMS. Other secreted factors like Slit1 and Slit2 (not shown) contribute to the regulation of tangential migration (a). After the exit of the RMS, cells switch to the slower and less direct radial migration mode (b).

1.3.1. Tangential Migration

In 2007, Nam et al. quantified the migratory behaviour of cells coming from the dorsal SVZ in three dimensions using a mouse model (P10 to adulthood). They showed that there are statistically different speeds in different classes of SVZ cells and proposed that this might be due to different level of maturation: older neuroblasts seemed to be faster than less mature neuroblasts. The average migration speed of a mixed population of neuroblasts in the RMS ranges from 60 to 80 µm/hr and ranks therefore amongst the highest in the brain (Nam et al. 2007). Nevertheless it takes 2-3 days before the newborn cells originating in the dorsal SVZ reach the rodent olfactory bulb. The migrating 1-7 days old neuroblasts have a simple, homogeneous morphology with a prominent leading and a small trailing process. Their orientation during RMS migration is not stringently uniform. Of course, nuclear translocation always follows

the leading process extension, but remarkably, cells move not only rostrally, but sometimes stop or even reverse their direction towards the SVZ (Nam et al. 2007). This is unexpected, taking into account the influence of the chemorepulsion signals, Slit1 and Slit2, expressed in the septum and ventricular zone which normally repel migrating SVZ neuroblasts (Nguyen-Ba-Charvet et al. 2004). Nonetheless, Slit can only act on neurons within a range of 1 mm and is therefore not effective within the entire 5 mm long mouse RMS. Possibly filling this gap, the OB itself could be a source of attracting cues. Even if the removal of the OB has surprisingly no large impact on tangential migration (Kirschenbaum et al. 1999), some grafting experiments showed later-on that a piece of OB is enough to allure and reorient migrating SVZ precursors (Liu and Rao 2003). Consequently, chemoattractants as directing clues are highly supposable. Unlike neuronal migration during embryonic development, RMS neuroblasts are not mediated by scaffolding radial glia, neither during tangential nor radial migration. After a postnatal period of 2-3 weeks, cells in the adult brain migrate rather in chains based on homophilic interactions via integrins (Murase and Horwitz 2002) and are associated with astrocytes. Those astrocytes surround neuroblasts and form glial tubes that act as boundaries to physically prevent premature RMS exit. Based on transplantation experiments it was demonstrated that neuroblast chains are mainly stabilized by adhesion molecules such as PSA-NCAM (Chazal et al. 2000) or N-Cadherin (Yagita et al. 2009). The lack of PSA-NCAM for instance leads to a decrease in migration. However, neuronal migration is not fully blocked showing that the mutant RMS is to a certain extent still functional. This suggests that other factors contribute to its performance. Due to the close contact between neuroblast chains and blood vessels, it can be assumed that those anatomical structures may provide such an additional scaffold for tangential migration (Whitman et al. 2009) as well as for radial migration within the olfactory bulb (Bovetti et al. 2007). Interestingly, astrocytes can regulate the vascular organization by releasing vascular endothelial growth factor (Bozoyan et al. 2012). Overall, astrocytes are a very important component in guiding migrating cells: they give directional cues (Gengatharan et al. 2016) and strictly control neuronal survival by releasing glutamate through the stimulation of N-Methyl-D-aspartate (NMDA) receptors (Platel et al. 2010). If neuroblast have not acquired NMDA receptors, they are eliminated prior to entering the OB synaptic network. By adjusting GABA and glutamate levels SVZ- and RMS-astrocytes provide one of the main homeostatic mechanisms to modulate neuroblast migration speed. For example, they express the GABA transporter GAT4 which allows them to partially control the extracellular GABA concentration. Upon GABA-increase, the migratory speed decreases (Platel et al. 2008b). Accordingly, the application of the $GABA_A$-receptor antagonist Bicuculline enhances the migration rate by 30% (Bolteus and Bordey 2004).

1.3.2. Radial Migration

As soon as neuroblasts have reached the core of the OB, they dissociate from their cellular chains and turn outwards to reach their target layer individually. At this point, the cells slow down, migrate less straight and start to have a more complex morphology. This radial migration mode lasts for about one week before integration takes place in the respective layer (Carleton et al. 2003).
So far, only few regulatory mechanisms for the switch from tangential to radial migration are described. The first discovered key signaling pathway involves the extracellular matrix protein Reelin which is synthesized in the mitral cell layer (MCL) (Hellwig et al. 2012). Secondly, Tenascin-R was found in the granule cell layer (GCL) (Saghatelyan et al. 2004). This extracellular matrix molecule does not only induce the detachment of arriving cell, like reported for Reelin, but also enhances radial migration itself. Interestingly, Tenascin-R expression seems to be mediated by activity as it is considerably deceased by odor deprivation (Saghatelyan et al., 2004). In addition, the detection of a reduced chain migration in favor for dispersed migration after the absence of Slit1 implicates, that Slit expression promotes the change from tangential to radial migration as well (Nguyen-Ba-Charvet et al. 2004).

After having left the RMS, migrating neuroblasts continue to follow blood vessels through an extracellular matrix–astrocyte-end-foot-interaction. In fact, this “vasophilic migration” seems to be only an initial guidance through the GCL, which is redundant and thus abandoned for crossing the EPL (Bovetti et al. 2007).
Next to the vasal, also cellular scaffold was hypothesized for neuroblast guidance after identifying a population of radial glia-like cells within the granule cell layer (Emsley et al. 2012). As the OB consists of a variety of cell types, a modulation of migration by this cellular network is probable. Foremost, MCs are possible candidates for modulating radial migration due to their expression of Reelin and stores of glutamate. Also, they form a physical barrier-like structure inevitably slowing down the crossing procedure.

Interestingly, two different ways of how OB interneuron subtypes finish migration were found by *in vivo* imaging upgraded with an optical cell positioning system based on repeated angiography. On the one hand, GCs keep their radial mode until they reach their final location in the GCL, on the other hand, PGCs undergo a switch in their migration pattern upon entering the GL (Liang et al. 2016). As soon as PGCs arrive in their target layer, they sharply change the angle of their motion vector. To describe this last subtype-specific migration mode, the term „lateral migration“ was introduced. During this unique long-distance lateral displacement, PGCs migrate saltatory for up to two weeks with a remarkable age-dependent decrease in velocity.

1.4. Neuronal activity as a multi-potent regulator of neuronal migration and differentiation

Considering that the olfactory bulb is an area that processes sensory input and seeing that radial migration of newborn neurons takes place surrounded by functional neurons, it could be possible that neuronal activity is important in the OB for the regulation of migration and layer positioning. This hypothesis is supported by the fact that many neurotransmitter receptors are expressed by neuroblasts during both modes of migration (Platel et al. 2008b). Recent findings demonstrate that the migration of newborn bulbar interneurons could be sensitive to neuronal activity. One publications shows for instance that sensory deprivation decreases tangential migration speed *in vivo* (Pothayee et al. 2017). Another demonstrates that migrating PGCs in the GL respond to odor presentation (Kovalchuk et al. 2015).
Both intrinsic factors and extrinsic signals are important for controlling neuronal migration. As main source of extrinsic cues, astrocytes and neurons release neurotransmitters or -modulators. This allows already integrated neurons to regulate the migration of later arriving interneurons, thereby generating a feedback loop. Applying this strategy, OB excitatory projection neurons can modulate interneuron migration and therefore regulate the future extent and mode of their inhibitory influence.
Interestingly, several parameters of this spontaneous activity like the time spent in the active state or the fraction of continuously active cells show a bell-shaped dependence on cell's age — peaking in 3-4 weeks old cells. This data underlines the *in vivo* presence of spontaneous Ca^{2+} signaling during the layer-specific maturation of adult-born neurons in the olfactory bulb and motivate to further investigate the functions of this activity.
To better understand which role neural activity plays in regulating OB migration and integration, I will review relevant facts in this subchapter. First, I will introduce the basic mechanism of neuronal migration before I describe some neurotransmitters and neuromodulators that are involved in the regulation of migration in the RMS. Finally, I will come to the contribution of the interneuron membrane potential to migration.

1.4.1. Basic mechanism of neuronal migration

Overall, neuronal modulations involve intrinsic and extrinsic clues which can be provided by both astrocytes and neurons themselves. In the case of the OB that means that the projection neurons which are already in place could shape the migration of the later added interneurones. Through this feedback loop, interneuron migration can be regulated and the future range of inhibitory modulation defined.
Neuronal signaling is mainly achieved by the intracellular release of Ca^{2+} which can either enter directly through ionotropic channels from the extracellular surrounding, or indirectly using metabotropic receptor transduction that activates Ca^{2+} transporters

within the membrane of the Endoplasmic Reticulum (ER) (Berridge et al. 2003). Fine regulations are achieved by the application of neurotransmitters which can either hyper- or depolarize the cell and therefore trigger additional Ca^{2+} influx.
Once the Ca^{2+} concentration in the cytoplasm has reached a certain threshold, diverse molecular pathways such as cytoskeleton rearrangements are initiated. Above all, the nucleus, as the largest intracellular organelle, has to be displaced in order to start cellular movement. This is achieved through an initial formation of a cup-like actin structure at the rear nuclear pole that later contracts progressively to realize nucleokinesis. The actin remodeling requires a distingue Ca^{2+} level provided by fast intracellular Ca^{2+} transients (Martini and Valdeolmillos 2010).
In migrating neuroblasts, spontaneous Ca^{2+} spikes last usually for 2–5 s and go along with an up to 6-fold increase in the intensity of a fluorescence probe (Garcia-Gonzalez et al. 2017). Whereas intracellular Ca^{2+} chelating decreases migratory speed in cortical interneurons and cerebellar granule cells, it does surprisingly not cause velocity changes in the RMS (Darcy and Isaacson 2009).

1.4.2. Receptors and neurotransmitters of migrating OB neuroblasts

The expression of receptors on migrating neuroblasts and differentiating NSCs suggests that both migration and integration processes are controlled by certain chemical messengers which I will subsequently explain in detail.
In the postnatal and adult SVZ, stem cells regulate the extracellular concentration of GABA via uptake through GAT4 GABA transporters (Bolteus and Bordey 2004). When $GABA_A$ receptors are activated in the SVZ and RMS, the rate of migration and the number of proliferative stem cells decrease (Platel et al. 2008a).
Functional AMPA/kainate receptors (GLUK5) as well as metabotropic glutamate receptors subtype 5 (mGluR5) are expressed in SVZ and RMS neuroblasts. Although both of them increase Ca^{2+} levels upon activation, only GLUK5 receptors tonically reduce the speed of neuroblast migration along the lateral ventricle (Platel et al. 2008b).
Additionally, neuroblasts born in the postnatal subventricular zone acquire NMDA receptors during their migration to the olfactory bulb. Those provide early survival cues to neuroblasts before they enter the OB network. At the same time, genetic or pharmacological manipulations of NMDA receptors did not affect the speed of neuroblast migration (Platel et al. 2010).
Glutamate in the RMS could be the released by astrocytes, since activity-dependent, vesicular glutamatergic signals from astrocyte-like cells to neuroblasts have been shown (Platel et al. 2010).
GLUK5, mGluR5 and $GABA_A$ receptors are expressed as a mosaic on migrating neuroblasts. Only 40% of rostral SVZ cells express all three receptors, ~30% express either GLUK5 or mGluR5 with $GABA_A$ receptors while ~90% of neuroblasts express

$GABA_A$ receptors either alone or with other receptors. Furthermore, a raising amount of neuroblasts expresses GLUK5 and mGluR5 along the rostral–caudal axis suggesting that the acquisition of those receptors is part of the neuroblast maturing process during tangential migration (Platel et al. 2008a).

1.4.3. Membrane potential

The tight link between migration and electrophysiological properties was first discovered in the developing cerebellum, where granule cell movement is regulated via KCl-induced depolarization (Komuro and Rakic 1992). Numerous studies testified later that this regulatory mechanism is not unique but exists in various regions of the nervous system such as the spinal cord (Spitzer 2006) and the ventricular zone (De Marco Garcia et al. 2011) to only name a few. Therefore, it seems to be probable that OB kinetics, too, are linked to the membrane potential.
The basis of changing membrane potentials are ion channels that allow certain currents to pass though and consequently lead to an electrical charge.
Neuroblasts in the RMS express voltage-dependent, delayed-rectifier K^+ currents and less frequently also voltage-gated Na^+ currents (Belluzzi et al. 2003). When all extracellular Ca^{2+} concentration was removed artificially, K^+ currents were partially decreased at the same time, suggesting that the K^+ channels depend on the presence of Ca^{2+} (Wang et al. 2003). During tangential migration, spontaneous Ca^{2+} transients are mediated by the serotonin 3 A receptor-activation (Garcia-Gonzalez et al. 2017). Through this Ca^{2+} mechanism, speed and directionality are regulated either directly or via the activation of Ca^{2+} dependent potassium channels.
While adult-born cells during tangential migration do not yet generate own action potentials and have mainly a delayed-rectifier potassium conductance, they become odor responsive two days after their arrival at the glomerular layer (Kovalchuk et al., 2015). Given the fact that odorant sensitivity occurs even before definite integration, it is indicated that migration and final positioning could be guided by stimulating input.
After having left the RMS, OB neural progenitors generate a different kind of Ca^{2+} transient mediated by Dihydropyridine-sensitive L-type Ca^{2+} channels (Darcy and Isaacson 2009). These Ca^{2+} gates are independent of voltage-gated Na^+ channels as well as NMDA, AMPA and $GABA_A$ receptors and do, astonishingly, not influence migratory parameters. As soon as one week after future PGCs have reached their OB layer, they start to fire action potentials and carry well-developed voltage-gated sodium and potassium conductances which allow depolarization. P14 old PGCs show electrophysiological properties *grosso modo* similar to those of the neighboring resident neurons indicating that their structural and functional differentiation occurs at a high pace (Belluzzi et al. 2003).
Recently, a final switch of Ca^{2+} mechanisms in OB neural progenitors has been reported. Using in vivo imaging techniques, it was shown that the intracellular Ca^{2+}

levels in neuroblasts are highly increased upon their arrival in the destination layer (Maslyukov et al. 2018). Due to the fact, that those spontaneous Ca^{2+} transients are sensitive to Tetrodotoxin, a blocker of voltage-gated Na^{+} channels, they seem to be mechanistically different from those observed in earlier migration steps (Darcy and Isaacson 2009).

1.4.4. Neurophysiological differentiation and integration of interneurons in the OB

Integration processes have to be particularly well-coordinated, because synaptogenesis of adult-born neurons could interfere with the circuit operation already in place. If we want to fully understand how SVZ neurogenesis works, we have to look not only at regulatory mechanisms of cell production and migration but also at those signals that guide each subtype to its final layer. Somehow, cells have to switch from migration to an integration program.

At this point, I will give an insight in the way OB interneurones mature morphologically and electrophysiologically and how their synapses are formed, focusing on the role of neurotransmitters.

Prior to the integration process, tangentially and radially migrating cells in the adult brain have a relative plain morphology and do not release spontaneous postsynaptic currents, but already express functional $GABA_A$ and excitatory AMPA receptors (Carleton et al. 2003, Platel et al. 2007). Once stationary, their simple dendrite extends within the GCL towards the MCL, progressively becoming more and more complex. As discussed earlier, migrating interneurones express functional GABA receptors already in the RMS (Bolteus and Bordey 2004). Thus it is not surprising that the first synapses they make in their final layer are GABAergic, followed by glutamatergic synapses after several weeks. Through the stabilization of lamellipodial protrusions in dendritic growth cones, ambient GABA contributes to the proper initiation and elongation of dendrites (Gascon et al. 2006). The observed GABAergic effects are associated with an increased stability of microtubules and depend on depolarization and Ca^{2+} influx. At 20 the maturation process is finally completed with spine acquirement.

Interestingly, newly arrived neurons already react synaptically to olfactory nerve stimulation and can establish axodendritic and dendrodendritic synaptic contacts within the OB network (Belluzzi et al. 2003). The initial glutamatergic contacts can be received through axodendritic synapses from centrifugal fibers and/or axon collaterals of mitral and tufted cells. These connections are established in the GCL as early as P10 when cells that have just stopped migration and do not yet possess dendrites long enough to reach the EPL.

As soon as GCs have stopped migration, they show spontaneous inhibitory and excitatory postsynaptic currents. However, only those with a mature cell morphology are able to fire action potentials. This delay in spiking ability relative to the capacity of

receiving synaptic input can be exclusively found in the postnatal development of the OB (Carleton et al. 2003).
Whereas all new fully mature GCs present spontaneous synaptic potentials (Carleton et al. 2003), only a small percentage of the arrived PGCs show spontaneous excitatory synaptic currents (Belluzzi et al. 2003). The fact that not all PGCs are connected to existing synaptic circuitry hints that some of them are blocked or delayed during the competition for synaptic contacts. Also, PGCs younger than 4 weeks regardless of their functional GABA receptors do not respond to glutamate (Belluzzi et al. 2003). However, olfactory input enhances synaptogenesis of adult-born PGCs during their early development (Livneh et al. 2009).
As soon as dendritic elongation within the EPL has taken place (around P21) a second wave of excitatory inputs though reciprocal dendrodendritic synapses appears (Whitman and Greer 2007). The initial formation of basal synapses in the GCL allows new neurons to receive information about the preexisting network. This might contribute to the way they later integrate into the local circuits found in the EPL, where they then actively participate through inhibitory dendrodendritic synapses. Overall, this two-step sequential formation in the adult brain with input synapses appearing before output synapses, may represent a cellular mechanism to down-regulate the interruption caused by new neurons trying to integrate into preexisting circuits (Kelsch et al. 2008).

1.5. Cell death in the OB and its link to migration

When hippocampal pyramidal neurons are injured or apoptosis locally induced in non-neurogenic brain regions, the migration of adult-born neurons towards those places is enhanced (Nakatomi et al. 2002) proposing that neuronal death and migration are linked. This regulatory mechanism could also work in the OB, but has been so far merely understood. Since I aim to clarify the complex regulations of OB interneurons, it is inevitable to take a closer look at survival and cell death as possible influencing parameters. It will be essential to see if during migration there is a selection phase and if non-selected cells will disappear. It has been already shown that death could be present during the migration phase and that NMDAR acquisition is crucial for neuroblast survival prior to entering a synaptic network (Platel et al. 2010).
In Bax-KO mice, where programmed cell death of migrating neuroblasts and olfactory interneurons is reduced, neuronal migration was impaired in the RMS. However, after Bax-KO SVZ explants were embedded in 75% Matrigel, they showed normal chain migration patterns, both at the age of 4 days and 12 month, implying that the mechanism behind harmed cell migration under non-apoptotic conditions is not cell autonomous. Instead, external factors such as damaged glial tubes or neurotransmitter alterations could be causes (Kim et al. 2007).

As the link between migration and death is especially interesting for cell therapies at sites of neurological damage — where impaired cells undergoing apoptosis urge to be replaced — it will be essential in the future to understand the underlying processes in depth.

1.5.1. Elements that influence survival

Since cells are constantly added to a preexisting neuronal network, it seems to be evident that the final number of participating neurons has to be somehow regulated. Until recently, competitive selection was proposed to be the main principle of neuronal homeostasis regulation during synaptic integration. However, applying novel more physiological methods, different observations have been made putting this models under scrutiny. As this ongoing debate could probably cause a change in how we understand the whole process of OB neurogenesis in the future, I will look at different theories in more detail after reviewing influences and possible functions of apoptosis in the OB.

Activity plays most likely a distinct role as it is well known that complex sensorial stimulations modify brain functioning and its anatomical organization. In adult mice, the exposure to an odor-enriched environment for 40 days increases the number of surviving progenitors (Rochefort et al. 2002), presumably by upraising cellular activity. On the other hand, naris occlusion decreases the number in both the glomerular and the deep granular layer, notably only during a specific time window, suggesting that sensory input dependency begins not until the cells have reached their final destination (Yamaguchi and Mori 2005). In addition, nostril closure in the perinatal period decreases the complexity of dendritic arborisation as well as the spine density in newborn GCs without affecting the preexisting GC-population (Saghatelyan et al. 2005). Indeed, sensory deprivation by naris closure leads to extensive neuronal death among neonatal and adult born GABAergic inhibitory interneurons (Sawada et al. 2011). Interestingly though, glutamatergic juxtaglomerular cells survive sensory deprivation. Which leads to the assumption that the response of inhibitory and excitatory populations to environmental input differs (Angelova et al. 2019).

The literature about molecular signaling concerning survival in the OB is very complex to the extent, that some data even seem to be controversial. Taking the example of cholinergic inputs, it has been shown on the one hand, that intraperitoneal administration of donepezil, a potent and selective acetylcholinesterase inhibitor given also to Alzheimer's disease patients, significantly enhanced the survival of newborn neurons while the rate of SVZ progenitor proliferation stayed unchanged (Kaneko et al. 2006). On the other hand a diminution of newborn neurons was observed after chronic nicotine exposure which normally binds to the same acetylcholine receptor (Mechawar

et al. 2004). When cell-intrinsic neuronal activity was suppressed using the Kir 2.1-approach, the number of newly generated GCs in the OB was largely reduced at P28 (Yamaguchi and Mori 2005) - a time point just after their integration phase, when survival is most sensitive to olfactory deprivation. This underlines once more the role of neuronal activity during the maturation of adult-generated neurons in a cell-autonomous manner. In contrast, the spine density was indistinguishable between Kir 2.1+ and control group neurons, suggesting that a Ca^{2+} decrease affects synaptic development only marginally (Lin et al. 2010).

The plasticity-associated transcription factor “cAMP response element-binding protein” (CREB) is expressed by SVZ neuroblasts though-out their entire development. However, its phosphorylation (pCREB) is transient - peaking at the late phase of tangential migration and declining as dendrite and spine formation is completed (Giachino et al. 2005). A number of experiments confirmed that CREB controls differentiation and survival of newborn neurons in the OB: in transgenic mice lacking CREB the morphological differentiation of SVZ-derived neuroblasts was troubled and their survival rate significantly reduced (Lonze and Ginty 2002). Likewise, peripheral afferent denervation experiments, where functional connections from the olfactory epithelium to the OB were disrupted, lead to the down-regulation of pCREB and consequently apoptosis (Giachino et al. 2005).

Not only signalling pathways but also local selection criteria of neuronal apoptosis remain to be fully understood. One critical factor could be network activity. Through excitatory synaptic input of pyramidal cells during postnatal development, the number of inhibitory cells in local cortical circuits is dynamically adjusted (Wong et al. 2018). Seeing this activity-dependent mechanism that provides the final signal for appropriate proportioning of excitatory and inhibitory neurons in the cortex, might allow us to hypothesize that a similar regulation also takes place in the OB layers.

Further given spatial activation patterns during olfactory discrimination tasks, learning processes could be another parameter in adjusting survival of newborn neurons in the OB. Indeed, after a 6-days-training for olfactory discrimination, the distribution was altered and survival increased specifically in those circuits to which odors were repetitively presented (Alonso et al. 2006). The fact that learning influences survival raises the question whether *argumentum e contrario* apoptotic selection is needed for memory. The sheer observation that neural activity increases survival and therefore shapes the final distribution of newly arriving cells hints that future sensory pathways are installed at those sites that have been activated earlier on. Investigations seeking to link activity of newly generated bulbar neurons to the time course of their survival and death, compared the density of BrdU+ cells of mice housed either in an odor-enriched environment or in usual laboratory cages. In agreement with previous studies

(Rochefort et al. 2002), the stimulation resulted in a 50% increase in surviving BrdU-positive cells. However, only one month after animals were withdrawn from the enriched environment, the quantity of survived adult-born neurons was the same in the two tested groups (Rochefort and Lledo 2005). This transient increase of the number of adult-generated neurons at periods of stimulation points to the possibility that survival contributes to an adapting olfactory network.

1.5.2. The role of survival and death in correct OB functioning

Often, adult interneuron maturation is classified as a competitive process where apoptosis leads to the elimination of about half of the newly generated population, while the remaining cells can afterwards survive for periods longer than one year. Following an early peak in the number of adult-born cells, an extensive BrdU+ cell loss was demonstrated both in the rat glomerular (Kato et al. 2000) and mouse granule cell layer (Petreanu and Alvarez-Buylla 2002). Currently, most studies provide evidence for this concept suggesting that adult olfactory bulb neurogenesis utilizes the overproduction and selection of young neurons rather than simply replacing old ones. Double-labelling of the apoptotic marker TUNEL with doublecortin (expressed by migrating neuroblasts and early stage neurons) supports the idea that programmed cell death is limited to progenitor cells instead of effecting also the embryonically developed cell population. This leads to the conclusion that apoptosis puts selective pressure on immature neurons (Winner et al. 2002).
Further substantiating this assumption, new neurons exposed to either sensory deprivation or administration of diazepam, a $GABA_A$ receptor modulator, die in particularly when they are differentiating and integrating into the circuit between 14-28 days after birth (Yamaguchi and Mori 2005). Immunostaining with activated Caspase-3 and BrdU indicates that GCs at days 14-20 are most vulnerable to cell death. This time interval, when GC-survival is explicitly determined in a sensory experience-dependent manner was consequently baptized ”critical period‟. However, once neurons have survived this early crucial time frame, they seem to escape endogenous apoptosis. Interestingly, naris occlusion that deprived sensory input unilaterally, effects PGCs and GCs differently. Between 15 and 180 days post-BrdU exposure, the density of labelled cells decreases about 70%, starting earlier in the GL than in the GCL (Mandairon et al. 2006).
Up to this point, the vast majority of survival studies is to a large extent based on BrdU labelling. Making use of the integration of thymidine analogs, like 3H-dT or BrdU, into the DNA of dividing cells allows the tracing of timed cohorts. Despite all its advantages, this method also introduces cellular changes due to the presence of the incorporated molecules that are significantly different from the natural thymidine structure. The resulting impact on the normal DNA conformation can harm transcription and translation leading to mutations and cell toxicity (Breunig et al. 2007).

In particular, BrdU administration increases the cell death of aNPCs in a dose-dependent manner which could lead to misinterpretations (Lehner et al. 2011). Although the critical effects of BrdU on neural progenitor destiny urge for caution, there are currently only few alternatives available to reliably label proliferating cells. Just recently, however, a novel conclusion was drawn from aNPCs data obtained through such an alternative approach. Using modern non-invasive long-term imaging with minimal concentrations of the thymidine analogue EdU, considerable cell death was observed neither among postnatal nor for adult generated neurons during their integration phase. Surprisingly, previous homeostatic models were contradicted. Instead, it was proposed that the OB development is a non-selective addition process (Platel et al., 2018). To further verify their claim, they looked at 3D reconstructions of the OB volume between 2 and 12 months via light sheet microscopy of CUBIC-treated transparent brains which, indeed, showed a permanent growth of the structure. (Platel et al., 2018). Even-though this outcome is unexpected, it is backed up by other data such as observations in Bax-KO mice. There, apoptotic cell death is inhibited, but the general structure and layer size of the OB remains similar to control conditions (Kim et al. 2007). That the programmed cell death of adult-produced interneurones is primarily dependent on Bax, a proapoptotic member of the Bcl-2 family, was demonstrated beforehand by showing a significant reduction in the number of dying OB cells under Bax knocked out conditions (Shi et al. 2005). When apoptosis is suppressed, neuronal migration and differentiation are altered, whereas stem cells proliferation as well as olfactory functioning remained normal (Kim et al. 2007).
This hypothesis is further supported by CREB-phosphorylation studies. In wild type mice, pCREB levels are higher in the part of the RMS that is proximal to the OB, the site where tangential migration ends and neuronal differentiation starts. In the Bax-KO, however, CREB-phosphorylation looses this specific distribution and instead is ubiquitously expressed along the entire migratory route (Kim et al. 2007). Possibly, programmed cell death is thereafter part of an “early selection“ molecular program that regulates the final number of OB neurons. Accordingly, the density of apoptotic cells is much higher in the RMS compared to the rest of the OB (Biebl et al. 2000). Another interesting observation in Bax-KO mice concerns PGCs. Although ~1–5% of adult produced cells become normally TH positive in the GL, none of the ectopically positioned cells in the Bax-KO RMS exhibited a TH+ genotype, clearly demonstrating that they have a different underlying control mechanism (Kim et al. 2007).

Taken together, these results challenge the well-established doctrine that during brain development a large proportion of neural progenitors are eliminated in a competitive process for synaptic input or trophic support. Looking at adult generated OB neurons by applying modern, more physiological techniques, reveals that cell loss and turnover are more complex and further research has to be done to finally clarify the impact of activity and competition during neuronal maturation.

2. AIMS

Even if the existence of human adult neurogenesis is debated, it is necessary to understand how brain circuits can incorporate new neurons and how we can improve their delivery to regions where neuronal replacement is needed if we want to advance in the development of medical brain repair (Paredes et al. 2016). Taking the example of the adult rodent olfactory system, I have therefore decided to study in detail the regulation of interneuron migration and their integration into preexisting OB circuits.

First, I aim to discover whether the two main OB interneuron subtypes share a uniform mode of migration in the postnatal brain. Observing GCs and PGCs in the RMS as well as the in the layers of the OB, I will compare relevant parameters such as the speed of nuclear translocation, the percentage of stationary phases, straightness and the overall displacement. Possibly, this could enable researchers in the future to distinguish GCs and PGCs solemnly by their dynamism instead of having to look at genetical markers.

Interestingly, a subpopulation specific role of activity was reported for cortical interneuron migration (De Marco Garcia et al. 2011). In the past, it has been hypothesized that foremost non-cell autonomous glutamatergic signals affect migration (Platel et al. 2010). However, a recent study brings up the idea that also olfactory activity has a regulatory function on neuroblast migration in the RMS: tangential migration speed was decreased when sensory stimuli were inhibited (Pothayee et al. 2017). I want to investigate in more detail the underlining regulatory mechanisms of the migration of the two main OB interneuron subtypes. A differential reaction to intrinsic activity could be not only part of the control of migratory parameters but also influencing radial segregation of the two cell types in the OB. In my study, I want to address the questions if GCs and PGCs are differently guided and how they reach their final position. Consequently, the main bulbar interneuron subpopulations have to be followed at a single cell level with *in vivo* imaging techniques. I will characterize calcium activity during migration and compare the results after neural activity deprivation or activation. As a matter of course, I attempt additionally to identify underlying mechanisms and responsible neurotransmitters.

It is already known that the development of olfactory bulb interneurons strongly depends on activity related input as their synaptic integration and survival are challenged upon olfactory deprivation (Mandairon et al. 2003). Furthermore, past studies suggest that neural activity is also tightly linked to the control of death and survival in the OB (Rochefort et al. 2002, Yamaguchi and Mori 2005, Lin et al. 2010). In order to improve cell therapies at sites of neurological damage, it is important to understand the link between migration and survival, which is why I finally aim to clarify the role of cell death in the postnatal OB.

3. Material and Methods

Animals

All mice were treated respecting the European Communities Council Directive and in accordance with the protocols approved by the French Ethical Committee (Comité d'Ethique pour l'expérimentation animale n°14; permission number: 62-12112012). Mice were group housed in regular cages under standard conditions, with up to 5 adult mice per cage on a 12-h light–dark cycle.
Rosa-RFP mice (Ai14, Rosa26-CAG-tdTomato) were obtained from the Jackson laboratory and used on a mixed C57Bl6/CD1 background. Nestin-CreERT2 mice were obtained from Amelia Eisch and crossed with Rosa-RFP mice. CD1 (Charles-River, Lyon, France), Ai14 transgenic reporter (Jackson Laboratories, stock-number 007914), hM3Dq mice (Jackson Laboratories, stock-number 026220), GCaMP6s mice (Jackson Laboratories, stock-number 028866) were used. Mice of both genders were part of our experiments. All efforts were made to minimize the number of animals used and their suffering.

Genotyping

To define the genotype of our mice a 1-2 mm sample from their tails was taken and lysed overnight using 10mg/ml Proteinase K (Sigma) at 55°C with vigorous shaking, in DirectPCR Lysis Reagent (VIAGEN Biotech). The next morning the Protein kinase K was inactivated by heating it to 95° for 15 minutes. For a PCR reaction 1 µl of the template DNA was added to sterile water, the corresponding primers as well as to the ingredients displayed below in order to amplify some of its precise parts.

Reagent	Final volume (µl)	Final concentration
Template DNA	1	10-500ng
Sterile dH2O to 30 µl	14,5	
Go taq Buffer 5X	6	1X
MgCl2 (25 mM)	2,5	1-4mM
dNTPs MIX (10 mM)	0,6	0,2 mM each dNTPs
Primers	0.1 each	0,1-1 µM
Go taq (5u/µl)	0,2	1,25 u
TOTAL	30	

In order to genotype the different mouse lines, the corresponding primers shown below were employed:

Primers	WT forward	WT reverse	Mutant forward	Mutant reverse	Annealing Temp.
TH-EGFP			ACGTAAACGGC CACAAGTTC	GCTCCTGGACGTAG CCTTC	56°C
Ai14 Rosa Tomato	AAGGGAGCTGC AGTGGAGTA	CCGAAAATCTGT GGGAAGTC	CTGTTCCTGTAC GGCATGG	GGCATTAAAGCAG CGTATCC	58°C
hM3Dq			CGCCACCATGT ACCCATAC	GTGGTACCGTCTG GAGAGGA	67°C
GCaMP6s	AAGGGAGCTGC AGTGGAGTA	CCGAAAATCTGT GGGAAGTC	ACGAGTCGGAT CTCCCTTTG	CCGAAAATCTGTG GGAAGTC	58°C
Nestin			ATTTGCCTGCAT TACCGGTC	ATCAACGTTTTCTT TTCGG	54°C

After about two hours in the Biometra UNO II PCR DNA thermal cycler our samples were ready to be visualized using a 2% agarose gel and SYBR safe DNA staining.
Each time positive as well as negative controls were made to ensure the proper functioning of the enzymes and the purity of our samples.

DNA plasmid preparation from E.coli

Preparation of plasmid DNA was done with anion-exchange chromatography using the NucleoBond® Xtra Maxi kit (MACHEREY-NAGEL, Düren, Germany) following the manufacturers protocol. DNA quality and quantity were validated using the Nanodrop 1000 (Thermo scientific).
For electroporation DNA plasmids at a concentration of 5 µg/µl in phosphate-buffered saline were used. The pCAGGS-CRE, pCAGGS-EGFP and pCAGGS-TdTomato vectors were subcloned into pCX-mcs2, a derivative of the pCAGGS expression vector (Morin et al., 2007). The construct of the used PCX Kir 2.1 plasmid is shown in Figure 5.

Postnatal electroporation

Studying the differences of the postnatally-born olfactory interneuron subpopulations is challenging due to the lack of early molecular markers. However, it is possible to specifically target future PGCs and GCs via in vivo electroporation (cf. Fig. 6).
Therefore, we injected the left lateral ventricle of neonatal (P0-P1) pups which were first anesthetized by hypothermia. Using a method described previously (Boutin, Diestel et al. 2008) we injected 2 µl of DNA plasmid. The success of injection was verified by looking at the shape of the darker colored lateral ventricle under a strong light source. Correctly injected animals were subjected to five 95 V electrical pulses (50 ms, separated by 950 ms intervals) using the CUY21 edit device (Nepagene) and 10 mm tweezer electrodes (CUY650P10, Nepagene). To ensure high conductibility, we coated the electrodes with gel (Control Graphique Medical). The electrodes were oriented according to the desired

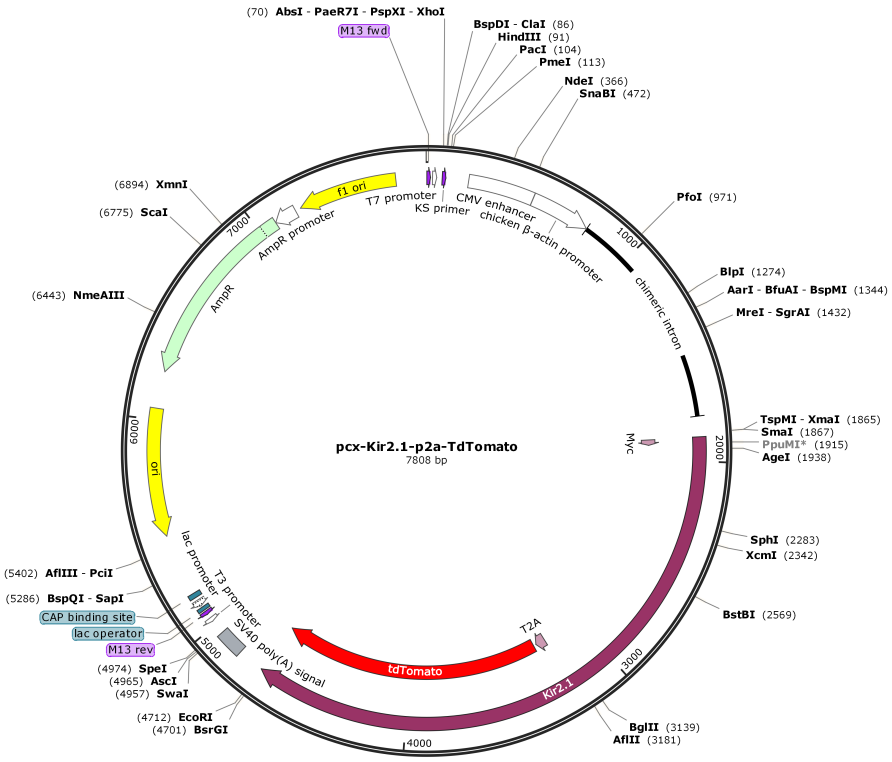

Figure 5: ***Plasmid card of PCX Kir 2.1-p2a-TdTomato***
This Ampiliciline- sensitive plasmid has an overall size of 7808 base pairs (bp). The Kir 2.1 part codes for an inward rectifying potassium channel which allows the hyperpolarization of neuroblasts. To see if cells recombined the plasmid, a tdTomato fluorescence reporter gene was incorporated into to construct.
The image was generated with SnapGene by Stéphane Burgeon.

targeting. Reanimation took place in an 37°C-incubator. Fully recovered pups were finally reunited with their mother. DNA plasmids were directly injected into the lateral ventricle of newborn or one day old mice.

Nucleic acids are charged negatively. That is why they follow the anode to cathode current gradient which leads them to cells lining the ventricle on the positively charged side. By placing the electrodes accordingly, different cell populations can be targeted (de Chevigny, Core et al. 2012). Applying this technique, Stéphane Burgeon quantified in 2017 the cell proportion in different OB layers three weeks after lateral, dorsal and medial electroporation of a pCAGGS-EGFP plasmid. The time-point was chosen because green fluorescent protein (GFP) labeled cells stop migrating by then, having reached their final position. Burgeon demonstrated that dorsal electroporation targets a mixed population, consisting of ~70% GCs and ~30% PGCs while electroporating laterally generates ~80% GCs and medially almost 80% of peripheral PGCs. Thanks to this method it is now possible to label future GCs and PGCs with a relatively high purity at the stem cell level.

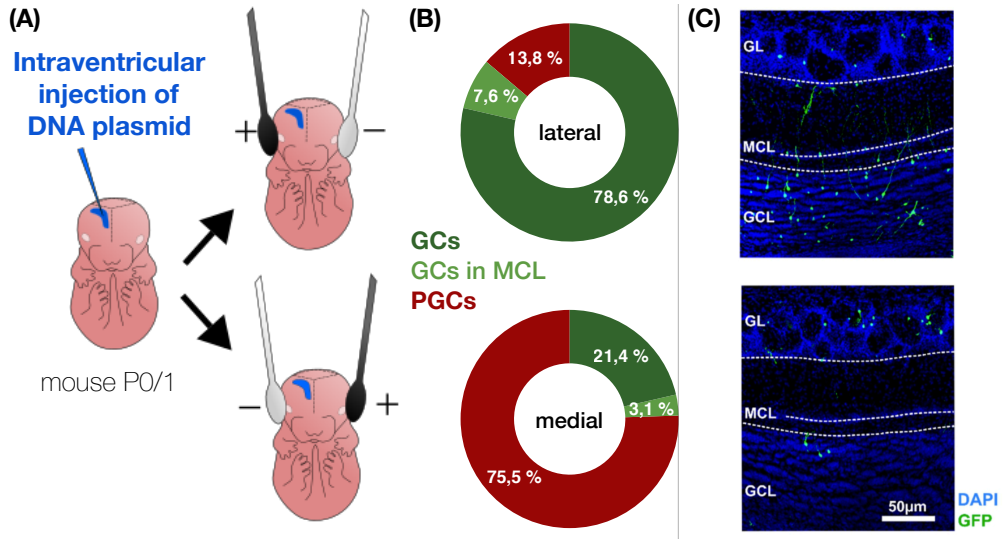

Figure 6: ***OB populations specifically labelled by postnatal electroporation***
(A) Illustration of in vivo electroporation: P0-P1 mice are first anesthetized by hypothermia, then a DNA plasmid is injected into the ventricle (blue area represents the target region). Applying pulses with electrodes (depicted as +/- sign) the cells lining the ventricle are forced to open their membrane to let the negatively charged DNA enter. The orientation of electrodes (lateral = positive electrode on the lateral ventricle side; medial = positive electrode on the medial ventricle side) is determining for the result. (B) Quantification of the mean percentage of GFP+ cells in each OB layer after lateral and medial electroporation. The majority of cells generated by lateral stem cells have migrated to the GCL while most cells produced by medial stem cells are located in the GL. Granule cells in the MCL were separately counted. Lateral: GCs-78.6±1.0%; GCs in MCL-7.77±0.3%; PGCs-13,8±0,8%. Medial: GCs-21.4±3.8%; GCs in MCL-3.1±0.8%; PGCs-75.5±3.9%. N = 12 coronal slices from 4 animals. (C) Coronal sections of OB after lateral or medial electroporation at P1 with a GFP encoding plasmid. At 21 dpe, mice were sacrificed to look at the repartition of green fluorescent cells in the different layers. DAPI stains cell nuclei. Scale bar: 50 µm

Immunohistochemistry and image analysis

To gain access to the histological cell information we analyzed fixed brain slices. Therefore, mice were deeply xylazine/ketamine anesthetized and perfusion was performed intracardiacally 4% paraformaldehyde (Electron Microscopy Sciences; Hatfield, PA, USA) in PBS. The brain was dissected out and incubated 24 hours at 4°C in the 4% PFA in PBS. With a microtome (Microm) brains were sliced into 50 µm thick sections. Sections were incubated overnight at 4°C with one of the following primary antibodies: rabbit anti-EGFP (1:500; Life Technologies), rabbit anti-cFos (1:5000; Millipore), mouse anti-Cre recombinase (1:4000; Millipore), chicken anti-caspase (1:1000; Abcam) or rabbit anti-pCREB (1:500; Cell Signaling) and then washed 3x in PBS before the second incubation for 2h at 20°C with the corresponding fluorescent labelled secondary antibody. Nuclei were stained with Hoechst or TOPRO3 (1:1000) before mounting. Imaging was performed with a fluorescence microscope (Axioplan2, ApoTome system, Zeiss, Germany) or a laser confocal scanning microscope (LSM510 or LSM780, Zeiss, Germany). The cytoplasmic fluorescence intensity was detected using ImageJ software on z-stack images.

In vivo slices

One week after electroporation, P7-8 animals were anesthetized with ketamine/xylazine. We then pumped cold (4°C), oxygenated (95% O2 / 5% CO2) dissection solution (250mM Sucrose, 3 mM KCl, 1.25 mM NaH_2PO_4, 3 mM $MgSO_4$, 10 mM D-Glucose, 26 mM $NaHCO_3$ and 0.5 mM $CaCl_2$) into the left chamber of their heart to cool their brain and keep neurons alive while removing all blood from the interior of the cranium. Next, we quickly removed the brain and glued it on a vibratome platform to cut it in 300 µm thick sagittal slices. Sections were made with a Leica VT1200S vibratome in 4°C-cold, oxygenated (95% O_2 / 5% CO_2) dissection solution. Afterwards we stored them in oxygenated DMEM, high glucose, GlutaMAX (Gibco) (124mM NaCl, 3mM KCl, 1.25 mM NaH_2PO_4, 1.3 mM $MgSO_4$, 10mM D-Glucose, 26 mM $NaHCO_3$ and 2mM $CaCl_2$) at room temperature for at least 30 minutes prior to imaging.

Two-photon time-lapse imaging and image processing

To image the acute brain slices we placed them under the 20X objective (1,0 NA) of a two-photon ZEISS 7MP microscope equipped with a Mai-Tai laser (ONE BOX TI:SAPPHIRE LASERS, Spectra-Physics). To obtain a physiological environment we installed a flow-through warming chamber (Warner instruments, Open Diamond Bath Imaging Chambers, RC-26G) perfused (Compact Peristaltic Pump, Harvard Apparatus; ~1 ml/min) with the appropriate recording solution which was ventilated with 95% O2/5% CO2 using a dual automatic temperature controller with an in-line heater (Warner Instruments). Aiming to prevent movement while recording we positioned the slice under a special mesh (Warner instruments, SHD-26GH/10).

Recording radial migration, we took z-stacks (step size: 3µm) every 5 minutes and for tangential migration every 2 minutes. Each picture had a size of 1024x1024 pixels with an 0.53µm axial resolution. Later on, the Z-stack maximum projection of every time point was taken, and registered to avoid horizontal drifting. For this, we employed the StackReg plugin function of the ImageJ software. To register the Ca^{2+} activity we recorded the same plane one-second long for at least two minutes. Again, movies were edited with the StackReg plugin. For the reason that the cutting process leaves traces on the superficial part of the slices we started the acquisition at a depth of at least 50µm.

Approaches to manipulate the membrane potential

During the last years many revolutionary techniques have been developed to address activity related questions very precisely with and without pharmacology (Fig. 7). Concretely, through the introduction of chemogenetic approaches, neuroscientists gained strong tools to enhance or inhibit neuronal activity in a cell type–specific and noninvasive manner.

Generally, the chemogenetical idea is based on engineering macromolecules such as G protein–coupled receptor in a way that they start to interact with small molecules

that they previously did not recognize (Urban and Roth 2015). Consequently, they are activated exclusively upon addition of their specific ligand resulting in the great advantage of a high temporal resolution. This raises hope that not only effects of activity modifications, but also underlining fundamental signaling pathways can be discovered (Bradley et al. 2018).

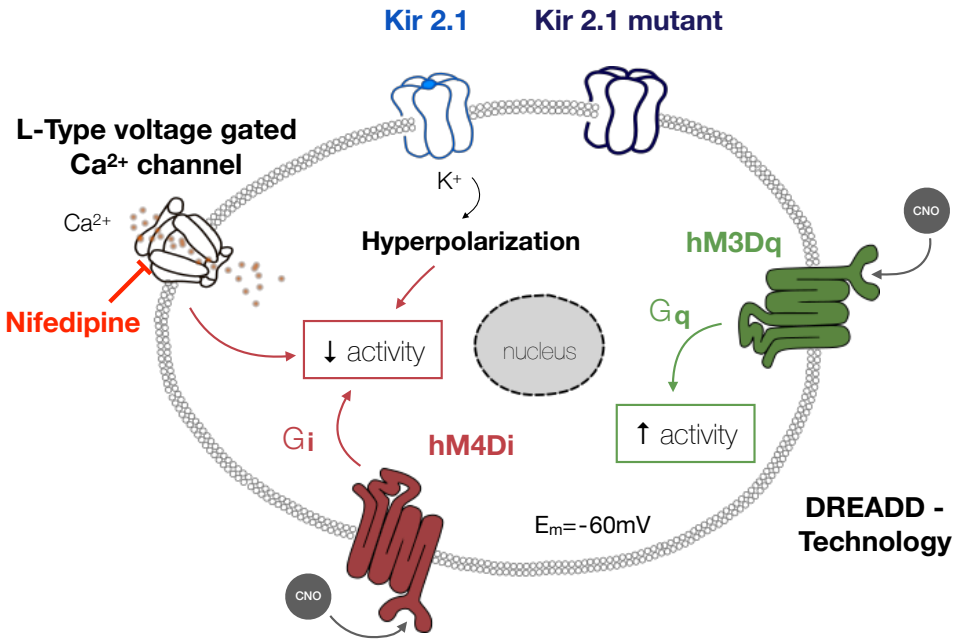

Figure 7: ***Tools to modify activity in olfactory NPCs***
In this schematic representation selected modulators of the intracellular voltage are shown. *1) pharmaceutical approach:* L-type voltage gated channels generate Ca^{2+} transients in OB interneuron precursors. These channels can be blocked specifically upon Nifedipine-addition. *2) genetic tools:* The DREADD-technology (Designer receptor exclusively activated by a designer drug) uses engineered human muscarinic receptors that respond exclusively to the synthetic ligand clozapine *N*-oxide (CNO). The pattern of signaling evoked by the CNO-hM3Dq chemogenetic platform efficiently mimics the effect of native M3 receptors activated by acetylcholine and, thus, allows *in vivo* investigations of the role that depolarization plays in migrating cells. Over-expression of hM4Di induces not only hyperpolarization, but also silences spontaneous and depolarization-evoked firing. Another possibility to decrease cellular activity is to electroporate the Kir 2.1- plasmid. The over-expression of this inward rectifying potassium channel reduces the membrane potential by inducing potassium efflux. The silent Kir 2.1 mutant channel can be used as control. E_m, resting membrane potential

The so-called “designer receptor exclusively activated by a designer drug” (DREADD) for instance is solely stimulated by the clozapine analog clozapine-N-oxide (CNO), a synthetic ligand possessing almost no biologic activity. Using the human M3 muscarinic cholinergic G_q-coupled receptor (hM3Dq) as base for DREADDs, CNO-addition allows *in vivo* investigations of the role that depolarization plays in migrating cells (see also: methods and materials “Pharmacology”). In past studies, where hM3Dq was expressed in glutamatergic projection neurons, the intrinsic excitability was increased which resulted in a higher frequency of spontaneous Ca^{2+} transients. Additionally, it induced premature branching of the leading process and prolonged the pausing time without directly modifying the instant migratory speed. Ergo, laminar positioning of projection neurons in deep cortical layers was affected, too (Hurni et al. 2017).

To fully understand the role of neuronal activity in regulating migration, it is necessary to look as well at effects of hyperpolarization. Over-expressing the mutant form of a non-rectifying Kir 2.1 potassium channel leads to a leak current and subsequently decreases the resting membrane potential. Since the required synaptic input for reaching the firing threshold is then higher, neuronal spiking becomes less likely (Lin et al. 2010). This construct has already been tested in cortical interneurons where migration was then greatly disturbed. Noticeably, only the development of Reelin+ and CalR+ but not of Vasointestinal Peptide+ neurons was impacted. When Kir 2.1 expression was turned off by Doxycycline addition before P5, the total length and complexity of Reelin+ interneuron axonal arbors did not change compared to physiological controls, maybe suggesting that genetic programs coming from the progenitor stage are modified according to later activity levels (De Marco Garcia et al. 2011).
Hyperpolarization *in vitro* and *in vivo* can be also achieved via the DREADD approach. In hippocampal neurons, the designer receptor hM4Di is known to induce neuronal silencing by activation of $G_{i/o}$ coupled receptors (Armbruster et al. 2007).
In another context, a chemogenetic cFos-based approach allowed the hM3Dq DREADD receptor to be expressed exclusively in neurons that were activated previously by an environmental stimulus (Garner et al. 2012). Taking advantage of the re-activation of only this type of neurons through CNO, elements that were part of an artificially induced neural network could be exclusively labeled. This underlines once more the great potential of chemogenetic tools to remotely control neuronal signaling *in vivo* which will facilitate investigations aiming to understand the role of defined neuronal populations in numerous physiological and pathological processes.

Pharmacology

To block specific receptors we applied different antagonists in the DMEM solution during the imaging procedure at the following concentration: D-APV (Tocris Bioscience, 50µM), NBQX (Tocris Bioscience, 10µM), MPEP (Tocris Bioscience, 30µM), Bicuculline (Tocris Bioscience, 10µM), Strychnine (Tocris Bioscience, 20µM), Dolasetron mesylate (Tocris Bioscience, 10µM), CNQX (Tocris Bioscience, 20µM), Scopolamine (Tocris Bioscience, 10µM). To specifically block L-Type Ca^{2+} channels, we added Nifedipine (Tocris Bioscience 10µM) to the recording solution while two-photon time lapse imaging after a 2h-control recording. For activation of the DREADD technology (Designer Receptors Exclusively Activated by Designer Drugs), which allows the controlled depolarization of cells, Clozapine-N-Oxide (CNO, Tocris Bioscience, Cat. No. 4936) was used and dissolved in Dimethylsulfoxyde (DMSO). *In vitro* experiments of the muscarinergic receptor 3 DREADD showed that upon CNO-addition, the engineered receptor was able to stimulate G protein-mediated singling pathways like phosphorylation of ERK1/2,

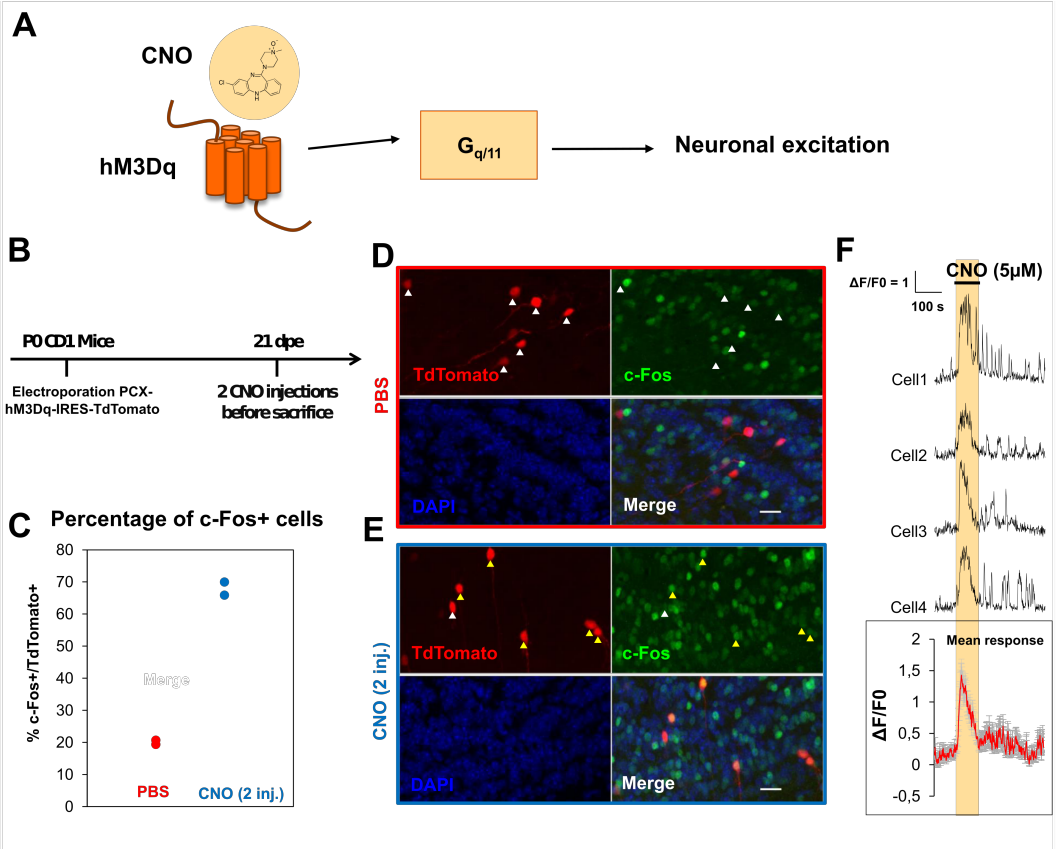

Figure 8: ***Validation of hM3Dq DREADD activator in OB interneurons***
(A) The DREADD receptor hM3Dq is specifically activated by Clozapine-N-Oxide (CNO). Upon binding, the activation of the Gq subunit will lead to depolarization and neuronal excitation. (B) Experimental setup for in vivo validation of hM3Dq. P0 mice were electroporated with hM3Dq and TdTomato. At 21 dpe, mice received two intraperitoneal injections of CNO or PBS. (C,D,E) Brain slices were then immunostained for cFos and the percentage of cFos positive cells among TdTomato was assessed. CNO injected animals had 70% of TdTomato cells that were also positive for cFos, while only 20% TdTomato co-expressed the immediate early gene in the control condition. Yellow arrowheads indicate cFos+/TdTomato+ cells and white arrowheads indicate cFos-/TdTomato cells. (N = 2 animals). (F) Acute brain slices from 7 dpe hM3Dq/ GcAMP6s animals electroporated with a Cre plasmid were recorded for calcium transients. Cells located in the GCL were recorded for 2 minutes in control solution. CNO was then bath applied inducing a large calcium entry in the cells showing efficient neuronal excitation of hM3Dq expressing cells.

inositol phosphate accumulation and calcium release (Armbruster et al. 2007). The efficiency of CNO-induced depolarization in electroporated cells in hM3Dq mice was previously assessed in our laboratory by Stéphane Burgeon both *in vivo* and *ex-vivo* (Fig. 8). First, he compared the number of cFos+ cells among TdTomato+ cells between hM3Dq electroporated animals that received two intraperitoneal injections per day of either CNO (1 mg/kg, 0,1% DMSO) or PBS (0,1% DMSO). The expression of the immediate early gene cFos was largely increased after CNO application which shows that it is sufficient to activate cells. Secondly, hMD3q/GCaMP6s animals were electroporated with a Cre plasmid and acute brain slices prepared 7 dpe. Then CNO was bath-applied at a concentration of 5µM to record calcium fluctuations of electroporated cells. The increased amplitude of calcium activity upon CNO addition proved again that CNO efficiently induced depolarization in migrating interneurones

Cell tracking and migration analysis

Using the Imaris software (Bitplane), every single cell was tracked manually to save their position at each time point in an Excel table. Non-migrating cells as well as those who moved back from the GCL to the RMS were not taken into account. During the next step, the gathered information of all cells considered was evaluated in R.

Saltatory migration was measured by instantaneous speed at time t by dividing the distance between the positions at t-1 and t+1 by two time intervals. Only cells moving with a speed higher than 20 µm/h (which correlates with a displacement of 1.3 µm for a 5 minutes time interval) were defined migrating. We introduced this threshold to circumvent the influence of artificial movement caused by shifting. Applying this fringe, the detection of unwanted noisy movement was successfully excluded. The obtained speed vector, allowed us to distinguish at the same time between active migration (Fig. 9; m, orange) phases and time intervals of relative immobility which we treated as stationary phases (Fig. 9; s, grey). Consequently, the following parameters could be to calculated:

- **Mean speed of nuclear translocations [µm/h]**
  mean of all speed above 20 µm/h (cf. Fig. 9 only ■)

- **Displacement per hour [µm/h]**
  mean of all speeds (cf. Fig. 9 ■ and ●)
  = total distance covered during the recording / time required to travel this distance

- **Percentage of stationary phases [%]**
  percentage of time points with a speed less than 20 µm/h
  $= \sum s_{1\text{-}n} / (\sum s_{1\text{-}n} + \sum m_{1\text{-}n})$

- **Straightness**
  directness of migratory behavior
  = straight vector between last and first time point / cumulative distance traveled

Note: Exclusively the data in-between the first and last migratory phase was taken into account. Furthermore, cells which migrated only once were not regarded when calculating the percentage of stationary phases.

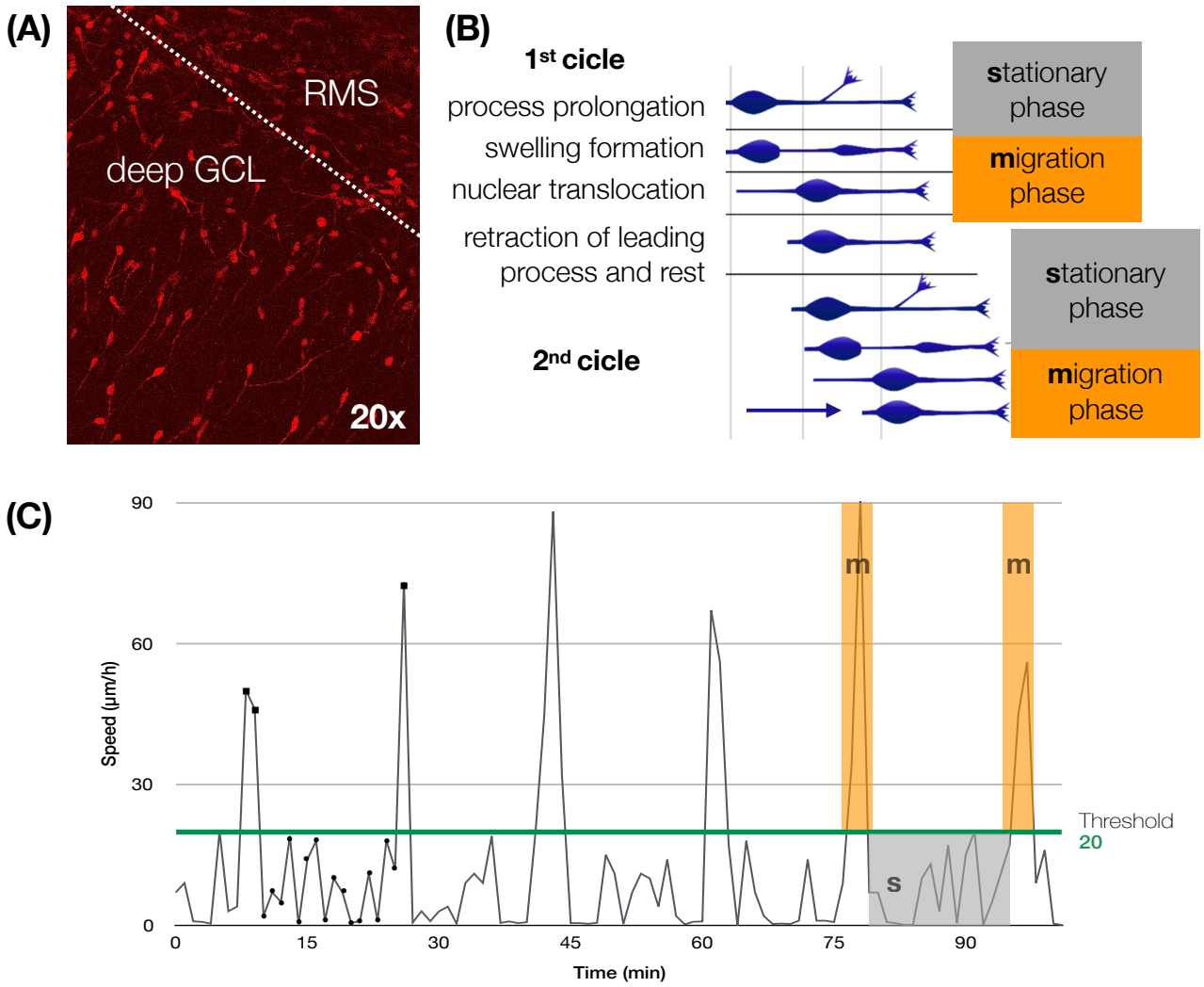

Figure 9: ***Quantifying the migration of olfactory interneurone progenitors***
(A) Image taken from a time lapse recording of TdTomato expressing neuroblasts in the granule cell layer (GCL) and rostral migratory stream (RMS) on acute brain slices at 7 days post Cre-electroporation. (B) Schematic overview of saltatory migration. During the active migration phase, neurones first extend their leading process. There, a swelling formation appears before the nucleus is finally dislocated. Afterwards, the leading process is retracted and the overall migration stops for a certain time. This alternation of "jumps" and pauses is characteristic for saltatory migration. (C) v(t)-diagram for the displacement of one single neurone. The threshold of 20µm/h separating migratory from stationary phases is represented as a green line.

Calcium imaging analysis

To facilitate in vivo activity studies and for monitoring neural activity, genetically encoding calcium indicators, such as the green fluorescent protein (GFP)-based G-CaMPs, have been developed to make Ca^{2+} fluctuations visible in the cytoplasm. As the abbreviation implies GCaMP6 was created by attaching a circularly permuted variant of enhanced green fluorescent protein to a CaM-binding M13 peptide (from myosin light chain) at the N-terminus as well as the calcium-binding protein calmodulin (CaM) at the C terminus (Nakai et al. 2001). When calcium is present, the protein undergoes a conformational change which results in a bright fluorescent signal (Sato et al. 2015). A wide range of neural activity can be reported since each G-CaMP variant shows own sensitivities, kinetics and signal-to-noise ratios (Akerboom et al. 2012). In order to observe Ca^{2+} fluctuation in the cell cytoplasm mice that were transgenic for the calcium indicator GCaMP6s were used. The GCaMP6s mice were bred with Ai14 TdTomato mice for the reason that the additional TdTomato

fluorescence highlighted cell contours and therefore increased accuracy during the imaging and quantification process. Removal of a stop sequence and expression of Ai14 and GCaMP6s was accomplished by either lateral or medial Cre electroporation. Seven days after electroporation the animals were sacrificed to obtain acute brain slices on which neurons were recorded during their tangential or radial migration. Making time-lapse recordings and averaging them over time allowed us to identify relative clear cell borders. With this orientation the image could be segmented and a binary mask created that was then treated with the “Analyse Particles” function in ImageJ. Next, the ROIs (Region Of Interest) calculated by the program were manually corrected to subtract duplicates or systematic errors. In the following step, the mean green fluorescence intensity of for every individual ROI was measured over time and stored as a text file. Using a Matlab interface, that has been programmed especially for this purpose by Jean-Claude Platel, the files were imported, filtered and normalized by intensities. All Ca^{2+} transients over the fixed threshold of 25% dF/F0 were automatically detected by the software. A Ca^{2+} transient was declared as over when at least 4 time points showed a consecutive decrease in amplitude. To prevent systematic software mistakes, we verified each peak manually. Finally, both the frequency and the mean amplitude of each cell’s calcium transient were determined and saved.

Statistical analyses

All statistical analyses were achieved with the software „R“ and the R Commander Package (https://CRAN.R-project.org/package=Rcmdr). The normality (Shapiro-Wilk Normality Test) and equality of variances (Levene’s Test for Homogeneity of Variance) were tested before we statistically analyzed our data. Depending on the outcome the following statistical test to access the mean difference were applied:

number of compared groups	normally distributed and/or unequal variances	not-normally distributed and homoscedastic
2	**Student two-sample t-test**	**non-parametrical Wilcoxon rank sum Test**
>2	**ANOVA**	**non- parametrical Kruskal-Wallis Test**

Data is presented as mean±SEM.

probability	assignment
> 0.05	not significant, ns
0.01< p < 0.05	*
0.001< p < 0.01	**
< 0.001	***

4. RESULTS

4.1. Comparing the migratory behavior of future PGCs and GCs

Until recently, the vast majority of migratory studies did not differentiate between the main OB interneuron subtypes lacking early molecular markers for labelling them specifically. However, thanks to new approaches like electroporation, the two interneuron populations can now be successively identified and therefore separately studied. We use this technique in order to characterize the tangential and radial migratory behavior of the two populations by two-photon time-lapse imaging. Briefly, this method consists in injecting a DNA plasmid coding for the gene of interest directly into the lateral ventricle of P0-P1 mice. The injection is then followed by the electroporation per se: application of 5 electrical pulses at 95 V on the animal's head (Fig. 6A). Given the anionic properties of nucleic acids, the molecules will enter the cells which line the ventricle and face the negative electrode, following the anode to cathode current gradient. Through the different positioning of the electrodes' orientation during the procedure, it is possible to transfect neural stem cells of three specific V-SVZ subdomains: targeting either the lateral, the dorsal or the medial wall of the lateral ventricle (Boutin et al. 2008, de Chevigny et al. 2012). Since neural stem cell population with different identity are regionalized, the neuronal populations generated from the different electroporated compartments result in labelling a defined composition of subtypes (Fig. 6B) which allows subsequently, the comparison of OB interneurons before their integration. Thus, we use lateral electroporation as a model for GCs neurogenesis and medial electroporation respectively for PGCs, comparing their migratory behavior first during tangential and later during radial migration.

4.1.1. Future PGCs and GCs share a uniform tangential migration mode

To characterize the migration of GCs and PGCs in the postnatal OB, we started by investigating whether the two main OB interneuron subtypes act differently on their way through the RMS.

To visualize their displacement, we electroporated Ai14 (Rosa-TdTomato reporter) animals either laterally or medially with a Cre plasmid driven by a CAG promoter. Five days post electroporation (dpe) we sacrificed the animals, making acute brain slices to launch a time-lapse recording via two-photon microscopy (Fig. 10A,B). The obtained speed profile of migrating cells (Fig. 10C,D) shows clearly that both populations alternate between short stationary phases and fast nuclear translocations, a typical so called "saltatory migration".

By quantifying the characteristic parameters of this saltatory migration, we found that the speed of nuclear translocations, representing the active phase of migration, was on average 75 µm/h (Fig. 1E). In 30% of the recorded time, cells stayed relatively immobile, meaning that they moved slower than the set threshold of 20µm/h (Fig.

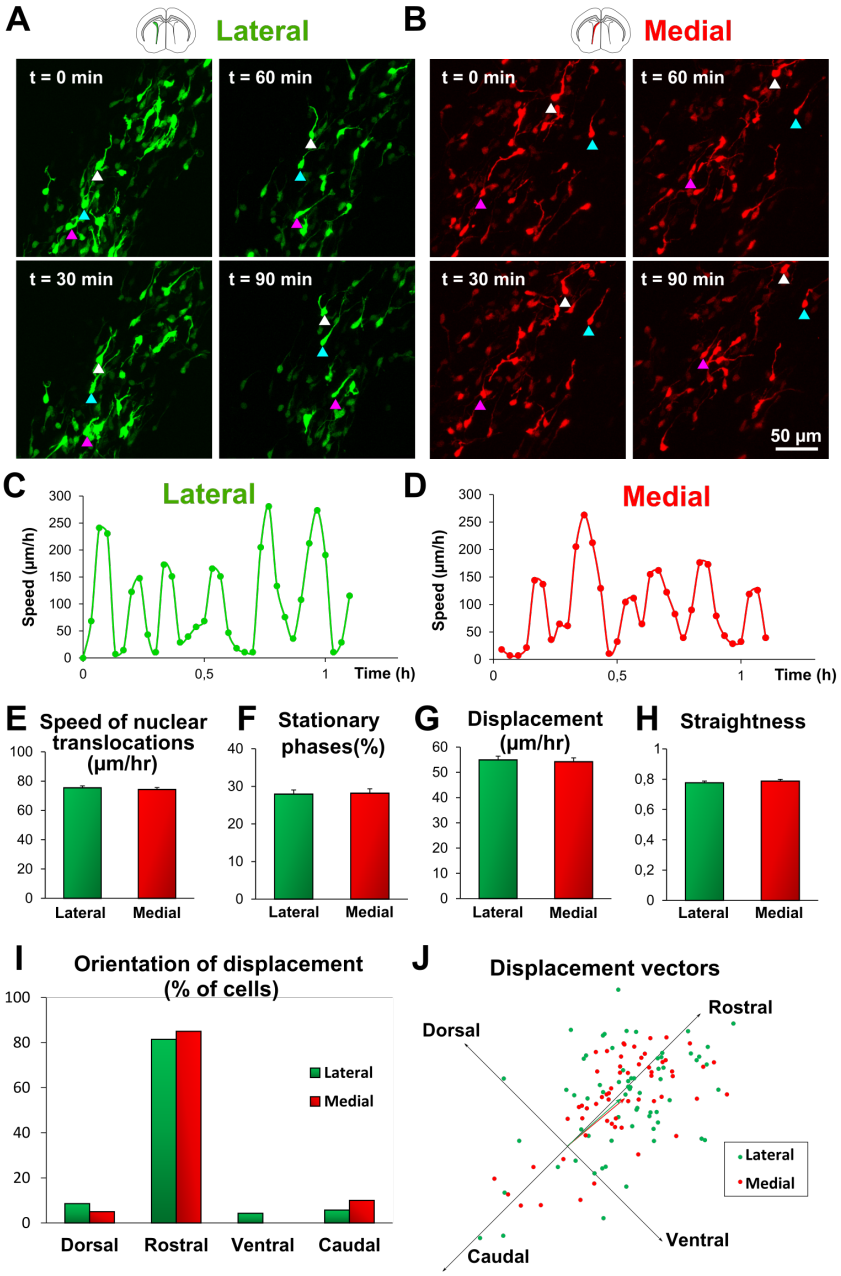

Figure 10: ***Comparison of medial and lateral originating cells during tangential migration***

Ai14 P0 animals received lateral or medial electroporation of a Cre encoding plasmid. The dynamic migration parameters of TdTomato expressing neuroblasts in the RMS were then assessed on acute brain slices at 7 dpe. (A,B) Snapshots of time-lapse two-photon imaging of lateral and medial cells respectively. For each panel, arrowheads indicate individual cells followed over time. Time is indicated in minutes. Scale bar: 50 µm. (C,D) Example of instantaneous speed recorded during a 1 hour movie for a lateral (C) and a medial (D) cell. Speed peaks correspond to "jumps", characteristic of the saltatory migration in the RMS. (E-H) Mean speed of nuclear translocations, percentage of stationary phases, displacement per hour and straightness for tangentially migrating lateral and medial cells. N = 232 cells on 3 slices. Error bars are SEM. (I) The trajectory of cells migrating in the RMS was categorized as rostral, caudal, dorsal and ventral oriented. N = 60 cells. (J) Representation of the displacement vectors of lateral (green dots) and medial (red dots) migrating cells. Vector direction is defined by the mean orientation of migration and vector length by the net distance covered. Most of cells migrate towards the rostral part of the RMS. N = 60 cells. (Adapted by Bugeon, 2017, p.46)

10F). Both, the percentage of stationary phases and speed of nuclear translocations were the same in the two migrating populations (Fig. 10E,F). Consequently, the ratio between the total distance travelled during imaging and the time needed for this route was as well similar (Fig. 10G).

To find out whether these cells employ a wide-range exploratory or a more direct migratory behavior, we divided the distance separating the first and last time points and the cumulated distance covered by migrating neurons. The resulting ratio characterizes migratory straightness - a parameter that varies between 0 and 1 and gives an idea of how efficient the trajectories are. In both conditions, the mean straightness was 0.8, corresponding to a highly efficient migration (Fig. 10H). Only few cells showed an exploratory behavior (straightness < 0.4). When we examined the orientation of these straight trajectories, we saw that the majority of them was oriented towards the rostral part of the brain i.e. the olfactory bulb. More than 80% of the future PGCs and GCs migrated in a caudal to rostral direction (Fig. 5I,J). In line with previous publications, we also observed some neuroblasts migrating towards the caudal part of the brain. However, the percentage of cells displaying this backward polarity was similar between conditions.

Overall, those results demonstrate that the kinetic parameters were broadly similar between the two cell populations in the RMS which makes it impossible to predict at this point their neuronal fate according to their movements.

4.1.2. Migratory parameters in the deep GCL are similar for the two populations

In comparison to tangential migration, radial migration has been poorly described. To better understand this process, we employed two-photon time-lapse imaging after media or lateral electroporation. To investigate radial migration, we made acute brain slices at 7 dpe, when most of the cells leave the RMS. Knowing that saltatory migration in the GCL is less fast, we prolonged the recording time to 3hrs. Our recordings confirmed that cells migrate radially with a lower speed of nuclear translocation and longer stationary phases compared to tangential migration.
In a 5hrs-time-lapse, we first quantified the percentage of cells migrating (Fig. 11A,B). Within the lateral cell population, over 60% of the cells located in the deep part of the GCL were moving during the recording period (Fig. 11C). Applying the same quantification for medial cells, the percentage was even higher: 80% (Fig. 11C). When we took only cells located in the superficial part of the GCL into account, this difference was further enhanced. There, less than 30% of lateral cells and still around 80% of medial cells were migrating during the recordings (Fig. 11D).
These significant differences fit into the existing model, because future GCs have to end migration in the GCL while future PGCs continue until they reach the GL.

Kinetic and trajectory parameters were quantified as previously to compare the two populations also in the deep GCL. Therefore, we took only those cells into account that were migrating during our recording.
In total, speed was twice as low for radial migration in contrast to tangential migration. Despite of that, our results were similar: revealing once more no significant variation between the lateral and medial population in regard of mean displacement, straightness, speed of nuclear translocation and percentage of stationary phases (Fig. 11E-H).

Taken together, these findings suggest that PGCs and GCs display similar parameters during radial migration. But still in our recording conditions, it seems that lateral cells abruptly stop their migration.
Nevertheless, it should be mentioned that our recording time was limited (<12hrs), which makes it possible that we missed a progressive, very slow increase in the percentage of stationary phases in lateral cells before their integration.
Combining the results for radial and tangential migration, we conclude that the two populations share a very similar migration mode from the SVZ all the way to the GCL and can be therefore only distinguished by their final arrest and not by their migration behavior.

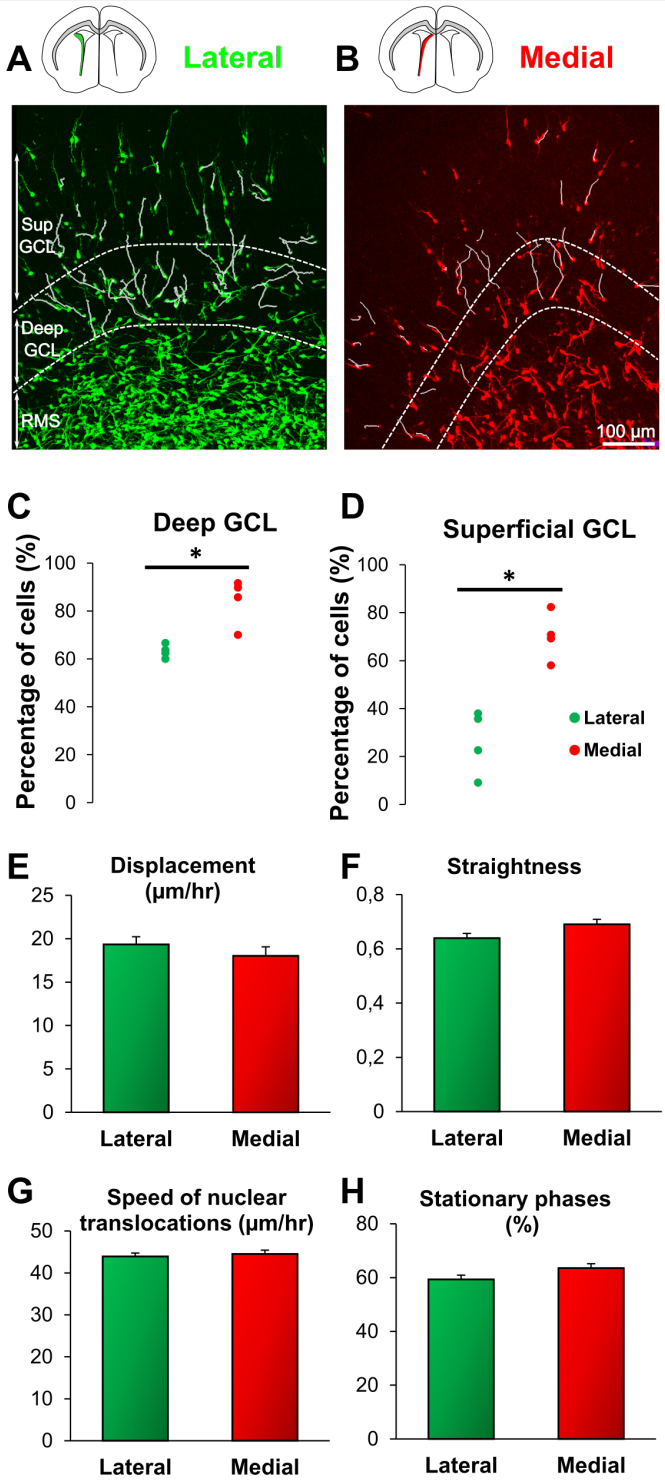

Figure 11: ***Migratory pattern comparison of medial and lateral originating cells during radial migration***

Ai14 P0 animals received lateral or medial electroporation of a Cre encoding plasmid. The parameters of radial migration of TdTomato expressing neuroblasts in the GCL were then assessed on acute brain slices at 7 dpe. (A,B) Example tracks (white lines) of radially migrating cells after lateral and medial electroporation. Dotted lines separate the RMS, deep GCL and superficial GCL. Scale bar: 100 µm. (C,D) Percentage of cells migrating in the deep (C) and superficial (D) GCL during a 5 hours recording period. Cells with at least one period of active migration were considered. Each dot represents a slice. N = 4 slices, $p<0.05$; Wilcoxon rank sum test for means. (E-H) Mean speed of nuclear translocations, percentage of stationary phases, displacement per hour and straightness for tangentially migrating lateral and medial cells.
N = 138 cells on 4 slices. Error bars are SEM. (Adapted by Bugeon, 2017, p.48)

4.2. Linking Ca^{2+} activity and OB interneuron migration

Taking into consideration that specific neuronal subtypes during the formation of the cortical network require different activity pattern to successfully integrate (De Marco Garcia et al. 2011), we hypothesize that PGCs and GCs have an individual migration-activity-pattern. To address this question, we compared first the spontaneous Ca^{2+} activity of both populations in the RMS as well as in the GCL and investigated later the underlining mechanisms.

4.2.1. The spontaneous Ca^{2+} activity of interneuronal subtypes is the same in the RMS, but differs upon GCL entry

As our previous results had revealed that medial and lateral cells share a uniform mode of migration, we hypothesized that their final layer positioning could dependent on external cues. In order to identify the role that neuronal activity plays during the segregation phase of radial migration, we have chosen to perform Ca^{2+} imaging for each population. Therefore, we used a genetically encoded Ca^{2+} sensitive probe called GCaMP6s which allows to see Ca^{2+} fluctuations with a high spatial resolution in the cytoplasm and cell processes. GCaMP6s/TdTomato mice were either laterally or medially electroporated with a Cre plasmid. To record intracellular calcium fluctuations in the RMS elbow and in the deep GCL (Fig. 12A), we made acute slices at 7 dpe. TdTomato allowed us to determine stable cell contours which is important to facilitate imaging and quantification.

To characterize the spontaneous Ca^{2+} transients of tangentially migrating neurons, we measured amplitude and frequency of Ca^{2+} fluctuations in the cytoplasm. Calcium transients have a typical rapid elevation of fluorescence followed by a slow decrease (Fig. 12B-E). When comparing activity between lateral and medial cells, we saw that about one-third of both populations showed at least one detectable transient during the 2 minute recording in the RMS. However, there was a significant increase only in the lateral population in regard of the active cell percentage as soon as they had entered the deep GCL. While only 30% of lateral cells showed detectable calcium transients in the RMS, more than 60% of them were active during radial migration (Fig. 12G). Amplitude and frequency of calcium transients were similar for the two populations in the RMS (30% dF/F0 and 0.015 Hz) (Fig. 12H,I). After the switch from tangential to radial migration though, lateral cells (60% dF/F0 and 0.03 Hz) were much more active, showing a doubled frequency and amplitude in comparison to the medial population in the GCL (40% dF/F0 and 0.018 Hz).

Interestingly, there was no significant increase for medial cells after RMS exit: neither in the percentage of active cells nor in their frequency of Ca^{2+} transients (Fig. 12H,G). To summarize, we detected a significant rise of Ca^{2+} activity in the deep GCL exclusively for future GCs. This suggests that only the lateral and not the medial cell population receives a signal after RMS exit.

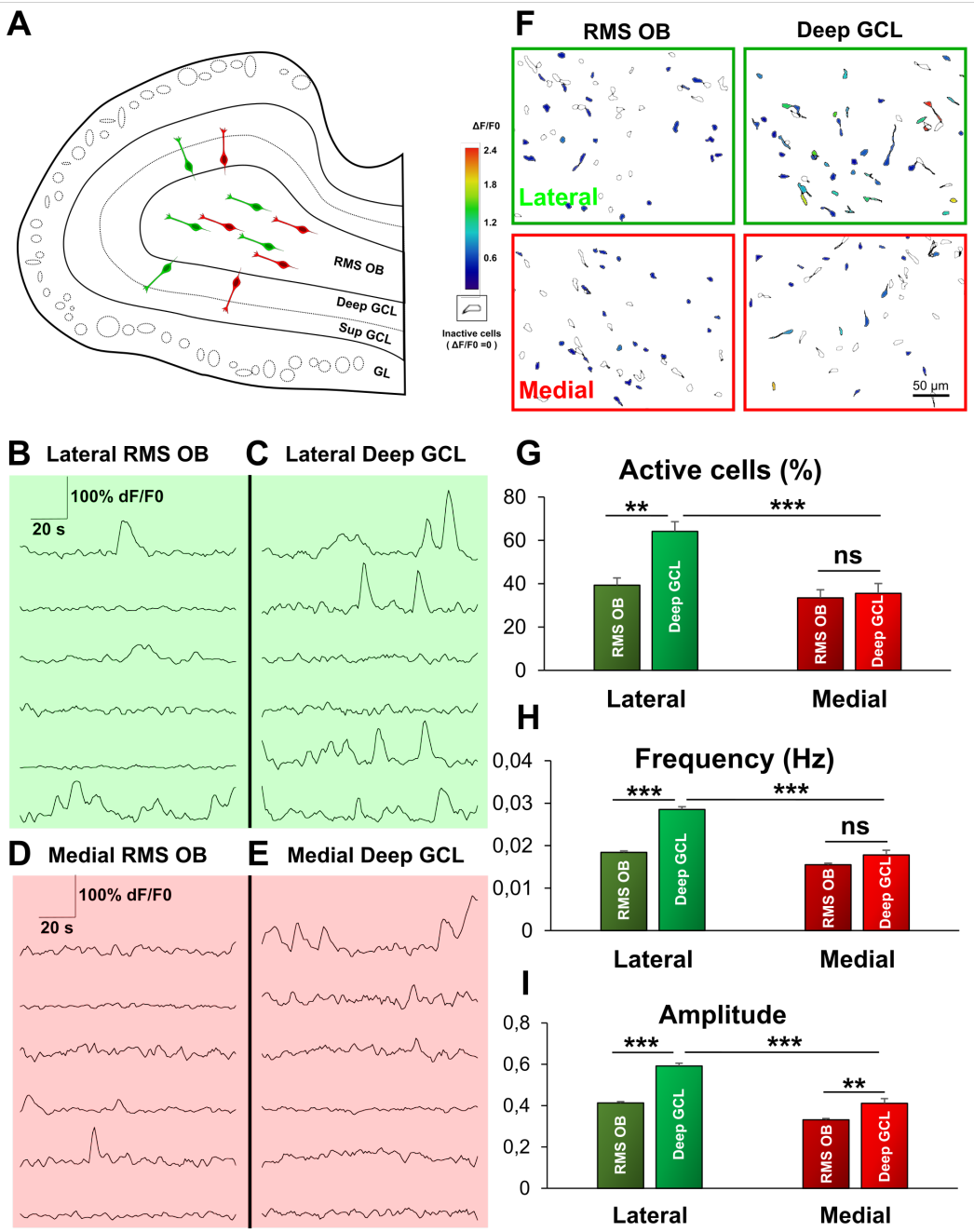

Figure 12: ***Calcium fluctuations in lateral and medial neuroblasts in the RMS OB and deep GCL***

Ai14/GCaMP6s P0 animals received lateral or medial Cre electroporation. Calcium activity was recorded on acute brain slices at 7 dpe. TdTomato fluorescence was used to ensure absence of drifting and to delineate the cells. (A) Schematic representation of an OB sagittal slice. Red and green cells represent medial and lateral cells migrating in the RMS OB or in the deep GCL. (B,C) Example calcium track recording for medial cells respectively recorded in the RMS OB and deep GCL. (D,E) Example calcium track recording for lateral cells respectively recorded in the RMS OB and deep GCL. Tracks are 2 minutes long. (F) Colour-coded representation of mean calcium transients amplitude for some recorded cells. Left panels are cells in the RMS OB and right panels cells in the deep GCL. Scale bar: 50 µm. (G) Percentage of active cells in a 2 minutes recording. Cells were defined as active if they showed at least one detectable calcium transient. N = 6 slices. Error bars are SEM. (H,I) Mean amplitude and frequency of calcium transients in lateral and medial cells recorded in RMS OB and deep GCL. N = 537 and 139 cells respectively, N = 6 slices. Error bars are SEM. The calcium activity of lateral cells greatly increased upon arrival in the deep GCL, in contrast with medial cells' activity.
(Adapted by Bugeon, 2017, p.53)

4.2.2. Screening for the signal that activate lateral cells

In order to identify the signals responsible for the drastic increase in Ca^{2+} activity for the lateral population at the beginning of radial migration, we performed a pharmacological screening. Therefore, we applied specific antagonists to acute slices and evaluated their effects on calcium transients. In a first step, we observed the basal Ca^{2+} activity of cells located in the deep GCL during a 4 minutes recording. Next, the slice was incubated 1 hour long with the chosen antagonist. Finally, we imaged the cells again for 4 minutes to see if their baseline activity was decreased (Fig. 13A). Our choice of antagonists was based on two factors: on one hand, the blocked neurotransmitters had to be previously mentioned in the context of cortical and/or cerebellar migration. On the other hand, migrating olfactory interneurons had to express the relevant functional receptors.

We started by testing glutamatergic receptors since it had been published before that NMDA-receptors mediated currents are necessary for the survival of migrating neurons in the RMS (Platel et al. 2010). We added D-APV (50µM), a selective NMDA antagonist, to the slice. Interestingly, blocking NMDA-receptors which are permeable to calcium, did not largely lower the amplitude of calcium transients (Fig. 13B). Other papers mentioned that functional AMPA-receptors, mGluR5 receptors as well as GLUK5 kainate receptors are expressed by V-SVZ cells (Di Giorgi Gerevini et al. 2004, Platel et al. 2008b). For this reason, we repeated the procedure with NBQX (10µM) to block AMPA-receptors, CNQX (20µM) for Kainate-receptors and MPEP (30µM) for mGluR5 receptors. Curiously, none of the antagonists affected the Ca^{2+} activity of lateral cells significantly (Fig. 13B).

Thereafter, we shifted our focus to GABA mediated currents which are supposed to still be depolarizing at this developmental point (Bolteus and Bordey 2004, Mejia-Gervacio et al. 2011). $GABA_A$ receptors are expressed by RMS neuroblasts where they are depolarized when the Na-K-2Cl co-transporter NKCC1 is present. Testing the role of $GABA_A$ receptors in lateral activity, we performed an antagonist experiment with Bicuculline. The $GABA_A$ receptor-blocker lead to a slight but significant increase of calcium transients amplitude (Fig. 13C). Likewise, the blockade of glycine receptors via Strychnine-application significantly rose the Ca^{2+} amplitude (Fig. 13C), indicating that inhibition of the two receptors for Glycine and $GABA_A$ promotes Ca^{2+} activity in laterally electroporated neuroblasts.

Another candidate that could likely be able to regulate lateral Ca^{2+} transients is Serotonin, probably acting through its 5HT3 receptor (Garcia-Gonzalez et al. 2017). Thus, in a new attempt we measured the effect of its specific antagonist Dolasetron mesylate (10µM) in our acute slice set-up. We observed that the 5HT3 receptor blocker lead to no significant decrease in calcium activity (Fig. 13C).

The glomerular and granule cell layers of the bulb receive extensive cholinergic input from the basal forebrain (Devore et al. 2012). Therefore hypothesizing that a

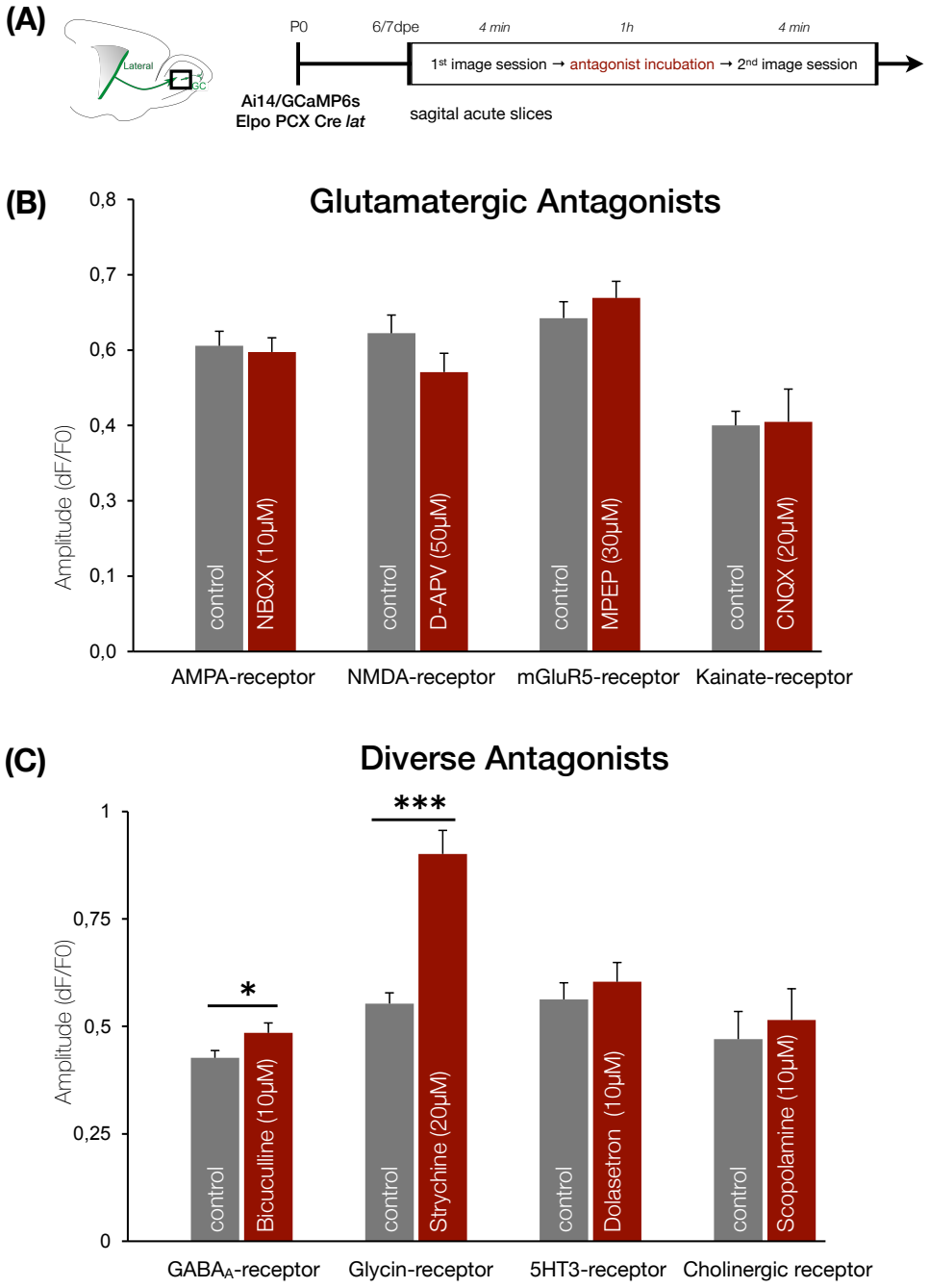

Figure 13: ***Pharmacological screening for the regulator behind lateral calcium activity in the deep GCL***

(A) Ai14/GCaMP6s animals received lateral electroporation of Cre at birth. After making acute slices of their brains at 7 dpe, calcium activity was recorded at two sessions. The first 4-minute long imaging session served as control before slices were incubated with a specific antagonist for at least 1 hour, and then re-imaged for 4 minutes. Afterwards, the mean amplitude of calcium transients was analysed and compared before and after antagonist incubation. (B) Mean amplitude of calcium transients before (grey bar) and after (red bar) incubation with glutamate related antagonists: NMDA-R antagonist D-APV, N=180 on 2 slices; AMPA-R antagonist NBQX, N=200 on 2 slices; mGluR5 receptor antagonist MPEP, N=163 on 2 slices; Kainite receptor antagonist CNQX, N=175 on 2 slices. (C) Mean amplitude of calcium transients before and after incubation with the $GABA_A$ receptor antagonist Bicuculline, N=134 on 2 slices; Glycine receptor antagonist Strychnine, N=154 on 2 slices. 5HT3 receptor antagonist Dolasetron mesylate, N=175 on 2 slices. Muscarinic cholinergic receptor antagonist Scopolamine, N=137 on 2 slices. Bar charts represent mean amplitude for all cells. Error bars are SEM.

competitive antagonist of Acetylcholine at muscarinic receptors could potentially increase lateral Ca^{2+} activity upon GCL entry, we tested Scopolamine (10µM). Yet again, the amplitude of Ca^{2+} transients was unchanged after stimulation (Fig. 13C). Since our analyses did not confirm any of the tested antagonists as strong inhibitor we wanted to understand in more detail how Ca^{2+} activity functions in the newborn neurons in order to gather more information for identifying potential regulators.

4.2.3. Depolarization is responsible for increase in lateral calcium activity

To gain comprehension of the entire activity cascade, we investigated activity in slices that had been incubated in a Ca^{2+} free environment. We observed that the amplitude of lateral Ca^{2+} transients and the percentage of active cells decreased a lot (Fig. 14A-D) providing evidence that the majority of Ca^{2+} comes from outside the cell. Consequently, we assumed that Ca^{2+} entry through the membrane must be mediated by ionotropic calcium channels. As it had been previously proven that L-type voltage gated calcium channels which connect the cytoplasm to the extracellular space influence calcium activity in the RMS (Darcy and Isaacson 2009), we asked if we could see similar effects upon their blockage. For this reason, we used Nifedipine which specifically blocks L-Type channels that open upon depolarization. Indeed, we detected a smaller amplitude of Ca^{2+} transients as well a diminished active cell

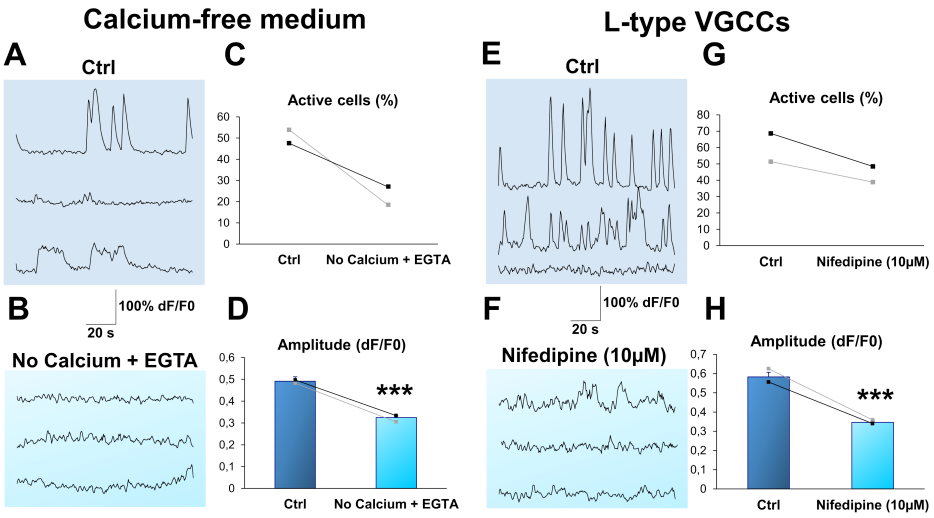

Figure 14: ***Ca^{2+} source identification for lateral activity in the deep GCL***
Ai14/GCaMP6s P0 animals received lateral electroporation of Cre encoding mRNAs. Calcium activity was recorded during a first imaging session for 4 minutes on acute brain slices at 7 dpe. Slices were then incubated with a specific antagonist for at least 1 hour and re-imaged for calcium activity for 4 minutes. The percentage of cells active and the mean amplitude of calcium transients was then compared before and after antagonist incubation. (A,B) Examples of calcium fluctuation tracks in control and calcium-free medium (No Calcium + EGTA). (C,D) Percentage of cells active and mean amplitude of calcium transients before and after incubation in calcium-free medium. N=192 cells on 2 slices. (E,F) Examples of calcium fluctuation tracks in control and Nifedipine supplemented medium. (G,H) Percentage of cells active and mean amplitude of calcium transients before and after incubation with Nifedipine. N=296 cells on 2 slices. Grey and black dot plots represent individual slices, bar charts represent mean amplitude for all cells. (Adapted by Bugeon, 2017, p.57)

percentage when we applied Nifedipine to the slice (Fig. 14E-H). This concludes, that the calcium fluctuations that we detected in lateral cells seem to be based on an entry of calcium from the extracellular space via voltage dependent calcium channels on voltage dependent calcium entry.

Since Nifedipine can successfully block neuronal activity in lateral cells we can draw the conclusion that depolarization is involved in the cascade of interneuron excitation. Hence, this drug can be further used to address the question whether OB interneuron migration on this increase of activity via activation of voltage dependent L-Type calcium channels.

4.3. Decreased excitability in migrating neuroblasts

As the lateral cell population is more active than medial neurons after leaving the RMS, we hypothesized that this increase in Ca^{2+} activity is part of the regulatory mechanism responsible for implementing different fate of interneuron subtypes. Thus, my next steps aimed to block activity in lateral cells for investigating if that was sufficient to impact migration and/or their final repartition. Given previous results showing that Nifedipine is an efficient inhibitor of lateral cell activity, we first used this drug before additional experiments were launched with the genetically expressed inward rectifying potassium channel Kir 2.1.

4.3.1. Nifedipine has no effect on radial migration in lateral cells

Aiming to decipher the role of neural excitation in the control of migration, blocking Ca^{2+} activity could reveal if migration depends on that Ca^{2+} signal and is consequently implemented or not. As a first approach, we took advantage of Nifedipine knowing that the L-type voltage gated calcium channel inhibitor efficiently prevents depolarization in lateral cells.
12-24 hrs after birth, Ai14 mice were laterally electroporated with a PCX Cre encoding DNA plasmid. Seven days later after lateral electroporation, we sacrificed the animals to prepare acute brain slices that were then imaged with a two-photon excitation microscope making a Z-stack every 5 minutes. During the first 1-hour recording the slice stayed in our standard dissection solution as control, before Nifedipine (10µM) was added for the second recording that lasted also 1 hour. Since the difference of activity between medial and lateral cells occurred in the deep GCL, we placed the imaging frame at the area where neurons leave the RMS (Fig. 15A). The analysis of those films showed that none of the tested migration parameters (Fig. 15B-E) changed significantly upon introduction of the Nifedipine treatment. However, we observed a slight tendency of longer stationary phases: 49% in control and 52% in Nifedipine condition (Fig. 15D) that lead to a non-significant increase of the overall displacement per hour (Fig. 15E).

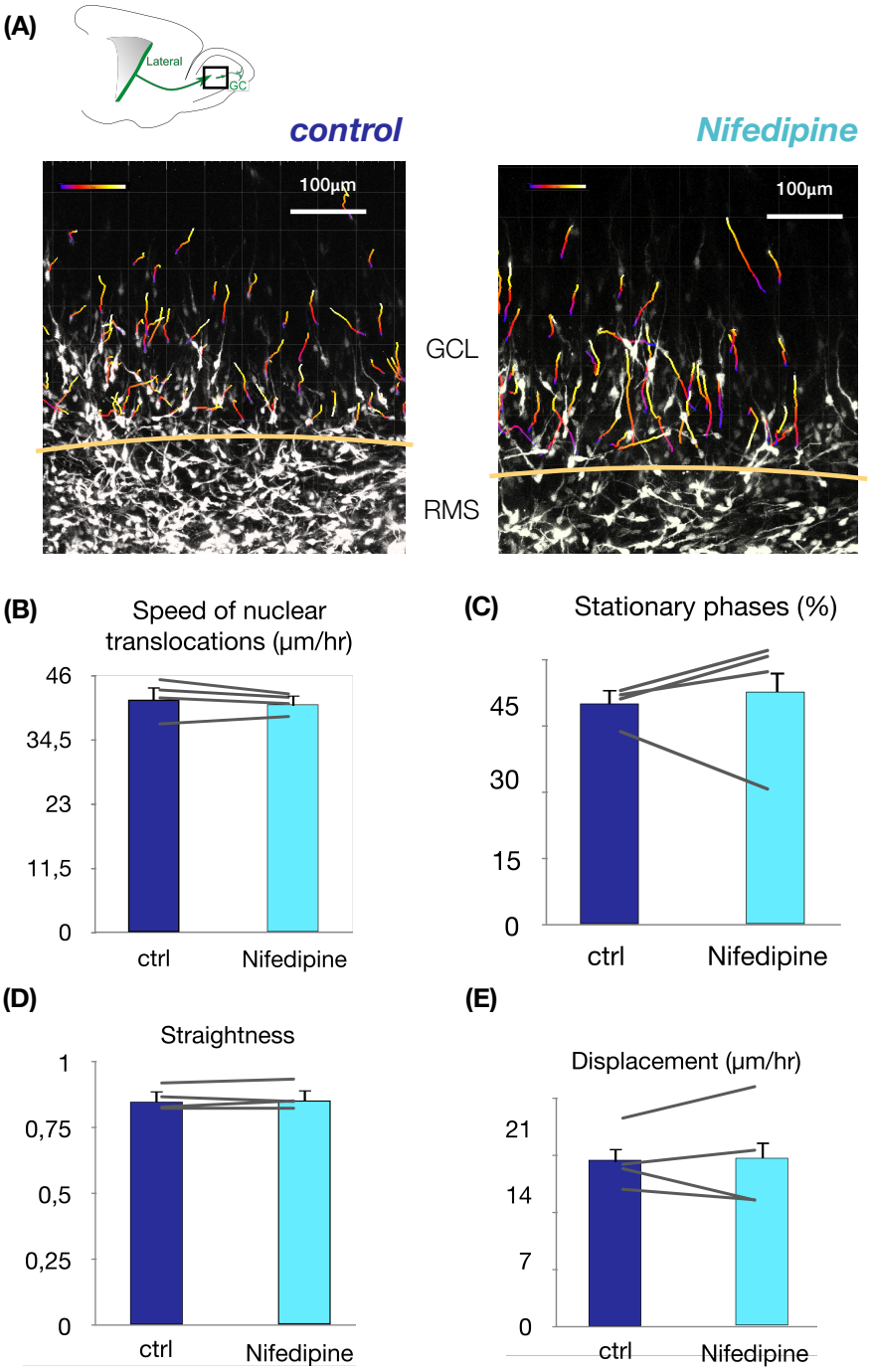

Figure 15: ***Migratory pattern comparison of lateral originating cells in the deep GCL under the influence of Nifedipine***

(A) P0 animals received lateral electroporation of a Cre encoding plasmid. The dynamic migration parameters of TdTomato expressing neuroblasts in the RMS were then assessed on acute brain slices at 7 dpe. Radial migration of individual cells in the deep GCL was imaged 1h long in a control medium before Nifedipine was added to the medium. The control condition is represented by dark blue cells, whereas the Nifedipine condition is shown in the picture with light blue cells. The border between RMS and deep GCL is indicated by a beige line. Scale bar: 100 µm (B-E) Mean speed of nuclear translocation, percentage of stationary phases, straightness and displacement per hour of radially migrating cells after lateral electroporation in control medium (dark blue), in the first hour and after Nifedipine addition (light blue). Note that Nifedipine addition does not change any of the tested parameters significantly. N=427 cells on 4 slices. Grey lines represent individual slices, bar charts represent the mean amplitude for all cells. Error bars are SEM.

Of course, this could simply mean that depolarization has no large effect on migration. Nevertheless, one has to be aware of the indirect effects that can appear within such a pharmacological experiment. Since the inhibitory drug is added to the entire set-up, it can possibly effect not only the channels of migrating lateral interneurones but also those of other cells which should ideally remain unchanged. Potentially, this can exaggerate or even conceal real effects. Those pharmacological perturbations can be hardly out-ruled forcing us to stay cautious while interpreting all concerned data. During the last decades, advanced genetic tools like the DREADD technology or the Kir 2.1 have been developed in order to avoid those kind of indirect effects and investigate the influence of cellular activity in a more precise and elegant way.

4.3.2 Activity-deprivation with Kir 2.1 shows subtype specific effects

To investigate the cell autonomous effect of decreased excitability in migration, we performed also non-pharmacological experiments manipulating exclusively the interneuron population that originates from the lateral wall of the lateral ventricle. For this reason the Kir 2.1 plasmid was used as a genetic tool since it will be specifically over-expressed only in the cell population targeted by electroporation. It codes for a modified potassium channel that leads to an increased inward current of potassium and triggers a hyperpolarization in the concerned interneurons. As consequence, those hyper-polarized cells can then not be excited anymore because the required depolarisation for reaching the firing threshold is largely elevated (Lin et al. 2010). As control we use a silent construct of this channel that is completely impermeable. The Kir-mechanism acts -unlike Nifedipine- independently of calcium sources.

The electroporation of Kir 2.1 efficiently decreases activity

To validate that this new tool is sufficiently decreasing Ca^{2+} activity in the lateral cell population, we performed two different tests to measure if the amplitude and frequency of Ca^{2+} transients can be diminished through Kir 2.1 expression. To compare Kir 2.1 positive and negative cells under the same conditions, we electroporated GCaMP6s mice at the same time with a Kir 2.1-RFP and a PCX Cre plasmid. Cells were observed 7 days later in the deep GCL on acute slices. GFP+ cells had only recombined Cre and served as control, whereas RFP+ and RFP+GFP+ cells were Kir-positive (Fig 16A,B). The comparison of those two populations confirmed that the amplitude and frequency of Ca^{2+} transients are lower in Kir+ cells (Fig 16D,F) proving that we can successfully block activity with our approach. To confirm the Kir 2.1 mutant as control we compared the amplitude and frequency in acute slices of Kir 2.1 and Kir 2.1-mutant electroporated animals (Fig 16 C). Again, activity was reduced in cells expressing the inward-rectifying potassium channel (Fig. 16 E,G). Hence, we can use both plasmids to study Ca^{2+} activity, migration and final positioning in OB interneurones.

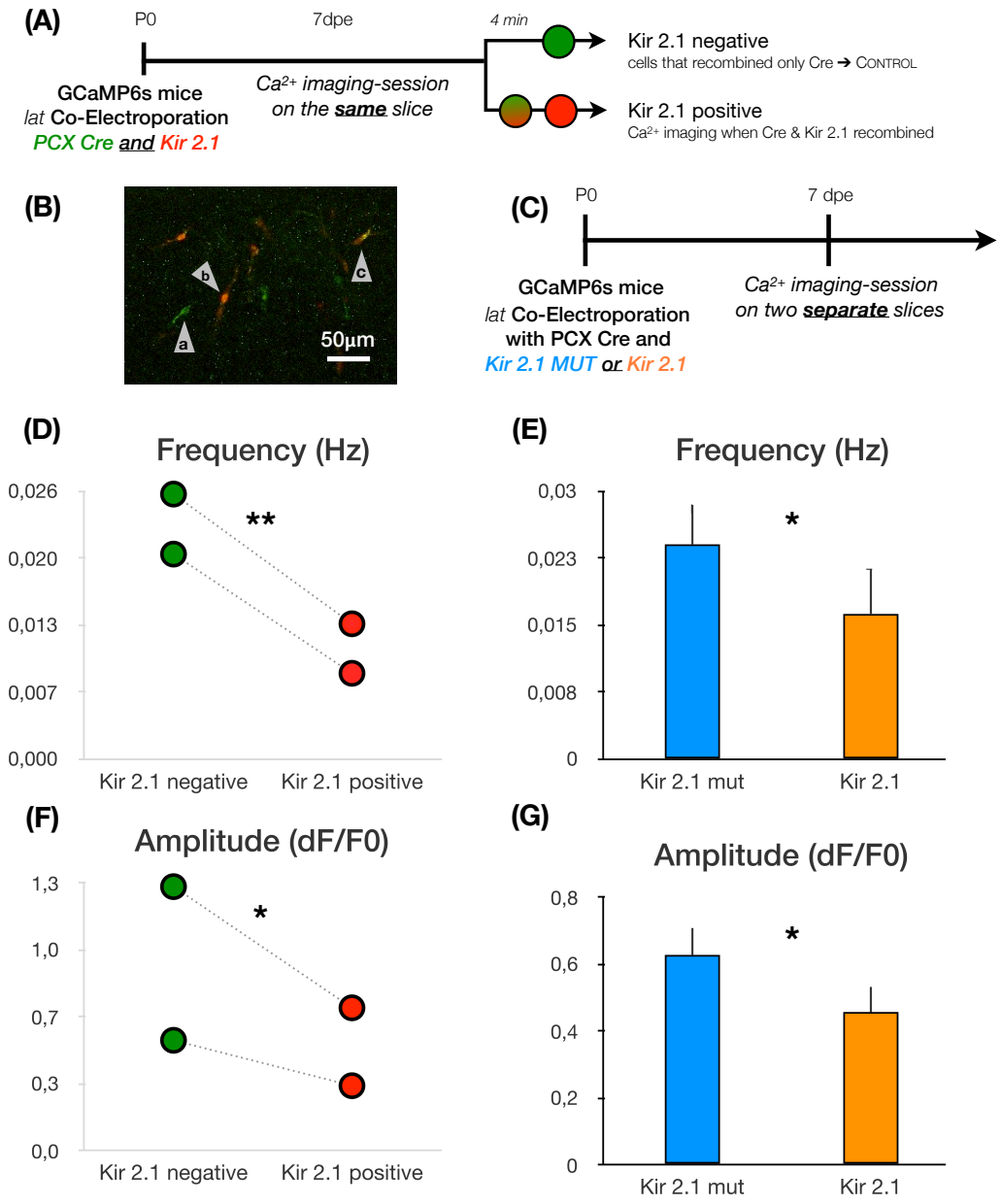

Figure 16: ***Validation of Kir 2.1 inhibitor on lateral OB interneurones***
(A) First validation experiment for Kir 2.1: at P0 GCamP6c mice were laterally co-electroporated with Kir 2.1 and Cre which activates the calcium sensitive probe in a transgenic mouse line. Calcium activity recordings were made at 7 dpe in the deep GCL. Both the Kir-condition and its control were observed on the same slice. Afterwards, Ca^{2+} analysis was made separately for Kir 2.1 positive (TdTomato and GFP-expressing cells in red&green) and Kir 2.1 negative cell population (only GFP-expressing cells in green). (B) Lateral cells in the deep GCL. The red TdTomato-expressing Kir 2.1+ cells (b) can be directly compared to the green GFP-expressing Kir2.1- cells (a). Two-coloured cells express both plasmids (c). Scale bar: 50 µm. (C) Second validation: P0 GCamP6c mice were laterally co-electroporated with Cre and either the Kir 2.1 plasmid or its control. Calcium activity recordings were then made at 7 dpe in the deep GCL on two different slices. (D,F) The mean amplitude and frequency of Kir 2.1 positive (red dot) and negative cells (green dot) were measured at the same time and under the exact same conditions. Both of the accessed parameters were remarkably lower in activity deprived Kir 2.1 positive cells. Grey lines connect populations on the same slice. N=119 on 2 slices (E,G) The mean amplitude and frequency are a lot less high in Kir 2.1 (orange) lateral cells compared to the or Kir 2.1 mutant (blue) control condition. Bar charts represent the average of each cell population. N=59 on 2 slices. Error bars are SEM.

Lateral electroporation of Kir 2.1 does not change migratory parameters

After having confirmed that the Kir 2.1 plasmid sufficiently lowers calcium activity, we wanted to investigate whether lateral cell migration can be manipulated using this tool. Therefore, either the Kir 2.1 or its mutant control plasmid were laterally electroporated into CD1 mice at P0. Later, we analyzed all migratory parameters as described before at three different locations (Fig. 17A). The first site was situated in the part of the RMS proximate to the SVZ in the so-called "RMS elbow" (Fig. 17B **I**). Secondly, registrations were made within the RMS of the OB right before the cells enter the deep GCL (Fig. 17B **II**). For observing the fast tangential migration, it was sufficient to set the total recording time to 1hr and apply a 2-min-interval between single scans. At last, Z-stacks were taken right after RMS exit (Fig. 17B **III**) when cells started to migrate radially. At this point, we prolonged the total recording time to 2hrs and the scanning interval to 5 minutes.

During tangential migration, neither at the RMS elbow nor in the centre of the bulb nor in the deep GCL significant differences in the mean speed of translocation, stationary phases and displacement were detected (Fig. 17F-H). However, during the imaging sessions in the deep GCL, we repetitively noticed more damaged or dying cells that were not moving. Also, the number of cells itself seemed to be diminished (Fig. 17D vs. E). Consequently, the percentage of stationary versus migratory cells was analyzed at each site for the Kir 2.1 as well as for the Kir mutant form. Indeed, more cells had stopped moving after the RMS exit (Fig. 17I). However, that applied for both conditions and can therefore not be specifically linked to the deprivation of activity. Nonetheless, we wondered if the subjective impression of an altered cell survival could be objectivized differently. This is why, additional experiments were launched to look at the final repartition after Kir-electroporation.

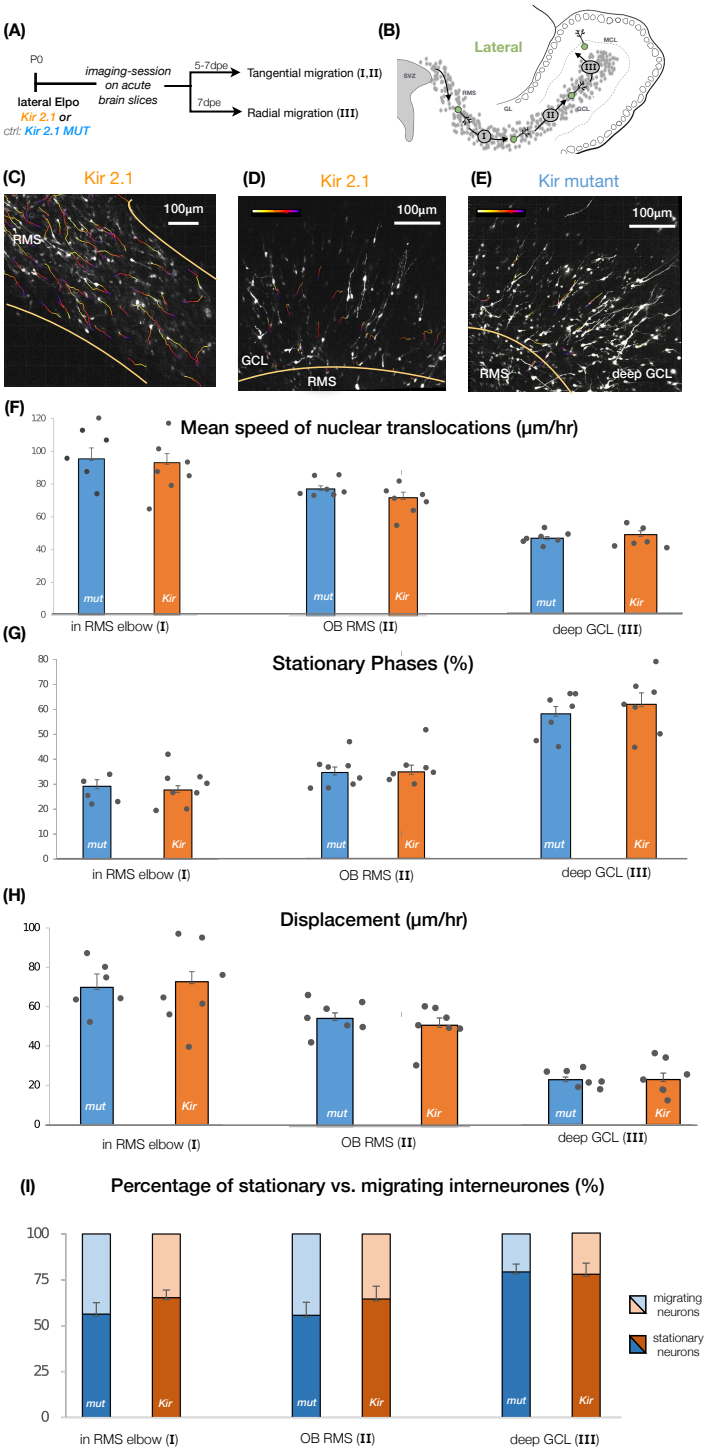

Figure 17: ***Kir 2.1 does not effect migration patterns of lateral cells***

(A) P0 animals received lateral electroporation of Kir 2.1 or its mutant form as control. The dynamic migration parameters of TdTomato expressing neuroblasts were then assessed on acute brain slices. Animals were sacrificed at 5-7 dpe for recordings in the RMS or at 7 dpe for recordings in the deep GCL. During tangential migration in the RMS we took a z-stack every 2 min for 1 hour. After RMS exit, the z-stack interval was adapted to 5min and the total recording time to 2h. (B) Schematic sagittal representation of the SVZ-OB pathway of future GCs. Roman numbers indicate the location for time laps recordings: (**I**) RMS elbow (**II**) RMS in OB (**III**) deep GCL. (C,D,E) Scale bar: 100µm. The first two images show Kir 2.1 positive cells in the RMS elbow (C) and the deep GCL (D). (E) shows cells expressing the mutant channel during RMS exit. Beige lines separate the RMS from the deep GCL in the bulb. (F-H) Mean speed of nuclear translocations, percentage of stationary phases and displacement per hour for Kir 2.1 (orange) or Kir 2.1 mutant (blue) lateral cells at different locations. Number of slices per location: RMS elbow n_{Kir}= 7 n_{mut}= 6; RMS in OB n_{Kir}= 7 n_{mut}= 7; deep GCL n_{Kir}= 8 n_{mut}= 7. (O) Percentage of cells either resting on one spot or migrating forward normed by the total cell amount. None of the assessed parameters shows a significant difference. Error bars are SEM.

Kir¡ 2.1 electroporation effects solely lateral cell repartition in the GCL

To investigate further *ex vivo* observations of a fragile lateral Kir 2.1 cell population in the GCL, we evaluated the cellular distribution 8dpe after lateral electroporation on whole bulbar mounts (Fig. 18A). *De facto*, manual blind counting of all TdTomato+ cells confirmed an impressive decay of the absolute GCs number in their final layer (Fig. 18C).

Seeing this large effect for the lateral population, one could asked whether this would equally apply for future PGCs. Repeating the experiment using medial electroporation revealed that the absolute number of interneurones in the GL was almost identical between the Kir 2.1 and its control mutant condition (Fig. 18B,D) indicating a cell type specific influence.

To out-rule the possibility that this measurement reflects only a transient artifact, OB interneuron repartition was evaluated also at two later time points: 10 and 12dpe. Again, a significant decrease in the final layer could exclusively be found for GCs (Fig. 18C,D). This strengthens further the hypothesis of two distinct control mechanisms: on the one hand, the activity-dependent GCs that seem sensitive to Kir 2.1 blockade of Ca^{2+} activity. On the other hand, the PGCs that act independently of activity - at least at this stage of their development.

Taking further into account the amount of cells in the RMS, those findings illustrate perfectly previous examinations on live slices: (1) both lateral and medial TdTomato+ cells display a normal phenotype during tangential migration, (2) yet, lateral Kir 2.1+ neuroblasts alone seem to be negatively effected during radial migration (3) resulting in a decreased cell number of migrating GCs after RMS exit. After having obtained the quantitative confirmation on fixed slices, we aimed to better understand the underlying pathways.

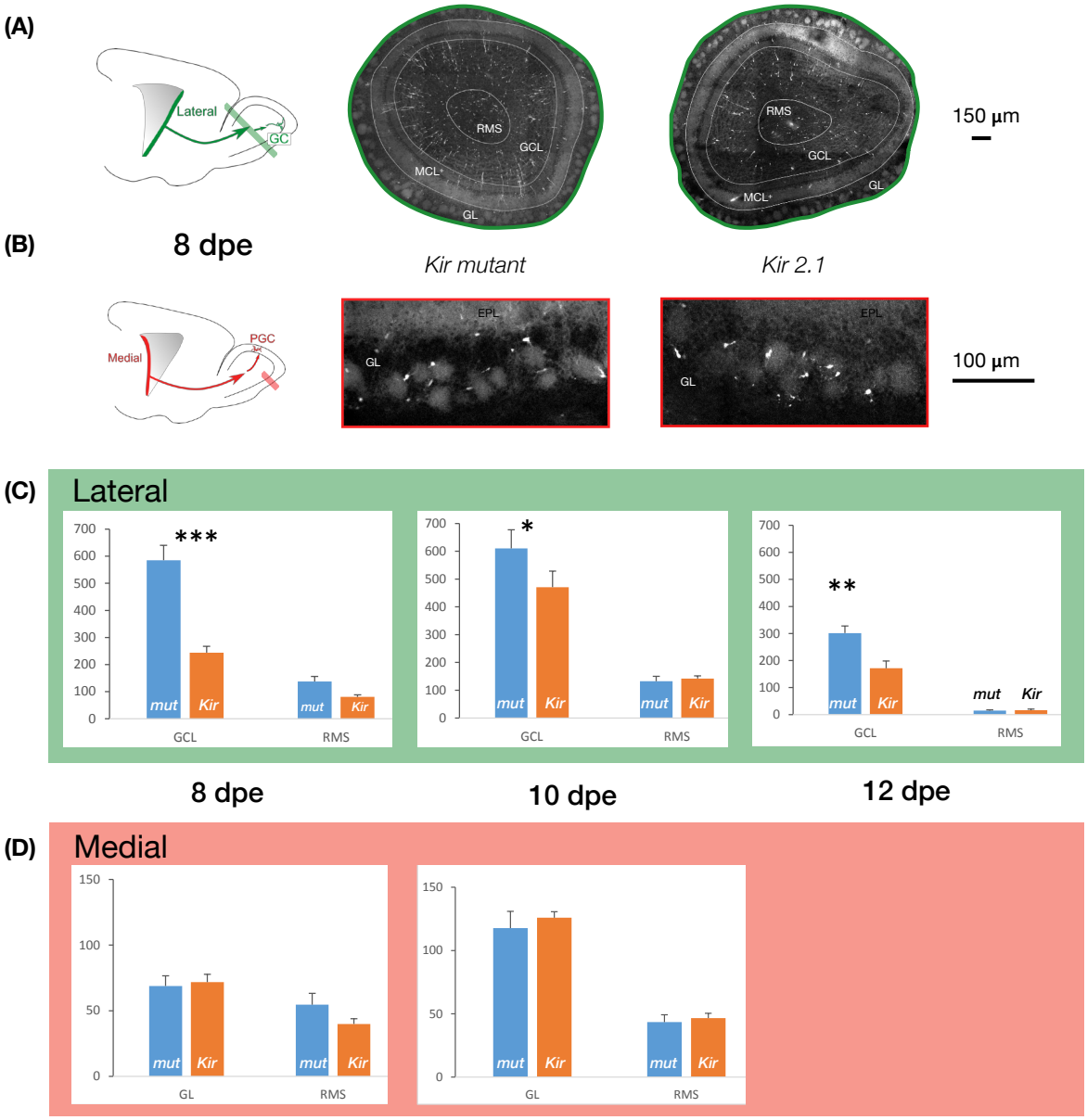

Figure 18: ***Activity deprivation decreases the absolute lateral cell number in the GCL while medial cell reparation remains unchanged***

P0 mice received lateral or medial electroporation of either the Kir 2.1 encoding plasmid or its mutant form as control. (A) Exemplary pictures of entire OB at 8dpe after lateral Kir 2.1 or mutant electroporation. The images show the different layers of the OB separated by white lines. The TdTomato+ cells (white) were counted manually. Note, that the internal and external plexiform layers are added to the MCL. Scale bar: 150µm (B) Detail of GL at 8dpe after medial Kir 2.1 or mutant electroporation. (C,D) Repartition in the final layers and RMS after lateral (C) or medial (D) electroporation. The absolute cell number of lateral cells in the GCL is significantly decreased at all tested ages (8/10/12dpe). At the same time, no effect was observed for the medial population. N=12730 cells on 34 slices; 7 Kir 2.1-animals, 8 mutant animals. Bar charts represent the absolute TdTomato cell number in the respective layer. Error bars are SEM.

Apoptosis is increased only in final layer of Kir 2.1-expressing GCs

As the link between neuronal activity and cell death has been already shown for adult born OB neurons (Rochefort et al. 2002), we decided to stain Kir 2.1/mutant fixed whole mount slices for the apoptotic marker Caspase 3 in order to investigate whether the quantitative decay in the GCL is due to an up-regulated programmed cell death (Fig. 19A). Having counted all cells that expressed the Kir 2.1/mutant plasmid

(TdTomato+; Fig. 19B red cells) and taking separately into account the ones positive for Caspase (TdTomato+/GFP+; Fig. 19B orange cells), we could compare their distribution in each OB layer at 12dpe. In-line with our previous data, the percentage of dying Kir 2.1+ cells was significantly elevated only in the GCL suggesting that this might be the place where final integration is regulated though activity-dependent survival.

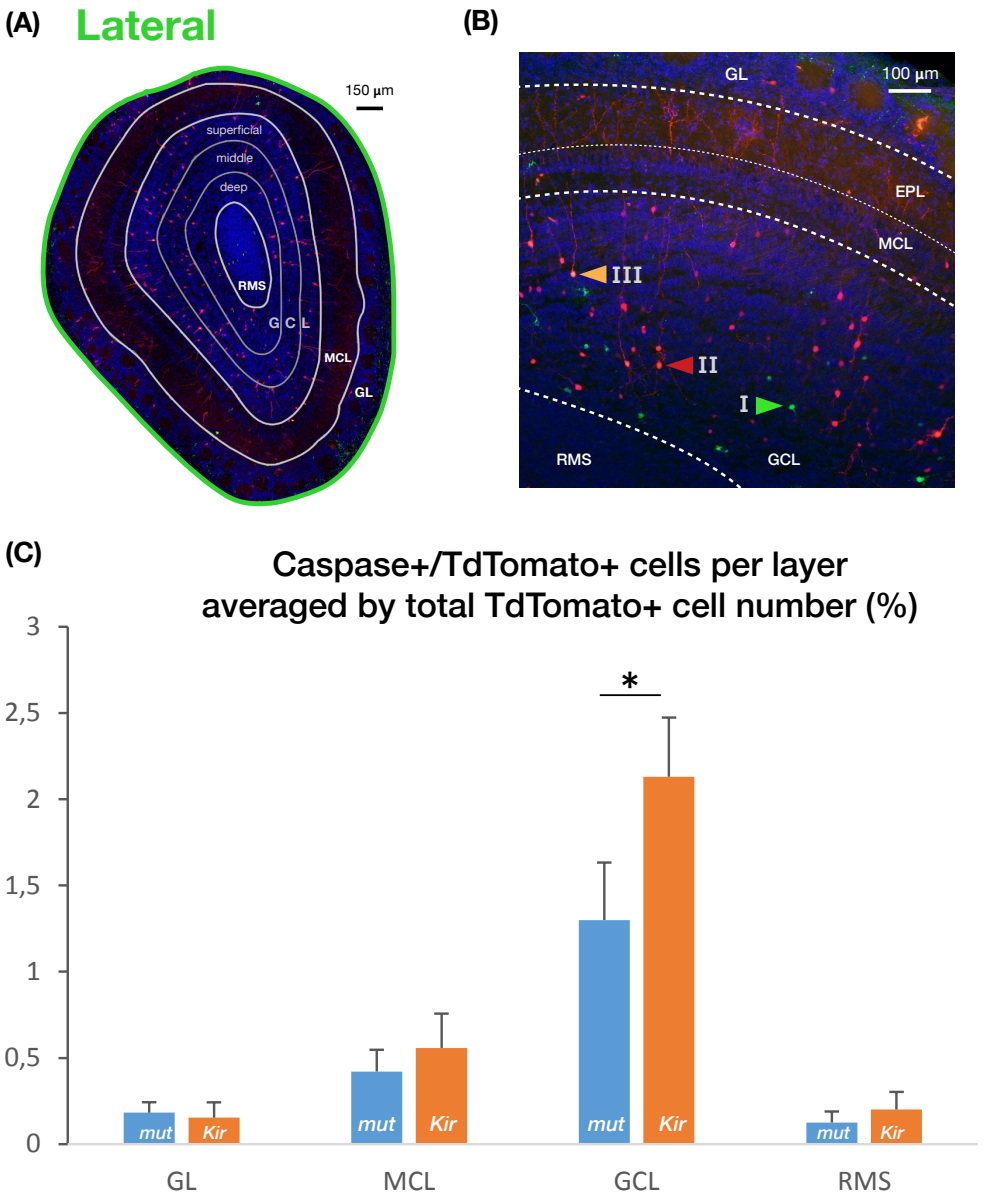

Figure 19: ***Kir 2.1 over-expression surpasses granule cells***
Lateral electroporation of Kir 2.1 or Kir mutant at P0. To look at the repartition of dying cells, mice were sacrificed at 12 dpe and OB slices incubated with Caspase. The distribution of Kir2.1/ mutant expressing interneurones (red) and Caspase+ cells in each layer of the OB was assessed. The obtained image (A) was analyzed in ImageJ. Grey lines separate the layers. Cells were counted manually. Note, that those cells that rarely accrued in the EPL were added to MCL. Scale bar: 150 µm (B) Detail of GCL. **I** Capase-positive Kir/mutant-negative (only green); **II** Capase-negative Kir/mutant-positive (only red); **III** Capase-positive Kir/mutant-positive (red and green). Layers are circumvent with white dotted lines. Scale bar: 100 µm (C) Graph showing percentage of dying cells among Kir/mutant positive cells for each layer. The deprivation of activity leads to a significantly increased apoptosis rate only in the GCL. N=12730 cells on 34 slices; 7 Kir 2.1- animals, 8 mutant animals. Bar charts represent the mean percentage of all type-**III** cells per layer averaged by the total number of Kir/mut expressing cells (**II**) in the respective layer.

4.4. Effects of increased excitability

To better understand the regulative mechanisms of OB interneurons, it is not only interesting to look at the consequences of decreased, but also of increased excitability. Making use of the chemogenetic DREADD-technique hM3Dq, it is possible to activate the M3 muscarinic cholinergic G_q cascade in a cell-autonomous manner and with temporal control upon the addition of the specific agonist CNO. As tested before, hM3Dq activation by CNO in 7 dpe neuroblasts efficiently induced depolarization resulting in a large calcium release in the cytoplasm (Fig. 8, Materials and Methods “Pharmacology”). This allowed *in vivo* investigations of the effects that increased neuronal activity has on lateral and medial migrating cells.
To access parameters of cellular movement in the deep GCL, transgenic Ai14/hM3Dq animals were sacrificed one week after P0 Cre electroporation. Their brains were then sliced and imaged with a biphoton microscope as described before (see Materials and Methods “In vivo slices”). First, cells were tracked by time-lapse imaging in control medium for 3 hrs, then CNO (5 µM) was added to the medium - triggering a large calcium entry (Fig. 20A). That way, we were able to measure and compare main kinetic parameters in control and CNO supplemented medium during radial migration.

The mean speed of nuclear translocations of medial radially migrating cells showed a small but significant increase after CNO induced depolarization (Fig. 20B). At the same time, the percentage of stationary phases remained unchanged (Fig. 20C). Taken together, this resulted in a faster displacement per hour (Fig. 20D). To test if this increase in speed for medial cells after depolarization is a general effect in radially migrating cells, the experiment was repeated on laterally electroporated cells. Surprisingly, there, excitation slightly decreased the overall displacement speed although the percentage of stationary phases as well as the mean speed of nuclear translocations were not significantly altered upon CNO addition (Fig. 20E-G).
These experiments confirm once more that in addition to having a different pattern of spontaneous calcium activity, lateral and medial cells react differently to activity. However, it has to be taken into account that the experimental approach of increasing excitation is less physiological than evaluating the effects of blocked activity since it remains uncertain if cells themselves would ever raise their natural level of excitement up to this point. Therefore, this data can be interpreted only cautiously.

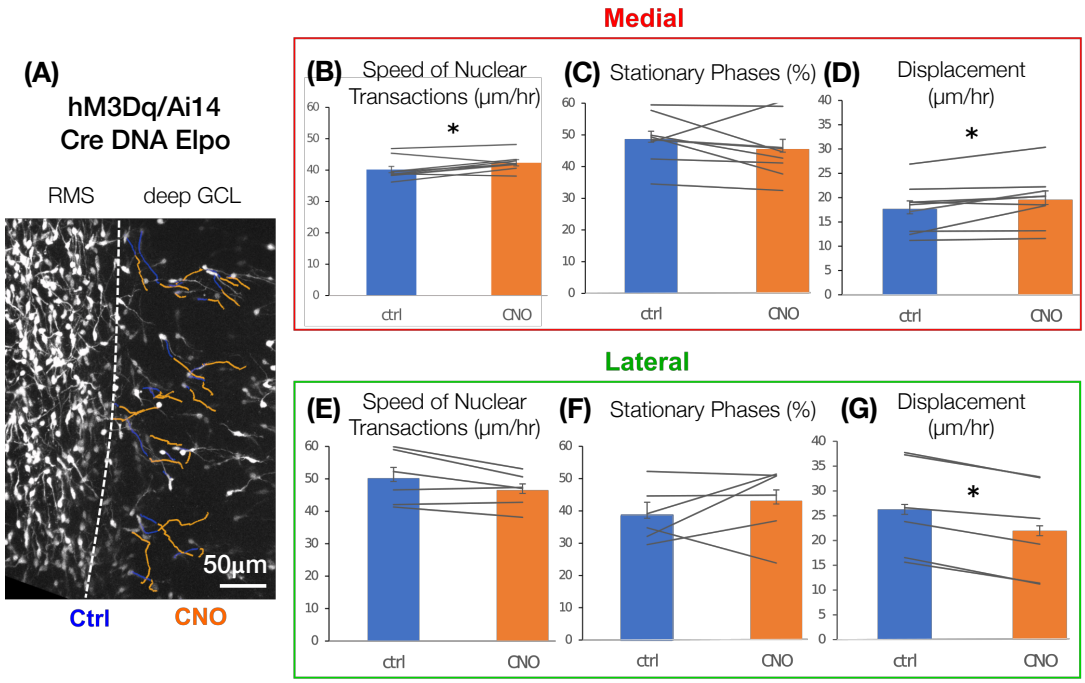

Figure 20: ***Increased excitability affects the speed of radial migration***
(A) Ai14/hM3Dq P0 animals received lateral or medial electroporation of Cre. Radial migration of individual cells in the deep GCL was imaged at 7dpe first for 1h in a control medium. Afterwards, CNO was added to the medium. Control condition is represented by blue tracks, the CNO condition by orange tracks. The border between the RMS in the OB and the deep GCL is indicated by a dotted white line. Scale bar: 50 µm (B,C,D) Mean speed of nuclear translocation, percentage of stationary phases and displacement per hour of radially migrating cells after medial electroporation in control medium (blue), between 0 and 1 hour and after CNO addition (orange). Note that CNO addition significantly increased the speed of nuclear transactions as well as the displacement per hour. N=1014 cells on 9 slices. (E,F,G) Mean speed of nuclear translocation, percentage of stationary phases and displacement per hour of radially migrating cells after lateral electroporation in control medium (blue), between 0 and 1 hour after CNO addition (orange) N=782 cells on 6 slices. Grey lines represent individual slices, bar charts represent mean amplitude for all cells. Error bars are SEM.

5. DISCUSSION

Neural stem cells have a great potential for cell-replacement strategies in brain repair due to their capacity of continuous self-renewal. Before this promising donor source is accessible though, certain prerequisites have to be met (Lledo and Saghatelyan 2005). Therefore, much intensive research concerning migration and differentiation of different neuronal cell types as well as a description of their regulatory mechanism is needed. Eventhough subpopulation specific behavior for cortical interneuron migration has been already reported (De Marco Garcia et al. 2011), little is known about the characteristics of different OB interneurons. One crucial mechanism during the development of olfactory bulb interneurons concerns sensory input (Saghatelyan et al. 2004, Yamaguchi and Mori 2005, Kelsch et al. 2009). For this reason, it is especially interesting to assess the role that neuronal activity plays in the regulation of interneuron populations in the postnatal OB. One has to keep in mind though, that a lot of intrinsic activity mechanism can exist completely independent of sensory activity.
Here, it was examined how PGCs and GCs, two interneuron populations deriving from the SVZ, migrate and integrate into their final bulbar layer. Using electroporation, we were able to separately target PGCs and GCs, compare for the first time their mode of migration and observe effects of altered activity on final positioning. We discovered that spontaneous calcium activity generated by depolarization is subtype-specific and probably responsible for different repartition patterns and survival of the two populations.

5.1. Specific labelling of subpopulations

The examination of two cellular populations requires reliable labeling. With postnatal electroporation, we utilized an efficient tool to distinguish and manipulate specific OB interneuron subpopulations already at the stem cell level. In our hands, specificity was sufficiently high, at minimum 80%. Former studies even claimed to reach slightly higher purity: 95% of GCs for lateral electroporation and 89% of PGCs for medial electroporation (Fernandez et al. 2011). Those differences may arise from individual handling e.g. during plasmid injection and the placement of electrodes. Although we considered that a purity of 80% is high enough for detecting significant differences, 20% of contamination still have to be taken into account when interpreting the obtained results, especially in regard of a decreased statistical power.

Our first experiments aimed to quantify migratory parameters of PGCs and GCs both during tangential migration in the RMS and radial migration in the GCL. In contrast to observations in the cortex (Tabata and Nakajima 2003), where direct visualization of cellular migration revealed subtype-specific migration modes, our recordings in the OB did not show any striking interneuron behavior differences. Albeit we expected outcomes similar to the ones in the cortex, our results are not highly surprising since it has been

previously described that regulatory mechanisms and migration differ in the RMS in comparison to other zones of the cortex (Metin et al. 2006, Nam et al. 2007).

5.2. Manipulating Ca^{2+} activity reveals subtype specific characteristics

If the mode of migration itself is not responsible for the different final positioning of PGCs and GCs, other clues must fulfill this regulatory task. As it has been published previously that sensory deprivation induces large changes during the maturating process of interneurons (Kelsch et al. 2009), we looked at intracellular Ca^{2+} activity at specific postnatal time points to clarify whether future GCs and PGCs are influenced differently. Indeed, we observed a substantial difference between the two populations regarding spontaneous calcium activity in the deep GCL, after the switch from tangential to radial migration. Reflecting on the underlying mechanisms of those distinguishing intracellular calcium fluctuations, one or both of the two following pathways seem probable: 1) gradient driven entry of Ca^{2+} from the extracellular space through ionotropic membrane receptors or 2) via the activation of IP3 receptors that triggers a release from internal stores (mostly smooth ER).

Seeing that the removal of extracellular Ca^{2+} resulted in major inactivation suggests that the first mentioned pathway could be more prominent. Further experiments revealed that blocking L-type voltage gated Ca^{2+} channels (VGCCs) sufficiently abolished Ca^{2+} transients - strengthening once more the hypothesis that the observed Ca^{2+} transients in radially migrating GCs are driven by the entry of Ca^{2+} through L-type channels which are opened by depolarization. It must be taken into account though, that blocking L-type VGCCs with Nifedipine on whole slices is a large intervention and addresses the question only in a non-cell autonomous way. Hence, it could likely be true that this kind of activity reduction causes cells to stop working physiologically. For instance, affected neurons might decrease their probability of releasing neurotransmitters. In this particular case, the observed diminution of Ca^{2+} transients could be due to a decrease in neurotransmitter release and not only because of the inhibition of L-type VGCCs. Yet, former experiments performed on tangentially migrating neurons in the RMS showed first that L-type VGCCs are expressed and second that Tetrodotoxin-induced blockage of neurotransmitter release leaves their spontaneous Ca^{2+} transients unchanged (Darcy and Isaacson 2009). These results add evidence to the fact that the L-type VGCCs blockage, that we perform in our experiments, is the real cause for the decrease in Ca^{2+} activity. Surprisingly, the application of Nifedipine on radially migrating lateral cells did not result in any significant modification on their parameters of migration. However, by applying recent genetical tools we were able to further test the causality between the difference in Ca^{2+} activity and radial migration without the mentioned pharmacological side effects that Nifedipine might imposes on brain slices.

The genetically encoded potassium channel Kir 2.1 allows the manipulation of cell-intrinsic excitability on a single cell level. Only those cells, that were electroporated with

the coding plasmid beforehand, express this channel that causes an hyperpolarization in neurons. To verify our hypothesis whereby the raise of Ca^{2+} activity exclusively during the radial migration of GCs is necessary for their correct development, we evaluated migration and final repartition of Kir 2.1 electroporated cells.
In line with our previous Nifedipine experiments, no evident alteration of lateral cell migration exists upon Kir-induced Ca^{2+} activity reduction neither in the RMS nor in the GCL. This underlines that the accessed parameters of migration such as the percentage of stationary phases or the overall displacement per hour are not regulated by Ca^{2+} activity.

Strikingly, we noticed a substantial difference between the control and the Kir 2.1 condition when we looked at the cellular distribution in the OB. On the one hand, a large decrease in the total amount of Kir 2.1 electroporated cells in the GCL could be seen for the lateral population at 8, 10 and 12dpe. On the other hand, the absolute numbers for medial cells in their final layer stayed the same, suggesting that the deprivation of Ca^{2+} activity was insignificant during their process of correct positioning. It had been already shown in the past that the number of new GCs decreases in a sensory-deprived OB (Yamaguchi and Mori 2005). However, former analysis were focused on GCs as the predominant population, whereas we now compared directly the two types of OB interneurons which are generated postnatally. Remarkably, our findings provide evidence that GCs and PGCs are regulated differently during radial migration: while the lateral population depends on Ca^{2+} activity triggered by depolarization, the medial distribution is not perturbed by an increase of Ca^{2+} activity.

It has to be critically mentioned though, that the influence of the activity decreasing Kir 2.1 channel begins at the stem cell level and is therefore not temporally restricted. Ideally, one ought to employ an inducible plasmid that can be specifically activated upon RMS exit. In order to investigate whether the effects of an altered distribution appears also when Ca^{2+} activity is blocked only during radial migration, our team is currently working on creating a genetic construct which will allow us to increase temporal control. Moreover, neuronal excitability can be decreased by using the DREADD technology as the modified receptor hM4Di has the ability to induce membrane hyperpolarization and neuronal silencing upon CNO addition (Armbruster et al. 2007). This additional experiment could further investigate the role that a decreased membrane potential plays during final migration and differentiation steps.

To quantify not only the effects of deprivation but also of activation, we artificially increased the membrane potential using the activator DREADD receptor hM3Dq. Again, we observed different effects depending on the population: a faster displacement for future PGCs and a decreased speed for future GCs. Those results confirm that the two populations react differently to activity manipulation in addition to having distinct Ca^{2+} levels during radial migration. The obtained data must be treated cautiously though,

because the stimulation of cells to an extent that succeeds physiological conditions can deliver results that would never appear under normal conditions. Also, it remains to be determined whether this up-regulated membrane potential also leads to differences in OB layer positioning. So far, only the cellular repartition after Ca^{2+} activity blockage was evaluated.

Finally, it should be noted that the effect of the hm3Dq receptor activation on migration is likely depending on the kinetics of its ligand CNO. In our validation experiments, we saw that CNO generates a large Ca^{2+} transient into the cell, which peaks during incubation (<2 minutes). Possibly, this could empty intracellular Ca^{2+} stores preventing further neuronal activation. To clarify the effect that CNO addition has on Ca^{2+} fluctuations, we aim to perform long-term experiments which will help to interpret the effect of DREADD activation on radial migration more reliably.

5.3. Relations between Ca^{2+} activity and survival

Given the impressive difference in lateral and medial Kir+ cell distribution, the search for an adequate explanation naturally represents the next step. One possible interpretation for the largely decreased lateral Kir+ cell number (compared to the Kir 2.1 negative control group in the GCL) could be that a lower Ca^{2+} activity slows down cells. Indeed, a decelerated velocity would result in later-arriving cells leading -at least temporarily- to a diminished absolute number. However, the data we generated through *ex vivo* imaging refutes this theory since the displacement per hour, both in the RMS and deep GCL, was similar for the Kir+ and control group.
Another answer could be that low Ca^{2+} activity levels trigger cell death. Addressing this option, fixed tissue slices were stained for caspase 3. The activation of this protein has been shown before to co-occur with DNA fragmentation of OB granule cells (Yamaguchi and Mori 2005). This strongly suggests that apoptosis is mediated through caspase activation and implements that caspase can serve as key molecule to reveal how Ca^{2+} activity acts as survival signal for newborn GCs.

In our study, we discovered that the rate of cell death is elevated for activity-deprived GCs at 12 dpe exclusively in their final layer. Surprisingly, the decrease of Ca^{2+} activity showed no effect in other parts of the OB, letting us hypothesize that their sensitivity might appear only at this specific locus or due to a certain level of maturation they have reached at this point of their differentiating process. For the reason that cells with caspase 3 activation might already start changing their morphology and then disappear completely due to fragmentation processes (Porter and Janicke 1999), our observations can solemnly encompass apoptotic cells during a narrow time frame. Therefore, the rate of cell death could be even higher than the value we detected.

Until now, the exact mechanisms of how Ca^{2+} activity in the adult brain can monitor a particular cell's survival and successful integration remain largely unknown. Former

studies claimed that synaptic input as well as membrane conductance which is determined by the cell's repertoire of ion channels, may play a major role in regulating both survival and network establishment (Lin et al. 2010). This suggests that the different behavior of GCs and PGCs could result from subtype specific membrane conductances that lead to altered activity sensitivity and consequently to distinct survival patterns. To test this assumption, we could repeat caspase staining for medial Kir+ interneurons comparing the correlation between cell death and activity deprivation in two different subpopulations. Additionally, analysis using caspase knockout mice and caspase inhibitors might present promising strategies (Ranger et al. 2001).

Figure 21 gives a visual overview of our main findings and proposes a working model that can be used as fundament for further research. Based on our results we hypothesize that OB interneuron populations are regulated differently as exemplified by their different level of Ca^{2+} activity. While the lateral population present an altered repartition after a decrease of activity, the medial cells seem to be insensitive to changing Ca^{2+} transients as their positioning stays the same.

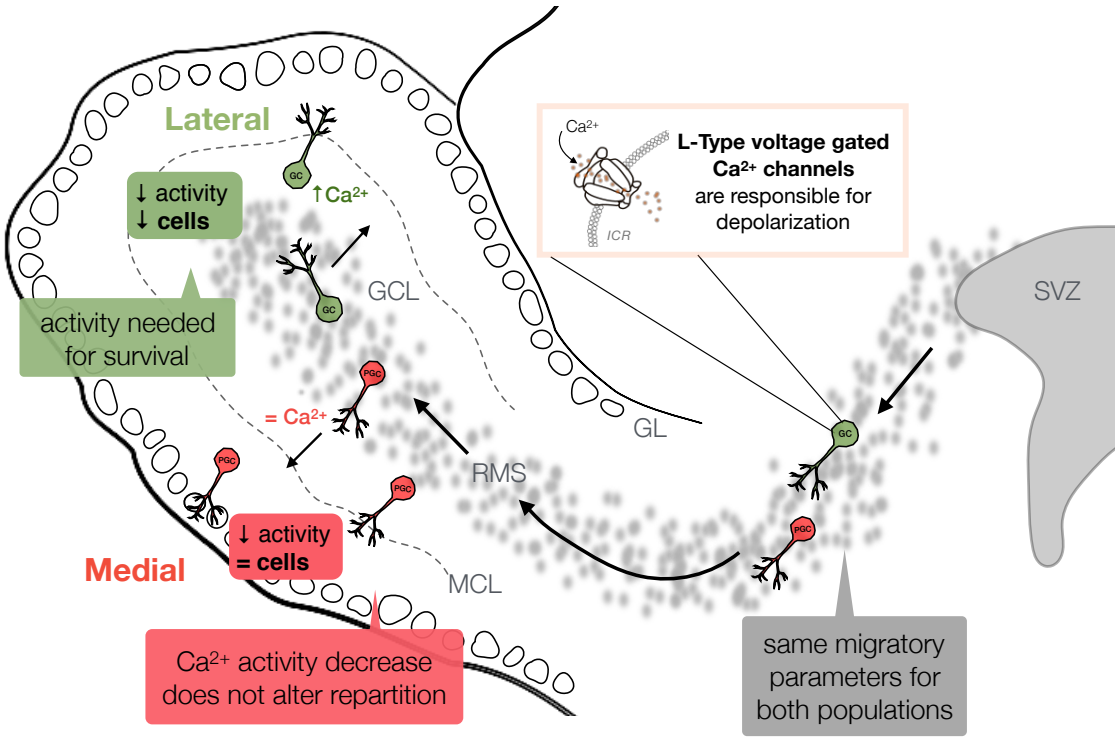

Figure 21: ***Working model***
Schematic overview of SVZ-RMS-OB pathway for lateral and medial neuroblasts. We have shown that the displacement parameters are the same for the two interneuron populations during migration. However, the level of Ca^{2+} activity increases upon RMS exit solely for future granule cells (GCs). Ca^{2+} activity is mediated through voltage gated calcium channels that depolarize the cell once opened. Activity deprivation triggered lateral cell death in the GCL leading to a decrease in the absolute cell number. At the same time, the final repartition of periglomerular cells (PGCs) remained unchanged when activity was blocked.

5.4. Approaching the complexity of regulatory mechanisms of adult born OB interneurons

Much research has already been done aiming to break down the tremendous complexity of adult neurogenesis. Still, underlying mechanisms remain vague since cellular subtypes of the entire brain present at each level of maturation different mechanisms of control. For instance, a study on the factor p27Kip1 revealed that neuronal differentiation and migration are individually controlled in newborn cortical neurons (Nguyen et al. 2006). Some years later, work on shRNA-mediated knockdown of Dcx showed an accumulation of cells within the RMS of the OB, but no affection of their capacity to differentiate (Belvindrah et al. 2011). Another study demonstrated that in mice lacking the zinc finger homeodomain factor TSHZ1, neuroblasts exhibit a normal tangential migration towards the OB, but that neuronal distribution is thereafter perturbed within the radial dimension and that many immature neuroblasts could not even exit the RMS (Ragancokova et al. 2014). In line with this data, our findings suggest that interneurons respond differently to signals during migration and segregation.

In the future, using TSHZ1 knockout mice could help to understand how different genetical settings influence the differentiation of PGCs and GCs. Also, we could address open questions about maturation processes in the OB by working with CREB, a transcription factor that activates target genes through cAMP response elements. CREB plays a predominant role e.g. in promoting interneuronal survival and precursor proliferation (Lonze and Ginty 2002). Its activation through phosphorylation correlates with neuronal differentiation, increasing during the late phase of tangential migration in the RMS and decreasing after dendrite elongation and spine formation (Giachino et al. 2005). On fixed OB slices, checking the level of phosphorylated CREB could reveal whether Kir+ lateral cells are less mature when they arrive in the GCL. Such a result would provide evidence for the assumption that Ca^{2+} activity is responsible for differentiation and survival rather than for controlling migration.

Conclusions drawn from previous experiments performed by Bolteus and Bordey underlined that an increase in extracellular GABA levels, instead of cell depolarization per se, affected the speed of cell migration (Bolteus and Bordey 2004). According to them, astrocyte-like cells create a microenvironment in which GABA release and uptake strictly control neuronal migration through the degree of $GABA_A$-receptor activation. Other data suggest that SVZ/RMS astrocytes may also be a source of glutamate and that NMDA-receptors provide early survival cues to neuroblasts prior to entering an existing synaptic network (Platel et al. 2010). This indicates that one has to take multiple factors such as the surrounding network into consideration in order to explain regulatory mechanisms. We tried therefore to identify additional signals affecting postnatal neurons.

However, in spite of persistent effort during pharmacological screening, we were unable to find a precise neurotransmitter responsible for the increase of calcium activity in future GCs. We tested not only several glutamatergic but also GABA-, Glycine-, Serotonin- and Acetylcholine-antagonists. Once more, the nature of interneuron regulation seems to be not straightforward. Instead of testing other candidates, we could now try to combine the effects of multiple signals by applying certain antagonists at the same time. Possibly, interneurons are not controlled through only one receptor but respond to the activation of a compound-signal. We could therefore block NMDA-, AMPA-, Kainate- and mGluR5 receptors at once. In case a signal can be identified in this manner, we will be able to clarify several open questions e.g. whether the difference of activity between lateral and medial cells in the GCL is caused by a delay in expression of certain receptors or by an absolute variation of expression between the two cell types.

Theoretically, integration and death of OB interneurons could also be intrinsically encoded. In the cortex, it has been shown that some developing interneurons are individually destined to die later during postnatal life, regardless of the nature of their local environment. About 40% of the total population is eliminated in a cell-autonomous manner through Bax-dependent apoptosis (Southwell et al. 2012). Here, we demonstrated that OB interneurons respond differently to implemented alterations of Ca^{2+} activity mimicking intrinsic mechanisms. In regard of the research in the cortex, it can be asked whether those Ca^{2+} signals that are crucial for survival in the GCL may be obtained through a cell-autonomous mechanism. Alternatively, it could also function in a population-autonomous way via cell-cell contact or synaptic transmission.

Taken together, interneurons play a critical role in neuronal physiology, and their dysfunction or loss has been implicated in several neurological disorders such as Parkinson's disease (Stoker and Barker 2018). The detailed examination of interneuron behavior, their migration and integration is thus expected to give new insights into the pathophysiology of brain disorders, and importantly the therapeutic application of neuronal transplantation.

6. SUMMARY

In the mammalian brain, neurogenesis persists at two sites: in the subgranular zone of the hippocampal formation as well as in the subventricular zone (SVZ). Neuroblasts generated by SVZ neural stem cells migrate first tangentially along the rostral migratory stream (RMS) into the olfactory bulb (OB). There, they exit the RMS and switch to a slower and less directed radial migration mode. Once the different populations of SVZ neuroblasts have reached their respective final layer, they start to differentiate into interneurons and become either periglomerular (PGCs) or granule cells (GCs). Finally, they form functional, mostly inhibitory synaptic connections with preexisting neurons. Overall, postnatal OB neurogenesis provides unique, advantageous properties to study the general process of neurogenesis, as the distinct steps of the neurogenic sequence (stem cell amplification, migration, final differentiation) are clearly spatially separated.

Since the knowledge about differential regulation of distinct cell populations has to be broadened in order to develop clinical treatments for patients who suffer from neuronal cell loss, it is especially interesting to study in detail the two different types of adult-born interneurons during their migration and integration.

In vivo postnatal electroporation was used to specifically label and manipulate peripheral (PGCs) and deep (GCs) interneurons. Combining this method with *ex vivo* imaging on acute brain slices, we showed that PGCs and GCs follow a similar pattern during both tangential and radial migration. However, subtype specific differences exist between their spontaneous calcium activity as soon as they have left the RMS suggesting that membrane potential could play a role in the segregation process. We observed that OB neuroblast Ca^{2+} activity depends on depolarization generated through voltage gated calcium channels. Novel chemogenetic tools allowed us to manipulate the intrinsic activity of future OB interneurons and enabled us to test effects on migratory behavior and final distribution. Even though activity deprivation had no influence on the migratory parameters of neither of the two populations, cellular repartition was changed. Interestingly, this effect was subtype specific as a decrease in the absolute cell number could be exclusively detected for GCs while the amount of PGCs in the GL remained the same. Since we found significant repartition results for activity-blocked cells at multiple time points (8/10/12 dpe), we can exclude that our conclusions are only based on transient observations. Additionally, immunostaining for the apoptotic marker Caspase 3 confirmed our findings: the survival of activity-deprived GCs is decreased specifically in the GCL. Further evidence for a subtype specific regulation is given by the results that we obtained after increasing Ca^{2+} activity chemogenetically. Even though this experimental set-up is less physiological, it proves clearly that the two types of interneurones react differently to activation as PGCs decrease and GCs increase their displacement velocity.

Taken together, our findings contribute to a better understanding of how different neuronal stem cell derived populations are controlled in the adult brain. In the future, this might help to develop and improve neuronal cell replacement therapies.

7. BIBLIOGRAPHY

Abrahams, J. M., C. J. Lenart and M. E. Tobias (2009). "Temporal variation of induction neurogenesis in a rat model of transient middle cerebral artery occlusion." Neurol Res 31(5): 528-33.

Akerboom, J., T. W. Chen, T. J. Wardill, L. Tian, J. S. Marvin, S. Mutlu, N. C. Calderon, F. Esposti, B. G. Borghuis, X. R. Sun, A. Gordus, M. B. Orger, R. Portugues, F. Engert, J. J. Macklin, A. Filosa, A. Aggarwal, R. A. Kerr, R. Takagi, S. Kracun, E. Shigetomi, B. S. Khakh, H. Baier, L. Lagnado, S. S. Wang, C. I. Bargmann, B. E. Kimmel, V. Jayaraman, K. Svoboda, D. S. Kim, E. R. Schreiter and L. L. Looger (2012). "Optimization of a GCaMP calcium indicator for neural activity imaging." J Neurosci 32(40): 13819-40.

Alonso, M., C. Viollet, M. M. Gabellec, V. Meas-Yedid, J. C. Olivo-Marin and P. M. Lledo (2006). "Olfactory discrimination learning increases the survival of adult-born neurons in the olfactory bulb." J Neurosci 26(41): 10508-13.

Angelova, A., J. C. Platel, C. Beclin, H. Cremer and N. Core (2019). "Characterization of perinatally born glutamatergic neurons of the mouse olfactory bulb based on NeuroD6 expression reveals their resistance to sensory deprivation." J Comp Neurol 527(7): 1245-1260.

Armbruster, B. N., X. Li, M. H. Pausch, S. Herlitze and B. L. Roth (2007). "Evolving the lock to fit the key to create a family of G protein-coupled receptors potently activated by an inert ligand." Proc Natl Acad Sci U S A 104(12): 5163-8.

Arvidsson, A., T. Collin, D. Kirik, Z. Kokaia and O. Lindvall (2002). "Neuronal replacement from endogenous precursors in the adult brain after stroke." Nat Med 8(9): 963-70.

Azim, K., A. Hurtado-Chong, B. Fischer, N. Kumar, S. Zweifel, V. Taylor and O. Raineteau (2015). "Transcriptional Hallmarks of Heterogeneous Neural Stem Cell Niches of the Subventricular Zone." Stem Cells 33(7): 2232-42.

Barker, R. A., M. Parmar, A. Kirkeby, A. Bjorklund, L. Thompson and P. Brundin (2016). "Are Stem Cell-Based Therapies for Parkinson's Disease Ready for the Clinic in 2016?" J Parkinsons Dis 6(1): 57-63.

Batista-Brito, R., J. Close, R. Machold and G. Fishell (2008). "The distinct temporal origins of olfactory bulb interneuron subtypes." J Neurosci 28(15): 3966-75.

Beitz, J. M. (2014). "Parkinson's disease: a review." Front Biosci (Schol Ed) 6: 65-74.

Belluzzi, O., M. Benedusi, J. Ackman and J. J. LoTurco (2003). "Electrophysiological differentiation of new neurons in the olfactory bulb." J Neurosci 23(32): 10411-8.

Belvindrah, R., A. Nissant and P. M. Lledo (2011). "Abnormal neuronal migration changes the fate of developing neurons in the postnatal olfactory bulb." J Neurosci 31(20): 7551-62.

Berridge, M. J., M. D. Bootman and H. L. Roderick (2003). "Calcium signalling: dynamics, homeostasis and remodelling." Nat Rev Mol Cell Biol 4(7): 517-29.

Biebl, M., C. M. Cooper, J. Winkler and H. G. Kuhn (2000). "Analysis of neurogenesis and programmed cell death reveals a self-renewing capacity in the adult rat brain." Neurosci Lett 291(1): 17-20.

Boldrini, M., C. A. Fulmore, A. N. Tartt, L. R. Simeon, I. Pavlova, V. Poposka, G. B. Rosoklija, A. Stankov, V. Arango, A. J. Dwork, R. Hen and J. J. Mann (2018). "Human Hippocampal Neurogenesis Persists throughout Aging." Cell Stem Cell 22(4): 589-599 e5.

Bolteus, A. J. and A. Bordey (2004). "GABA release and uptake regulate neuronal precursor migration in the postnatal subventricular zone." J Neurosci 24(35): 7623-31.

Boutin, C., S. Diestel, A. Desoeuvre, M. C. Tiveron and H. Cremer (2008). "Efficient in vivo electroporation of the postnatal rodent forebrain." PLoS One 3(4): e1883.

Bovetti, S., Y. C. Hsieh, P. Bovolin, I. Perroteau, T. Kazunori and A. C. Puche (2007). "Blood vessels form a scaffold for neuroblast migration in the adult olfactory bulb." J Neurosci 27(22): 5976-80.

Bozoyan, L., J. Khlghatyan and A. Saghatelyan (2012). "Astrocytes control the development of the migration-promoting vasculature scaffold in the postnatal brain via VEGF signaling." J Neurosci 32(5): 1687-704.

Bradley, S. J., A. B. Tobin and R. Prihandoko (2018). "The use of chemogenetic approaches to study the physiological roles of muscarinic acetylcholine receptors in the central nervous system." Neuropharmacology 136(Pt C): 421-426.
Breton-Provencher, V., M. Lemasson, M. R. Peralta, 3rd and A. Saghatelyan (2009). "Interneurons produced in adulthood are required for the normal functioning of the olfactory bulb network and for the execution of selected olfactory behaviors." J Neurosci 29(48): 15245-57.
Breunig, J. J., J. I. Arellano, J. D. Macklis and P. Rakic (2007). "Everything that glitters isn't gold: a critical review of postnatal neural precursor analyses." Cell Stem Cell 1(6): 612-27.
Bugeon, S. (2017). “Regulation of radial migration and synaptic integration in the postnatal forebrain: links with neuronal activity.” (Dissertation, Biology).Aix-Marseille Université.
Carleton, A., L. T. Petreanu, R. Lansford, A. Alvarez-Buylla and P. M. Lledo (2003). "Becoming a new neuron in the adult olfactory bulb." Nat Neurosci 6(5): 507-18.
Chaker, Z., P. Codega and F. Doetsch (2016). "A mosaic world: puzzles revealed by adult neural stem cell heterogeneity." Wiley Interdiscip Rev Dev Biol 5(6): 640-658.
Chazal, G., P. Durbec, A. Jankovski, G. Rougon and H. Cremer (2000). "Consequences of neural cell adhesion molecule deficiency on cell migration in the rostral migratory stream of the mouse." J Neurosci 20(4): 1446-57.
Colman, A. and J. C. Burley (2001). "A legal and ethical tightrope. Science, ethics and legislation of stem cell research." EMBO Rep 2(1): 2-5.
Darcy, D. P. and J. S. Isaacson (2009). "L-type calcium channels govern calcium signaling in migrating newborn neurons in the postnatal olfactory bulb." J Neurosci 29(8): 2510-8.
de Chevigny, A., N. Core, P. Follert, M. Gaudin, P. Barbry, C. Beclin and H. Cremer (2012). "miR-7a regulation of Pax6 controls spatial origin of forebrain dopaminergic neurons." Nat Neurosci 15(8): 1120-6.
De Marco Garcia, N. V., T. Karayannis and G. Fishell (2011). "Neuronal activity is required for the development of specific cortical interneuron subtypes." Nature 472(7343): 351-5.
De Saint Jan, D., D. Hirnet, G. L. Westbrook and S. Charpak (2009). "External tufted cells drive the output of olfactory bulb glomeruli." J Neurosci 29(7): 2043-52.
Deng, W., J. B. Aimone and F. H. Gage (2010). "New neurons and new memories: how does adult hippocampal neurogenesis affect learning and memory?" Nat Rev Neurosci 11(5): 339-50.
Devore, S., L. C. Manella and C. Linster (2012). "Blocking muscarinic receptors in the olfactory bulb impairs performance on an olfactory short-term memory task." Front Behav Neurosci 6: 59.
Di Giorgi Gerevini, V. D., A. Caruso, I. Cappuccio, L. Ricci Vitiani, S. Romeo, C. Della Rocca, R. Gradini, D. Melchiorri and F. Nicoletti (2004). "The mGlu5 metabotropic glutamate receptor is expressed in zones of active neurogenesis of the embryonic and postnatal brain." Brain Res Dev Brain Res 150(1): 17-22.
Doetsch, F. and A. Alvarez-Buylla (1996). "Network of tangential pathways for neuronal migration in adult mammalian brain." Proc Natl Acad Sci U S A 93(25): 14895-900.
Doetsch, F., I. Caille, D. A. Lim, J. M. Garcia-Verdugo and A. Alvarez-Buylla (1999). "Subventricular zone astrocytes are neural stem cells in the adult mammalian brain." Cell 97(6): 703-16.
Emsley, J. G., J. R. Menezes, R. F. Madeiro Da Costa, A. M. Martinez and J. D. Macklis (2012). "Identification of radial glia-like cells in the adult mouse olfactory bulb." Exp Neurol 236(2): 283-97.
Eriksson, P. S., E. Perfilieva, T. Bjork-Eriksson, A. M. Alborn, C. Nordborg, D. A. Peterson and F. H. Gage (1998). "Neurogenesis in the adult human hippocampus." Nat Med 4(11): 1313-7.
Fernandez, M. E., S. Croce, C. Boutin, H. Cremer and O. Raineteau (2011). "Targeted electroporation of defined lateral ventricular walls: a novel and rapid method to study fate specification during postnatal forebrain neurogenesis." Neural Dev 6: 13.

Fuentealba, L. C., S. B. Rompani, J. I. Parraguez, K. Obernier, R. Romero, C. L. Cepko and A. Alvarez-Buylla (2015). "Embryonic Origin of Postnatal Neural Stem Cells." Cell 161(7): 1644-55.

Gage, F. H., S. B. Dunnett, P. Brundin, O. Isacson and A. Bjorklund (1983). "Intracerebral grafting of embryonic neural cells into the adult host brain: an overview of the cell suspension method and its application." Dev Neurosci 6(3): 137-51.

Garcia-Gonzalez, D., K. Khodosevich, Y. Watanabe, A. Rollenhagen, J. H. R. Lubke and H. Monyer (2017). "Serotonergic Projections Govern Postnatal Neuroblast Migration." Neuron 94(3): 534-549 e9.

Garner, A. R., D. C. Rowland, S. Y. Hwang, K. Baumgaertel, B. L. Roth, C. Kentros and M. Mayford (2012). "Generation of a synthetic memory trace." Science 335(6075): 1513-6.

Gascon, E., A. G. Dayer, M. O. Sauvain, G. Potter, B. Jenny, M. De Roo, E. Zgraggen, N. Demaurex, D. Muller and J. Z. Kiss (2006). "GABA regulates dendritic growth by stabilizing lamellipodia in newly generated interneurons of the olfactory bulb." J Neurosci 26(50): 12956-66.

Gengatharan, A., R. R. Bammann and A. Saghatelyan (2016). "The Role of Astrocytes in the Generation, Migration, and Integration of New Neurons in the Adult Olfactory Bulb." Front Neurosci 10: 149.

Geramita, M. and N. N. Urban (2017). "Differences in Glomerular-Layer-Mediated Feedforward Inhibition onto Mitral and Tufted Cells Lead to Distinct Modes of Intensity Coding." J Neurosci 37(6): 1428-1438.

Giachino, C., S. De Marchis, C. Giampietro, R. Parlato, I. Perroteau, G. Schutz, A. Fasolo and P. Peretto (2005). "cAMP response element-binding protein regulates differentiation and survival of newborn neurons in the olfactory bulb." J Neurosci 25(44): 10105-18.

Gould, E. (2007). "How widespread is adult neurogenesis in mammals?" Nat Rev Neurosci 8(6): 481-8.

Grade, S. and M. Gotz (2017). "Neuronal replacement therapy: previous achievements and challenges ahead." NPJ Regen Med 2: 29.

Gritti, A., A. L. Vescovi and R. Galli (2002). "Adult neural stem cells: plasticity and developmental potential." J Physiol Paris 96(1-2): 81-90.

Hao, L., Z. Zou, H. Tian, Y. Zhang, H. Zhou and L. Liu (2014). "Stem cell-based therapies for ischemic stroke." Biomed Res Int 2014: 468748.

Hellwig, S., I. Hack, B. Zucker, B. Brunne and D. Junghans (2012). "Reelin together with ApoER2 regulates interneuron migration in the olfactory bulb." PLoS One 7(11): e50646.

Hurni, N., M. Kolodziejczak, U. Tomasello, J. Badia, M. Jacobshagen, J. Prados and A. Dayer (2017). "Transient Cell-intrinsic Activity Regulates the Migration and Laminar Positioning of Cortical Projection Neurons." Cereb Cortex 27(5): 3052-3063.

Kaneko, N., H. Okano and K. Sawamoto (2006). "Role of the cholinergic system in regulating survival of newborn neurons in the adult mouse dentate gyrus and olfactory bulb." Genes Cells 11(10): 1145-59.

Karow, M., R. Sanchez, C. Schichor, G. Masserdotti, F. Ortega, C. Heinrich, S. Gascon, M. A. Khan, D. C. Lie, A. Dellavalle, G. Cossu, R. Goldbrunner, M. Gotz and B. Berninger (2012). "Reprogramming of pericyte-derived cells of the adult human brain into induced neuronal cells." Cell Stem Cell 11(4): 471-6.

Kato, T., K. Yokouchi, K. Kawagishi, N. Fukushima, T. Miwa and T. Moriizumi (2000). "Fate of newly formed periglomerular cells in the olfactory bulb." Acta Otolaryngol 120(7): 876-9.

Kelsch, W., C. W. Lin and C. Lois (2008). "Sequential development of synapses in dendritic domains during adult neurogenesis." Proc Natl Acad Sci U S A 105(43): 16803-8.

Kelsch, W., C. W. Lin, C. P. Mosley and C. Lois (2009). "A critical period for activity-dependent synaptic development during olfactory bulb adult neurogenesis." J Neurosci 29(38): 11852-8.

Kempermann, G., F. H. Gage, L. Aigner, H. Song, M. A. Curtis, S. Thuret, H. G. Kuhn, S. Jessberger, P. W. Frankland, H. A. Cameron, E. Gould, R. Hen, D. N. Abrous, N.

Toni, A. F. Schinder, X. Zhao, P. J. Lucassen and J. Frisen (2018). "Human Adult Neurogenesis: Evidence and Remaining Questions." Cell Stem Cell 23(1): 25-30.
Khodosevich, K., J. Alfonso and H. Monyer (2013). "Dynamic changes in the transcriptional profile of subventricular zone-derived postnatally born neuroblasts." Mech Dev 130(6-8): 424-32.
Kim, W. R., Y. Kim, B. Eun, O. H. Park, H. Kim, K. Kim, C. H. Park, S. Vinsant, R. W. Oppenheim and W. Sun (2007). "Impaired migration in the rostral migratory stream but spared olfactory function after the elimination of programmed cell death in Bax knock-out mice." J Neurosci 27(52): 14392-403.
Kirschenbaum, B., F. Doetsch, C. Lois and A. Alvarez-Buylla (1999). "Adult subventricular zone neuronal precursors continue to proliferate and migrate in the absence of the olfactory bulb." J Neurosci 19(6): 2171-80.
Kohwi, M., N. Osumi, J. L. Rubenstein and A. Alvarez-Buylla (2005). "Pax6 is required for making specific subpopulations of granule and periglomerular neurons in the olfactory bulb." J Neurosci 25(30): 6997-7003.
Komuro, H. and P. Rakic (1992). "Selective role of N-type calcium channels in neuronal migration." Science 257(5071): 806-9.
Kosaka, T. and K. Kosaka (2008). "Tyrosine hydroxylase-positive GABAergic juxtaglomerular neurons are the main source of the interglomerular connections in the mouse main olfactory bulb." Neurosci Res 60(3): 349-54.
Kovalchuk, Y., R. Homma, Y. Liang, A. Maslyukov, M. Hermes, T. Thestrup, O. Griesbeck, J. Ninkovic, L. B. Cohen and O. Garaschuk (2015). "In vivo odourant response properties of migrating adult-born neurons in the mouse olfactory bulb." Nat Commun 6: 6349.
Lazarini, F. and P. M. Lledo (2011). "Is adult neurogenesis essential for olfaction?" Trends Neurosci 34(1): 20-30.
Lehner, B., B. Sandner, J. Marschallinger, C. Lehner, T. Furtner, S. Couillard-Despres, F. J. Rivera, G. Brockhoff, H. C. Bauer, N. Weidner and L. Aigner (2011). "The dark side of BrdU in neural stem cell biology: detrimental effects on cell cycle, differentiation and survival." Cell Tissue Res 345(3): 313-28.
Liang, Y., K. Li, K. Riecken, A. Maslyukov, D. Gomez-Nicola, Y. Kovalchuk, B. Fehse and O. Garaschuk (2016). "Long-term in vivo single-cell tracking reveals the switch of migration patterns in adult-born juxtaglomerular cells of the mouse olfactory bulb." Cell Res 26(7): 805-21.
Lin, C. W., S. Sim, A. Ainsworth, M. Okada, W. Kelsch and C. Lois (2010). "Genetically increased cell-intrinsic excitability enhances neuronal integration into adult brain circuits." Neuron 65(1): 32-9.
Liu, G. and Y. Rao (2003). "Neuronal migration from the forebrain to the olfactory bulb requires a new attractant persistent in the olfactory bulb." J Neurosci 23(16): 6651-9.
Livneh, Y., N. Feinstein, M. Klein and A. Mizrahi (2009). "Sensory input enhances synaptogenesis of adult-born neurons." J Neurosci 29(1): 86-97.
Lledo, P. M. and A. Saghatelyan (2005). "Integrating new neurons into the adult olfactory bulb: joining the network, life-death decisions, and the effects of sensory experience." Trends Neurosci 28(5): 248-54.
Lonze, B. E. and D. D. Ginty (2002). "Function and regulation of CREB family transcription factors in the nervous system." Neuron 35(4): 605-23.
Malvaut, S., S. Gribaudo, D. Hardy, L. S. David, L. Daroles, S. Labrecque, M. A. Lebel-Cormier, Z. Chaker, D. Cote, P. De Koninck, M. Holzenberger, A. Trembleau, I. Caille and A. Saghatelyan (2017). "CaMKIIalpha Expression Defines Two Functionally Distinct Populations of Granule Cells Involved in Different Types of Odor Behavior." Curr Biol 27(21): 3315-3329 e6.
Mandairon, N., F. Jourdan and A. Didier (2003). "Deprivation of sensory inputs to the olfactory bulb up-regulates cell death and proliferation in the subventricular zone of adult mice." Neuroscience 119(2): 507-16.
Mandairon, N., J. Sacquet, F. Jourdan and A. Didier (2006). "Long-term fate and distribution of newborn cells in the adult mouse olfactory bulb: Influences of olfactory deprivation." Neuroscience 141(1): 443-51.

Maresh, A., D. Rodriguez Gil, M. C. Whitman and C. A. Greer (2008). "Principles of glomerular organization in the human olfactory bulb--implications for odor processing." PLoS One 3(7): e2640.
Martini, F. J. and M. Valdeolmillos (2010). "Actomyosin contraction at the cell rear drives nuclear translocation in migrating cortical interneurons." J Neurosci 30(25): 8660-70.
Maslyukov, A., K. Li, X. Su, Y. Kovalchuk and O. Garaschuk (2018). "Spontaneous calcium transients in the immature adult-born neurons of the olfactory bulb." Cell Calcium 74: 43-52.
Mechawar, N., A. Saghatelyan, R. Grailhe, L. Scoriels, G. Gheusi, M. M. Gabellec, P. M. Lledo and J. P. Changeux (2004). "Nicotinic receptors regulate the survival of newborn neurons in the adult olfactory bulb." Proc Natl Acad Sci U S A 101(26): 9822-6.
Mejia-Gervacio, S., K. Murray and P. M. Lledo (2011). "NKCC1 controls GABAergic signaling and neuroblast migration in the postnatal forebrain." Neural Dev 6: 4.
Merkle, F. T. and A. Alvarez-Buylla (2006). "Neural stem cells in mammalian development." Curr Opin Cell Biol 18(6): 704-9.
Merkle, F. T., Z. Mirzadeh and A. Alvarez-Buylla (2007). "Mosaic organization of neural stem cells in the adult brain." Science 317(5836): 381-4.
Metin, C., J. P. Baudoin, S. Rakic and J. G. Parnavelas (2006). "Cell and molecular mechanisms involved in the migration of cortical interneurons." Eur J Neurosci 23(4): 894-900.
Michelsen, K. A., S. Acosta-Verdugo, M. Benoit-Marand, I. Espuny-Camacho, N. Gaspard, B. Saha, A. Gaillard and P. Vanderhaeghen (2015). "Area-specific reestablishment of damaged circuits in the adult cerebral cortex by cortical neurons derived from mouse embryonic stem cells." Neuron 85(5): 982-97.
Mombaerts, P. (2004). "Genes and ligands for odorant, vomeronasal and taste receptors." Nat Rev Neurosci 5(4): 263-78.
Mombaerts, P., F. Wang, C. Dulac, S. K. Chao, A. Nemes, M. Mendelsohn, J. Edmondson and R. Axel (1996). "Visualizing an olfactory sensory map." Cell 87(4): 675-86.
Mori, K., K. Kishi and H. Ojima (1983). "Distribution of dendrites of mitral, displaced mitral, tufted, and granule cells in the rabbit olfactory bulb." J Comp Neurol 219(3): 339-55.
Mori, K. and H. Sakano (2011). "How is the olfactory map formed and interpreted in the mammalian brain?" Annu Rev Neurosci 34: 467-99.
Mori, K. and Y. Yoshihara (1995). "Molecular recognition and olfactory processing in the mammalian olfactory system." Prog Neurobiol 45(6): 585-619.
Murase, S. and A. F. Horwitz (2002). "Deleted in colorectal carcinoma and differentially expressed integrins mediate the directional migration of neural precursors in the rostral migratory stream." J Neurosci 22(9): 3568-79.
Nagayama, S., R. Homma and F. Imamura (2014). "Neuronal organization of olfactory bulb circuits." Front Neural Circuits 8: 98.
Nagayama, S., Y. K. Takahashi, Y. Yoshihara and K. Mori (2004). "Mitral and tufted cells differ in the decoding manner of odor maps in the rat olfactory bulb." J Neurophysiol 91(6): 2532-40.
Nakai, J., M. Ohkura and K. Imoto (2001). "A high signal-to-noise Ca(2+) probe composed of a single green fluorescent protein." Nat Biotechnol 19(2): 137-41.
Nakatomi, H., T. Kuriu, S. Okabe, S. Yamamoto, O. Hatano, N. Kawahara, A. Tamura, T. Kirino and M. Nakafuku (2002). "Regeneration of hippocampal pyramidal neurons after ischemic brain injury by recruitment of endogenous neural progenitors." Cell 110(4): 429-41.
Nam, S. C., Y. Kim, D. Dryanovski, A. Walker, G. Goings, K. Woolfrey, S. S. Kang, C. Chu, A. Chenn, F. Erdelyi, G. Szabo, P. Hockberger and F. G. Szele (2007). "Dynamic features of postnatal subventricular zone cell motility: a two-photon time-lapse study." J Comp Neurol 505(2): 190-208.

Nguyen, L., A. Besson, J. I. Heng, C. Schuurmans, L. Teboul, C. Parras, A. Philpott, J. M. Roberts and F. Guillemot (2006). "p27kip1 independently promotes neuronal differentiation and migration in the cerebral cortex." Genes Dev 20(11): 1511-24.

Nguyen-Ba-Charvet, K. T., N. Picard-Riera, M. Tessier-Lavigne, A. Baron-Van Evercooren, C. Sotelo and A. Chedotal (2004). "Multiple roles for slits in the control of cell migration in the rostral migratory stream." J Neurosci 24(6): 1497-506.

Obernier, K., A. Cebrian-Silla, M. Thomson, J. I. Parraguez, R. Anderson, C. Guinto, J. Rodas Rodriguez, J. M. Garcia-Verdugo and A. Alvarez-Buylla (2018). "Adult Neurogenesis Is Sustained by Symmetric Self-Renewal and Differentiation." Cell Stem Cell 22(2): 221-234.e8.

Paredes, M. F., D. James, S. Gil-Perotin, H. Kim, J. A. Cotter, C. Ng, K. Sandoval, D. H. Rowitch, D. Xu, P. S. McQuillen, J. M. Garcia-Verdugo, E. J. Huang and A. Alvarez-Buylla (2016a). "Extensive migration of young neurons into the infant human frontal lobe." Science 354(6308).

Paredes, M. F., S. F. Sorrells, J. M. Garcia-Verdugo and A. Alvarez-Buylla (2016b). "Brain size and limits to adult neurogenesis." J Comp Neurol 524(3): 646-64.

Petreanu, L. and A. Alvarez-Buylla (2002). "Maturation and death of adult-born olfactory bulb granule neurons: role of olfaction." J Neurosci 22(14): 6106-13.

Pinching, A. J. and T. P. Powell (1971). "The neuropil of the periglomerular region of the olfactory bulb." J Cell Sci 9(2): 379-409.

Platel, J. C., Angelova, A., Bugeon, S., Wallace, J., Ganay, T., Chudotvorova, I., Deloulme, J. C., Béclin, C., Tiveron, M. C., Coré, N., Murthy, V. N., & Cremer, H. (2019). “Neuronal integration in the adult mouse olfactory bulb is a non-selective addition process.” eLife, 8, e44830. https://doi.org/10.7554/eLife.44830

Platel, J. C., K. A. Dave and A. Bordey (2008a). "Control of neuroblast production and migration by converging GABA and glutamate signals in the postnatal forebrain." J Physiol 586(16): 3739-43.

Platel, J. C., K. A. Dave, V. Gordon, B. Lacar, M. E. Rubio and A. Bordey (2010). "NMDA receptors activated by subventricular zone astrocytic glutamate are critical for neuroblast survival prior to entering a synaptic network." Neuron 65(6): 859-72.

Platel, J. C., T. Heintz, S. Young, V. Gordon and A. Bordey (2008b). "Tonic activation of GLUK5 kainate receptors decreases neuroblast migration in whole-mounts of the subventricular zone." J Physiol 586(16): 3783-93.

Platel, J. C., B. Lacar and A. Bordey (2007). "GABA and glutamate signaling: homeostatic control of adult forebrain neurogenesis." J Mol Histol 38(6): 602-10.

Porter, A. G. and R. U. Janicke (1999). "Emerging roles of caspase-3 in apoptosis." Cell Death Differ 6(2): 99-104.

Pothayee, N., D. M. Cummings, T. J. Schoenfeld, S. Dodd, H. A. Cameron, L. Belluscio and A. P. Koretsky (2017). "Magnetic resonance imaging of odorant activity-dependent migration of neural precursor cells and olfactory bulb growth." Neuroimage 158: 232-241.

Ragancokova, D., E. Rocca, A. M. Oonk, H. Schulz, E. Rohde, J. Bednarsch, I. Feenstra, R. J. Pennings, H. Wende and A. N. Garratt (2014). "TSHZ1-dependent gene regulation is essential for olfactory bulb development and olfaction." J Clin Invest 124(3): 1214-27.

Ranger, A. M., B. A. Malynn and S. J. Korsmeyer (2001). "Mouse models of cell death." Nat Genet 28(2): 113-8.

Rizek, P., N. Kumar and M. S. Jog (2016). "An update on the diagnosis and treatment of Parkinson disease." CMAJ 188(16): 1157-1165.

Rochefort, C., G. Gheusi, J. D. Vincent and P. M. Lledo (2002). "Enriched odor exposure increases the number of newborn neurons in the adult olfactory bulb and improves odor memory." J Neurosci 22(7): 2679-89.

Rochefort, C. and P. M. Lledo (2005). "Short-term survival of newborn neurons in the adult olfactory bulb after exposure to a complex odor environment." Eur J Neurosci 22(11): 2863-70.

Saghatelyan, A., A. de Chevigny, M. Schachner and P. M. Lledo (2004). "Tenascin-R mediates activity-dependent recruitment of neuroblasts in the adult mouse forebrain." Nat Neurosci 7(4): 347-56.

Saghatelyan, A., P. Roux, M. Migliore, C. Rochefort, D. Desmaisons, P. Charneau, G. M. Shepherd and P. M. Lledo (2005). "Activity-dependent adjustments of the inhibitory network in the olfactory bulb following early postnatal deprivation." Neuron 46(1): 103-16.

Samuels, B. A. and R. Hen (2011). "Neurogenesis and affective disorders." Eur J Neurosci 33(6): 1152-9.

Sanai, N., A. D. Tramontin, A. Quinones-Hinojosa, N. M. Barbaro, N. Gupta, S. Kunwar, M. T. Lawton, M. W. McDermott, A. T. Parsa, J. Manuel-Garcia Verdugo, M. S. Berger and A. Alvarez-Buylla (2004). "Unique astrocyte ribbon in adult human brain contains neural stem cells but lacks chain migration." Nature 427(6976): 740-4.

Sato, M., M. Kawano, M. Ohkura, K. Gengyo-Ando, J. Nakai and Y. Hayashi (2015). "Generation and Imaging of Transgenic Mice that Express G-CaMP7 under a Tetracycline Response Element." PLoS One 10(5): e0125354.

Sawada, M., N. Kaneko, H. Inada, H. Wake, Y. Kato, Y. Yanagawa, K. Kobayashi, T. Nemoto, J. Nabekura and K. Sawamoto (2011). "Sensory input regulates spatial and subtype-specific patterns of neuronal turnover in the adult olfactory bulb." J Neurosci 31(32): 11587-96.

Schaar, B. T. and S. K. McConnell (2005). "Cytoskeletal coordination during neuronal migration." Proc Natl Acad Sci U S A 102(38): 13652-7.

Seri, B., J. M. Garcia-Verdugo, L. Collado-Morente, B. S. McEwen and A. Alvarez-Buylla (2004). "Cell types, lineage, and architecture of the germinal zone in the adult dentate gyrus." J Comp Neurol 478(4): 359-78.

Shepherd, G. M. (2004). The Synaptic Organization of the Brain. New York, Oxford University Press.

Shi, J., L. F. Parada and S. G. Kernie (2005). "Bax limits adult neural stem cell persistence through caspase and IP3 receptor activation." Cell Death Differ 12(12): 1601-12.

Sorrells, S. F., M. F. Paredes, A. Cebrian-Silla, K. Sandoval, D. Qi, K. W. Kelley, D. James, S. Mayer, J. Chang, K. I. Auguste, E. F. Chang, A. J. Gutierrez, A. R. Kriegstein, G. W. Mathern, M. C. Oldham, E. J. Huang, J. M. Garcia-Verdugo, Z. Yang and A. Alvarez-Buylla (2018). "Human hippocampal neurogenesis drops sharply in children to undetectable levels in adults." Nature 555(7696): 377-381.

Southwell, D. G., M. F. Paredes, R. P. Galvao, D. L. Jones, R. C. Froemke, J. Y. Sebe, C. Alfaro-Cervello, Y. Tang, J. M. Garcia-Verdugo, J. L. Rubenstein, S. C. Baraban and A. Alvarez-Buylla (2012). "Intrinsically determined cell death of developing cortical interneurons." Nature 491(7422): 109-13.

Spitzer, N. C. (2006). "Electrical activity in early neuronal development." Nature 444(7120): 707-12.

Stoker, T. B. and R. A. Barker (2018). "Regenerative Therapies for Parkinson's Disease: An Update." BioDrugs 32(4): 357-366.

Tabata, H. and K. Nakajima (2003). "Multipolar migration: the third mode of radial neuronal migration in the developing cerebral cortex." J Neurosci 23(31): 9996-10001.

Takahashi, K. and S. Yamanaka (2006). "Induction of pluripotent stem cells from mouse embryonic and adult fibroblast cultures by defined factors." Cell 126(4): 663-76.

Tambasco, N., M. Romoli and P. Calabresi (2018). "Levodopa in Parkinson's Disease: Current Status and Future Developments." Curr Neuropharmacol 16(8): 1239-1252.

Tatti, R., K. Bhaukaurally, O. Gschwend, R. P. Seal, R. H. Edwards, I. Rodriguez and A. Carleton (2014). "A population of glomerular glutamatergic neurons controls sensory information transfer in the mouse olfactory bulb." Nat Commun 5: 3791.

Taupin, P. (2006). "Therapeutic potential of adult neural stem cells." Recent Pat CNS Drug Discov 1(3): 299-303.

Urban, D. J. and B. L. Roth (2015). "DREADDs (designer receptors exclusively activated by designer drugs): chemogenetic tools with therapeutic utility." Annu Rev Pharmacol Toxicol 55: 399-417.

Wachowiak, M. and M. T. Shipley (2006). "Coding and synaptic processing of sensory information in the glomerular layer of the olfactory bulb." Semin Cell Dev Biol 17(4): 411-23.

Waclaw, R. R., Z. J. Allen, 2nd, S. M. Bell, F. Erdelyi, G. Szabo, S. S. Potter and K. Campbell (2006). "The zinc finger transcription factor Sp8 regulates the generation and diversity of olfactory bulb interneurons." Neuron 49(4): 503-16.

Wang, D. D., D. D. Krueger and A. Bordey (2003). "GABA depolarizes neuronal progenitors of the postnatal subventricular zone via GABAA receptor activation." J Physiol 550(Pt 3): 785-800.

Whitman, M. C., W. Fan, L. Rela, D. J. Rodriguez-Gil and C. A. Greer (2009). "Blood vessels form a migratory scaffold in the rostral migratory stream." J Comp Neurol 516(2): 94-104.

Whitman, M. C. and C. A. Greer (2007). "Adult-generated neurons exhibit diverse developmental fates." Dev Neurobiol 67(8): 1079-93.

Winner, B., C. M. Cooper-Kuhn, R. Aigner, J. Winkler and H. G. Kuhn (2002). "Long-term survival and cell death of newly generated neurons in the adult rat olfactory bulb." Eur J Neurosci 16(9): 1681-9.

Wong, F. K., K. Bercsenyi, V. Sreenivasan, A. Portales, M. Fernandez-Otero and O. Marin (2018). "Pyramidal cell regulation of interneuron survival sculpts cortical networks." Nature 557(7707): 668-673.

Xiong, W. and W. R. Chen (2002). "Dynamic gating of spike propagation in the mitral cell lateral dendrites." Neuron 34(1): 115-26.

Yagita, Y., T. Sakurai, H. Tanaka, K. Kitagawa, D. R. Colman and W. Shan (2009). "N-cadherin mediates interaction between precursor cells in the subventricular zone and regulates further differentiation." J Neurosci Res 87(15): 3331-42.

Yamaguchi, M. and K. Mori (2005). "Critical period for sensory experience-dependent survival of newly generated granule cells in the adult mouse olfactory bulb." Proc Natl Acad Sci U S A 102(27): 9697-702.

Zigmond, M. J., E. D. Abercrombie, T. W. Berger, A. A. Grace and E. M. Stricker (1990). "Compensations after lesions of central dopaminergic neurons: some clinical and basic implications." Trends Neurosci 13(7): 290-6.

8. THESES

I. PGCs and GCs follow a similar pattern during radial and tangential migration.
II. There exists a considerable difference between subtypes at the level of spontaneous Ca^{2+} activity after the RMS exit.
III. Depolarization is responsible for generating Ca^{2+} activity.
IV. Activity deprivation does not influence the migratory behavior of GCs.
V. GC-repartition in the OB is modified when activity is blocked.
VI. Activity deprivation of future GCs leads to an increase of cell death only in their final layer.

PUBLICATION

2630 • The Journal of Neuroscience, March 24, 2021 • 41(12):2630–2644

Development/Plasticity/Repair

Intrinsic Neuronal Activity during Migration Controls the Recruitment of Specific Interneuron Subtypes in the Postnatal Mouse Olfactory Bulb

Stéphane Bugeon, Clara Haubold, Alexandre Ryzynski, Harold Cremer, and Jean-Claude Platel
Aix-Marseille University, Centre National de la Recherche Scientifique, Institut de Biologie du Développement de Marseille, Unité Mixte de Recherche 7288, 13009 Marseille, France

Neuronal activity has been identified as a key regulator of neuronal network development, but the impact of activity on migration and terminal positioning of interneuron subtypes is poorly understood. The absence of early subpopulation markers and the presence of intermingled migratory and postmigratory neurons make the developing cerebral cortex a difficult model to answer these questions. Postnatal neurogenesis in the subventricular zone (SVZ) offers a more accessible and compartmentalized model. Neural stem cells regionalized along the border of the lateral ventricle produce two main subtypes of neural progenitors, granule cells and periglomerular neurons that migrate tangentially in the rostral migratory stream (RMS) before migrating radially in the olfactory bulb (OB) layers. Here, we used targeted postnatal electroporation to compare the migration of these two populations in male and female mice. We do not observe any obvious differences regarding the mode of tangential or radial migration between these two subtypes. However, we find a striking increase of intrinsic calcium activity in granule cell precursors (GC-Ps) when they switch from tangential to radial migration. By decreasing neuronal excitability in GC-Ps, we find that neuronal activity has little effect on migration but is required for normal positioning and survival of GC-Ps in the OB layers. Strikingly, decreasing activity of periglomerular neuron precursors (PGN-Ps) did not impact their positioning or survival. Altogether these findings suggest that neuronal excitability plays a subtype specific role during the late stage of migration of postnatally born OB interneurons.

Key words: postnatal neurogenesis; migration; SVZ; olfactory bulb; neuronal activity

Significance Statement

While neuronal activity is a critical factor regulating different aspects of neurogenesis, it has been challenging to study its role during the migration of different neuronal subpopulations. Here, we use postnatal targeted electroporation to label and manipulate the two main olfactory bulb (OB) interneuron subpopulations during their migration: granule cell and periglomerular neuron precursors (PGN-Ps). We find a very striking increase of calcium activity only in granule cell precursors (GC-Ps) when they switch from tangential to radial migration. Interestingly, blocking activity in GC-Ps affected mainly their positioning and survival while PGN-Ps were not affected. These results suggest that neuronal activity is required specifically for the recruitment of GC-Ps in the OB layers.

Received July 22, 2020; revised Jan. 11, 2021; accepted Jan. 15, 2021.
#H.C. and J.-C.P. are co-last authors.
Author contributions: S.B., H.C., and J.-C.P. designed research; S.B., C.H., A.R., and J.-C.P. performed research; H.C. and J.-C.P. contributed unpublished reagents/analytic tools; S.B., C.H., A.R., and J.-C.P. analyzed data; S.B., H.C., and J.-C.P. wrote the paper.
Acknowledgements: We thank the Cremer lab, Jenelle Wallace, and Dominique Debanne for critical reading of the manuscript. We also thank the local PiCSL-FBI core facility [Institut de Biologie du Développement de Marseille (IBDM), Aix-Marseille University] supported by the French National Research Agency through the "Investments for the Future" program (France-BioImaging, ANR-10-INBS-04) as well as the IBDM animal facilities. This work was supported by Fédération pour la Recherche sur le Cerveau (H.C.), the Agence National pour la Recherche Grant ANR-13-BSV4-0013, ANR-17-CE16-0025-02 Fondation pour la Recherche Medicale Grants ING20150532361, Equ 201903007806 (to H.C.) and FDT20160435597 (to S.B.), and the Fondation de France Grant FDF70959 (to H.C.).
The authors declare no competing financial interests.
Correspondence should be addressed to Jean-Claude Platel at jean-claude.platel@univ-amu.fr.
https://doi.org/10.1523/JNEUROSCI.1960-20.2021

Introduction

Neuronal networks comprise different subtypes of interconnected neurons in a precise region-specific stoichiometry and organization. For example, in the mouse neocortex ~85% of all neurons are glutamatergic, whereas 15% are inhibitory GABAergic interneurons. The mechanisms that regulate the migration and recruitment of appropriate numbers of inhibitory neurons in precise brain regions remain largely unknown.

Electrical activity has been identified as a key regulator of network development. For example, activity controls numerical population matching in the cortex. Electrical input from pyramidal neurons to interneurons determines their survival or death thereby controlling the amount of interneurons to the needs of the principal neuron pool (Lodato et al., 2011; Wong et al., 2018).

In addition, there are evidence that electrical activity impacts on neuronal migration and consequently final positioning of cortical interneurons. For example, specific subpopulations of interneurons show a shift in laminar positioning when their activity is inhibited by the expression of the Kir2.1 channel (De Marco García, 2011).

However, despite such first observations, the specific role of neuronal activity during migration is not well understood. This is mainly due to of a paucity of early markers, that allow the identification of interneuron subpopulations already during their migratory phase and before reaching terminal positions. Moreover, specifically during corticogenesis, migratory and postmigratory populations are intermingled and homogeneous compartments are not identifiable. Thus, to understand the impact of activity on interneuron migration and terminal positioning, lineage tracing and developmental models with clear compartmentalization are needed.

Activity has also been shown to be a major regulation factor of interneuron integration in the olfactory system. Indeed, in the postnatal and adult rodent, new interneurons are produced throughout life (Lois and Alvarez-Buylla, 1994) and permanently added to the preexisting circuitry of the olfactory bulb (OB; Platel et al., 2019). In this system neural stem cells localized in the ventricular-subventricular zone (V-SVZ) along lateral ventricles generate neuronal precursors that migrate tangentially via the rostral migratory stream (RMS) into the core of the OB. Here, they detach from the RMS and switch from tangential to radial migration. Granule cell precursors (GC-P) migrate short distances and settle in the granule cell layer (GCL). These represent ~90% of all new neurons. Periglomerular neuron precursors (PGN-Ps) traverse the entire GCL to reach the peripheral glomerular layer (GL) before their integration. Importantly, the generation of these interneuron subtypes relies on the regionalization of the stem cell compartment in the V-SVZ. For example, GCs are lineage related to stem cells localized in lateral aspects of the ventricular wall, whereas dopaminergic/GABAergic, calretinin-positive/GABAergic, and pure GABAergic PGN are predominantly derived from stem cells in the dorsal and medial walls (Merkle et al., 2007; Fernández et al., 2011). Several lines of evidence suggest that, like in the cortex, activity is a major regulator of this interneuron integration process. For example, increasing neuronal activity via olfactory training (Mouret et al., 2008) or overexpressing the bacterial sodium channel NaChBac (Lin et al., 2010) enhanced the number of newborn neurons integrated. By contrast, sensory deprivation via naris occlusion decreased the survival of newborn neurons in the OB (Saghatelyan et al., 2005; Yamaguchi and Mori, 2005; Platel et al., 2019).

Altogether, the highly compartmentalized environment of the OB neurogenic system provides the possibility to trace interneuron subpopulations destined for different target layers and study their specific migratory behavior and activity patterns during tangential and radial phases. Finally, because of the fact that defined stem cell pools can be efficiently manipulated, it is particularly well suited to analyze and manipulate activity patterns.

Here, we use targeted brain electroporation to label specifically the lateral and medial ventricular wall and show that this approach labels with high predominance either future GCs or PGNs. We compared their migratory behavior and neuronal activity at high resolution, combining acute forebrain slices with two-photon microscopy. Tangential and radial migration were indistinguishable between both populations. However, GC-P showed increased calcium activity already in the distal RMS, before exit and onset of radial migration. Moreover, we find that inhibition of activity in GC-P but not in PGN-P affects the transition from tangential to radial migration, their final positioning and survival. Our results indicate that activity during migration is specifically implicated in the recruitment process of GC-P before they enter the OB neuronal network. In constrast, the migration of PGN-P to the OB network seems largely independent on activity.

Materials and Methods

Animals

All mice were treated according to protocols approved by the French Ethical Committee (#5223-2016042717181477 v2). Mice were group housed in regular cages under standard conditions, with up to five mice per cage on a 12/12 h light/dark cycle. CD1 (Charles River), Ai14 (Rosa tdTomato) transgenic reporter (The Jackson Laboratory, stock #007914) and GCaMP6s (The Jackson Laboratory, stock #028866) mice were used. All experiments were performed on males and females.

Plasmids and mRNA preparation

pCAG-Kir2.1-T2A-tdTomato (https://www.addgene.org/60598/; Xue et al., 2014), pCAG-Kir2.1Mut-T2A-tdTomato (https://www.addgene.org/60644/). The pCAGGS-EGFP vectors was derived from pCX-MCS2 (Morin et al., 2007). All plasmids were used at a concentration of 5 µg/µl (0.1% Fast Green). mRNAs were provided by Miltenyi Biotec (Miltenyi Biotec): CRE Recombinase mRNA (130-101-113; a kind gift from A. Bosio, Miltenyi Biotec). For electroporation, mRNAs were diluted in RNase-free PBS at a concentration of 0.5 µg/µl (same range of molarity compared with 5 µg/µl DNA plasmid).

Immunohistochemistry and image analysis

For histologic analysis, pups were deeply xylazine/ketamine anaesthetized. Perfusion was performed intracardiacally with a solution of 4% paraformaldehyde in PBS. The brain was dissected out and incubated overnight in the same fixative at 4°C. Sections were cut at 50 µm using a microtome (Microm). Floating sections were first incubated overnight at 4°C with the following primary antibody: cleaved-caspase 3 antibody (cell signaling technology), before incubation 2 h at room temperature with the corresponding fluorescent labeled secondary antibody. Before mounting, cell nuclei were stained with Hoechst 33258. Optical images were taken either using a fluorescence microscope (Axioplan2, ApoTome System, Zeiss) or a laser confocal scanning microscope (LSM510 or LSM780, Zeiss).

For quantifications of cell distribution, layers were manually drawn based on the nuclear staining. Then, the CellCounter plugin from ImageJ was used to manually count cells in each layer. All experiments and quantifications were performed blindly to experimental groups.

Postnatal electroporation

Postnatal electroporation was performed as described previously (Boutin et al., 2008; Bugeon et al., 2017). Briefly, postnatal day (P)0–P1 pups were anesthetized by hypothermia. A glass micropipette was inserted into the lateral ventricle, and 2 µl of plasmid or RNA solution was injected by expiratory pressure using an aspirator tube assembly (Drummond). Successfully injected animals were subjected to five 95V electrical pulses (50 ms, separated by 950-ms intervals) using the CUY21 edit device (Nepagene) and 10 mm tweezer electrodes (CUY650P10, Nepagene) coated with conductive gel (Control Graphique Medical). Electrodes were oriented according to the desired targeting: for an electroporation of the left hemisphere, the cathode was placed on the left side and anode on the right side for lateral electroporation; for medial electroporation cathode on the right side and anode on the left side. Because of the lower number of cells generated from the medial V-SVZ, electroporations were preferentially performed at P0, when it is the most efficient. Electroporated animals were then reanimated in a 37°C incubator before returning to the mother.

Acute brain slices

P5–P10 animals were ketamine/xylazine anesthetized, and perfused intracardiacally with cold (4°C), oxygenated (95% O_2/5% CO_2) dissection solution (250 mM sucrose, 3 mM KCl, 1.25 mM NaH_2PO_4, 3 mM $MgSO_4$, 10 mM D-glucose, 26 mM $NaHCO_3$, and 0.5 mM $CaCl_2$). The brain was then quickly removed, and glued on a vibratome platform. 300 µm thick sagittal slices were taken with a vibratome (Leica VT1200S) in chilled (4°C), oxygenated (95% O_2/5% CO_2) dissection solution. Thick sections were then placed in oxygenated DMEM, high glucose, GlutaMAX (Invitrogen), or artificial CSF (ACSF; 124 mM NaCl, 3 mM KCl, 1.25 mM NaH_2PO_4, 1.3 mM $MgSO_4$, 10 mM D-glucose, 26 mM $NaHCO_3$, and 2 mM $CaCl_2$) at room temperature for at least 1 h before imaging.

Two-photon time-lapse imaging

Acute brain slices were imaged with a two-photon Zeiss 7MP, equipped with a 20× objective (1.0 NA) and a Mai-tai laser (ONE BOX TI: SAPPHIRE LASERS, Spectra-Physics). Slices were imaged in a flow-through warming chamber (Warner Instruments, Open Diamond Bath Imaging Chambers, RC-26G) and continuously superfused (Compact Peristaltic Pump, Harvard Apparatus; ~1 ml/min) with the appropriate recording solution bubbled with 95% O_2/5% CO_2 using a dual automatic temperature controller with an in-line heater (Warner Instruments). Slices were maintained with a slice anchor (Warner Instruments, SHD-26GH/10).

For migration, z-stacks (step size: 3 µm) were taken every 2 min for tangential migration and every 5 min for radial migration. All images were 1024 × 1024 pixels large, with an axial resolution of 0.52 µm. Z-stack maximum projections were then realized on every time points, and registered for horizontal drifting using the StackReg plugin from ImageJ software. The number of cells being stationary at every given time point (2- or 5-min interval) was sufficient to use them as landmarks for the registration (see Movie 5).

For calcium imaging, single plane time lapse were acquired every 0.5 or 1 s, for at least 2 min. Only movies with low Z drifting were analyzed. Again, movies were registered using the StackReg plugin from ImageJ.

All acquisitions were done at least 50 µm below the surface of the slice, to avoid strong slicing artefacts.

Cell tracking and migration analysis

Individual cells were manually tracked using Imaris software (Bitplane). Cell positions were then saved in individual excel files for each movie. The parameters of saltatory migration were then analyzed in R.

Instantaneous speed at time t was calculated by dividing the distance separating the positions at t − 1 and t + 1 by two time intervals. A cell was considered as moving when this speed reached 20 µm/h corresponding to a displacement of 1.3 µm per time frame (for a 5-min time interval), a distance sufficient to avoid noisy movements detection. From the speed vector, we could determine phases of active migration and phases of relative immobility (stationary phases). This allowed the calculation of the mean speed of nuclear translocations corresponding to the mean of all speed above 20 µm/h and the percentage of stationary phases which is the percentage of time points with a speed lesser than 20 µm/h. These parameters were calculated from the first migratory phase to the last one. Displacement per hour was calculated by dividing the total distance covered during the recording divided by the time required to travel this distance. Straightness was defined as the ratio between the displacement vector length and the cumulative distance traveled. Cells with no migratory phase were not taken into account. Cells with a single migratory phase were excluded from the calculation of the percentage of stationary phases.

For quantifying the percentage of cells migrating in the superficial versus deep GCLs, we considered time lapses which were 5 h long. Then the GCL was divided in two equal halves (deep and superficial). A cell was considered migrating if it showed a least one migratory period during this 5-h period.

Neurite length and swelling formation distance were measured manually with ImageJ. Mean neurite length extension was calculated over periods when neurite length was above the mean neurite length plus 2 SD. Similarly, the frequency of neurite extensions was calculated as the number of neurite extensions (mean neurite length + 2 SD) per hour. The threshold for the swelling distance was set at 4 µm, above this value it was considered as a swelling formation. From this, the frequency of swelling formation was defined as the number of swelling formation per hour. The mean duration of swelling was the mean time spent with a swelling formation.

Calcium imaging analysis

All calcium imaging experiments were performed on GCaMP6s/Ai14 mice electroporated with the RNA Cre recombinase. The expression of this calcium sensitive probe in electroporated cells allows the visualization of intracellular calcium fluctuations.

Calcium time-lapse movies were averaged over time to obtain cell contours. Averaged images were then segmented to obtain a binary mask that was treated with the "Analyze Particles" methods in ImageJ software. Automatically drawn ROIs (Region Of Interest) were then manually curated to remove lost cells, duplicates or mistakes. The mean intensity of green fluorescence for each ROI was measured over time and saved as text file. A homemade Matlab interface was used to import, filter (with running average) and normalize intensities. Calcium transients were automatically detected by the software, with a fixed threshold of 25% dF/F0. The end of each calcium transients was defined as more than three time points with a consecutive decrease of amplitude. Each peak was then manually curated to avoid systematic errors from the software. The mean amplitude and frequency of calcium transients from each cell were then calculated and saved.

Pharmacology

Antagonists were bath applied at the following concentrations: D-APV (Tocris Bioscience, 50 µM), NBQX (Tocris Bioscience, 10 µM), MPEP (Tocris Bioscience, 30 µM), bicuculline (Tocris Bioscience, 10 µM), strychnine (Tocris Bioscience, 20 µM), and nifedipine (Tocris Bioscience, 10 µM).

Calcium-free solution was prepared from modified ACSF (124 mM NaCl, 3 mM KCl, 1.25 mM NaH_2PO_4, 1.3 mM $MgSO_4$, 10 mM D-glucose, 26 mM $NaHCO_3$, and 1 mM EGTA).

Experimental design and statistical analysis

All statistical test results and data given as mean ± SD are presented in each figure legends. For all experiments (except Fig. 3), one slice per animal was used, we therefore indicate only the number of animal used. Statistical analyses were performed using R software and R Commander Package (https://CRAN.R-project.org/package=Rcmdr). Data are presented as boxplots using the ggplot2 package, where the lower and upper hinges correspond to the first and third quartiles, and the upper (or lower) whisker extends from the hinge to the largest (or smallest) value no further than 1.5 * IQR from the hinge. The middle line represents the median value. Probability assignment: $p > 0.05$ (not significant, ns), $0.01 < p < 0.05$ (*), $0.001 < p < 0.01$ (**), and $p < 0.001$ (***).

For linear mixed effects model (LMEM), R package nlme (lme function) was used to fit a linear mixed model to the data with slices as a random effect and the experimental group as a fixed effect, to account for the dependance between cells analyzed in the same slices. Statistical results are given as: LMEM, χ^2(degrees of freedom) = χ^2 score, p value for experimental group effect [Figs. 1*G*, 2*D*, 4*F*,*G* (for frequency amd amplitude), 6*B*,*C*,*E*–*G*].

For Figure 3*H*,*I*, the mixed model contained two fixed effects: the electroporation type (lateral vs medial) and the area of recording (RMS vs RMS-OB vs DeepGCL). Again, slices were considered as a random effect in the LMEM. Here, statistical results are given as: LMEM, χ^2(degrees of freedom) = χ^2 score, p value for interaction effect between electroporation type and area of recording. *Post hoc p* values were computed using the lsmeans function (R lsmeans package) and Tukey adjustment for multiple comparisons.

For Figure 3*G* (% active cells), a two-way anova was used with two fixed effects: the electroporation type (lateral vs medial) and the area of recording (RMS vs RMS-OB vs DeepGCL). Statistical results are given as F(degrees of freedom) = F ratio, $p = p$ value for interaction effect. Tukey's HSD test was used for *post hoc* multiple comparisons.

Mann–Whitney–Wilcoxon tests were used to compare two groups when the number of samples was insufficient to use parametric tests: Figures 2*B*,*G*, 4*F*,*G* (% active cells), 7*C*,*D*, 8*C*,*D*.

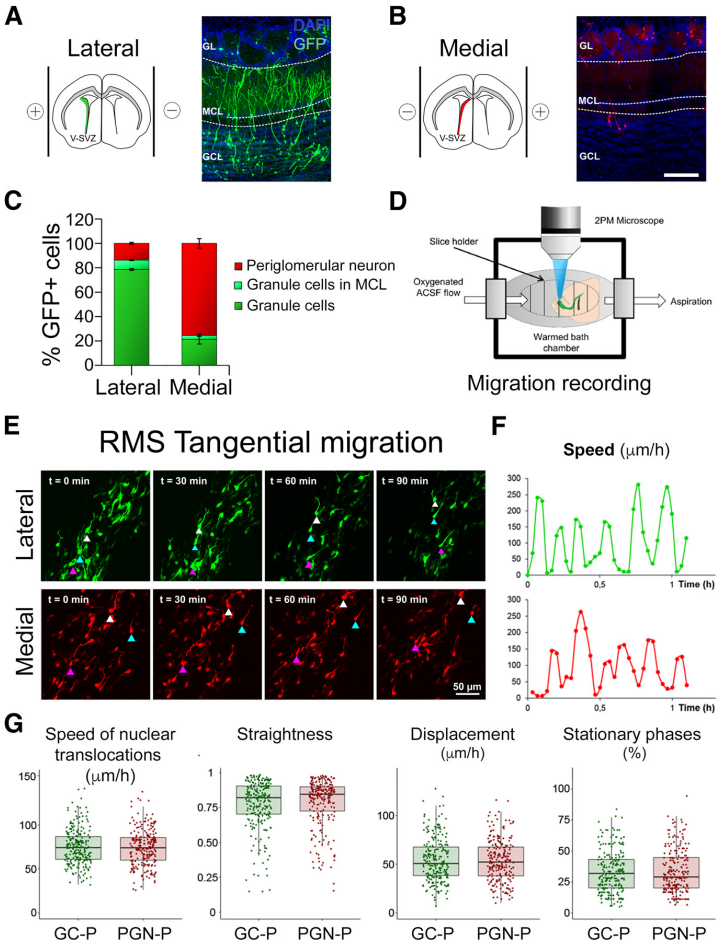

Figure 1. Tangential migration recording of postnatally generated subpopulation of OB interneurons. ***A***, left, Schematic of the V-SVZ from animals electroporated laterally. Right, Coronal sections of the OB at 21 dpe after lateral electroporation at P1 with a GFP encoding plasmid. Most of the neurons generated by lateral stem cells are located in the GCL. ***B***, left, Schematic of the V-SVZ from animals electroporated medially. Right, Coronal sections of the OB at 21 dpe after medial electroporation at P1 with a GFP encoding plasmid. Most of the neurons generated by medial stem cells are located in the GL. Scale bar: 50 µm. ***C***, Quantification of the mean percentage of GFP-positive cells in the different OB layers after lateral or medial electroporation. ***D***, Experimental setup for two-photon time lapse imaging of acute brain slices. ***E–G***, R26-Ai14 P0 animals received lateral or medial electroporation of Cre mRNAs. The parameters of tangential migration of tdTomato-expressing neuroblasts in the RMS were then assessed on acute brain slices at 5 dpe. ***E***, Snapshots of time-lapse two-photon imaging of lateral (up) and medial cells (down) at 5 dpe. For each panel, arrowheads indicate individual cells followed over time. Time is indicated in minutes. Scale bar: 50 µm. ***F***, Example of instantaneous speed recorded during a 1-h movie for a lateral (up) and a medial cell (down). ***G***, Mean speed of nuclear translocations, straightness, displacement per hour and percentage of stationary phases for RMS tangentially migrating lateral and medial cells. $n = 237/231$ cells on three animals per condition. Speed of nuclear translocations [mean ± SD: 75.4 ± 20.2 vs 74.2 SD 20.6 µm/h; LMEM, $\chi^2(1) = 0.05$, $p = 0.83$ (group effect)], straightness of cell body progression [0.78 ± 0.17 and 0.79 ± 0.17; LMEM, $\chi^2(1) = 0.09$, $p = 0.76$ (group effect)], cell body displacement per hour [54.6 ± 22 and 53.7 ± 21.4 µm/h; LMEM, $\chi^2(1) = 0.01$, $p = 0.93$ (group effect)], or percentage of time spent stationary [33.2 ± 17% and 33.6 ± 17%; LMEM, $\chi^2(1) = 0$, $p = 0.99$ (group effect)] were similar between both populations.

Similarly, Wilcoxon rank-sum tests (paired Wilcoxon test) were used when comparing the same slices before and after addition of an antagonist: Figures 4*B–D*, 5*B–F*.

Results

A new model to study interneuron migration

Previous work showed that terminal positioning of interneurons in the OB is dependent on the position of their respective stem cells along the walls of the lateral ventricles. Neurons born along the lateral wall tend to remain in the deep positioned GCL, whereas neurons derived from the medial wall preferentially migrate into the peripheral GL (Merkle et al., 2007; Fernández et al., 2011).

In order to quantify this correlation, we used targeted in vivo brain electroporation, which allows specific introduction of genetic material in the lateral or medial stem cell compartments (Fernández et al., 2011; Bugeon et al., 2017). Animals were electroporated at P1 and the OB was analyzed 21 d later [21 d post-electroporation (dpe)] when newborn neurons reached the OB

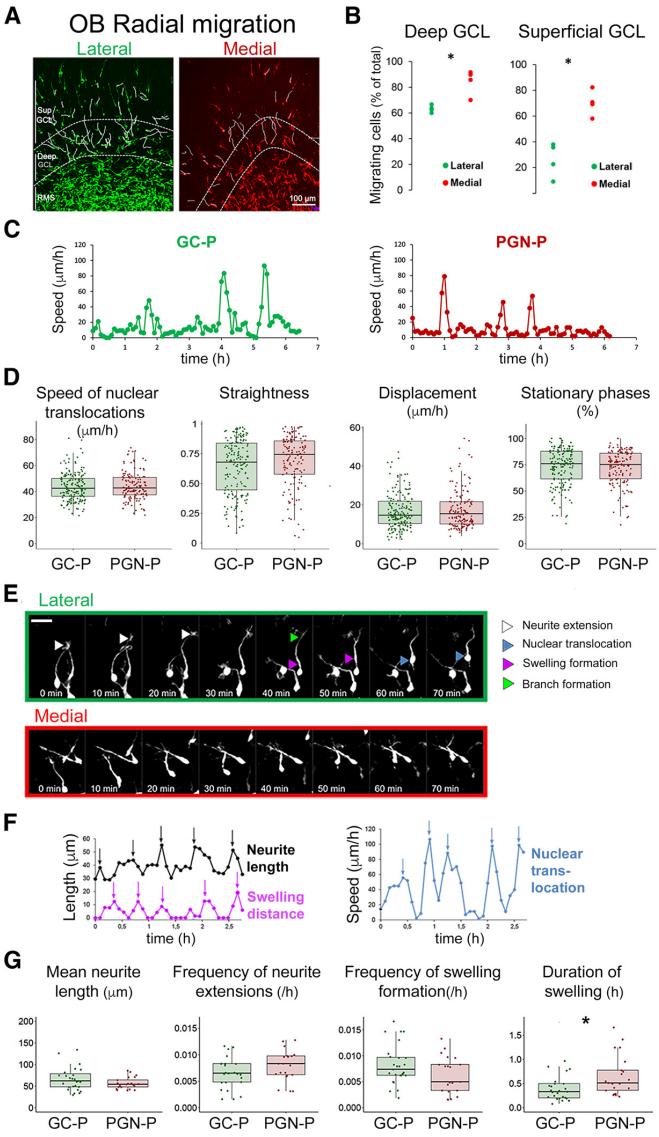

Figure 2. Characterization of radially migrating GC-P and PGN-P in the GCL. ***A***, R26-Ai14 P0 animals received lateral or medial electroporation of Cre mRNAs. The parameters of radial migration of tdTomato-expressing neuroblasts in the GCL were then assessed on acute brain slices at 7 dpe. Example tracks (white lines) of radially migrating cells after lateral and medial electroporation. Dotted lines separate the RMS, deep GCL, and superficial GCL. Scale bar: 100 µm. ***B***, Percentage of cells migrating in the deep and superficial GCL during a 5-h recording period. Cells with at least one period of active migration were considered. Each dot represents a slice, each slice comes from a different animal. $N = 4$ animals. Wilcoxon rank-sum test for means: deep GCL: $W = 0$, $p = 0.03$; superficial GCL: $W = 0$, $p = 0.03$. ***C***, Example of instantaneous speed recorded during a 6-h movie for a lateral and a medial cell. ***D***, Mean speed of nuclear translocations, straightness, displacement per hour, and percentage of stationary phases for tangentially migrating lateral and medial cells. We found no significant differences regarding speed of nuclear translocation [44 ± 10.7 vs 44.5 ± 10.7 µm/h; LMEM, $\chi^2(1) = 0$, $p = 0.99$ (group effect)], straightness [0.64 ± 0.23 vs 0.69 ± 0.22; LMEM, $\chi^2(1) = 0.7$, $p = 0.42$ (group effect)], mean displacement [16.9 ± 8.9 vs 17.8 ± 10 µm/h; LMEM, $\chi^2(1) = 0.09$, $p = 0.76$ (group effect)], or percentage of time spent in stationary phases [73.2 ± 17.2% vs 72.3 ± 16.6%; LMEM, $\chi^2(1) = 0.07$, $p = 0.8$ (group effect)] between both populations. $N = 178/138$ cells on four animals. ***E***, Snapshots of time-lapse two-photon imaging of radially migrating lateral (higher panel) and medial (lower panel) cells at high magnification. White arrowheads indicate the time of neurite extension, blue arrowheads indicate the occurrence of nuclear translocation, purple arrowheads indicate swelling formations and green arrowhead indicate a neurite branching appearance. Scale bar: 15 µm. ***F***, Example showing the sequence of neurite extension, swelling formation and nuclear translocation periods for one cell. Left chart, Neurite length and swelling distance are represented over time in µm. Right chart, Instantaneous speed of the cells in µm/h. Arrows indicate the peaks of each events. ***G***, Mean neurite extension length, frequency of neurite extension events, frequency and duration of swelling formations. We found no major differences in neurite length (71 ± 36.8 vs 57 ± 13.7 µm, Mann–Whitney–Wilcoxon test, $W = 340$, $p = 0.25$), frequency of neurite extension (0.007 ± 0.003 vs 0.008 ± 0.003, Mann–Whitney–Wilcoxon test, $W = 203.5$, $p = 0.1$), frequency of swelling (0.008 ± 0.004 vs 0.006 ± 0.004, Mann–Whitney–Wilcoxon test, $W = 361$, $p = 0.1$) between GC-P and PGN-P. The duration of swelling (0.44 ± 0.36 vs 0.66 ± 0.42) was slightly increased for PGN-P (Mann–Whitney–Wilcoxon test, $W = 162$, $p = 0.012$). $N = 21$ cells per condition, three animals. Individual points represent cells.

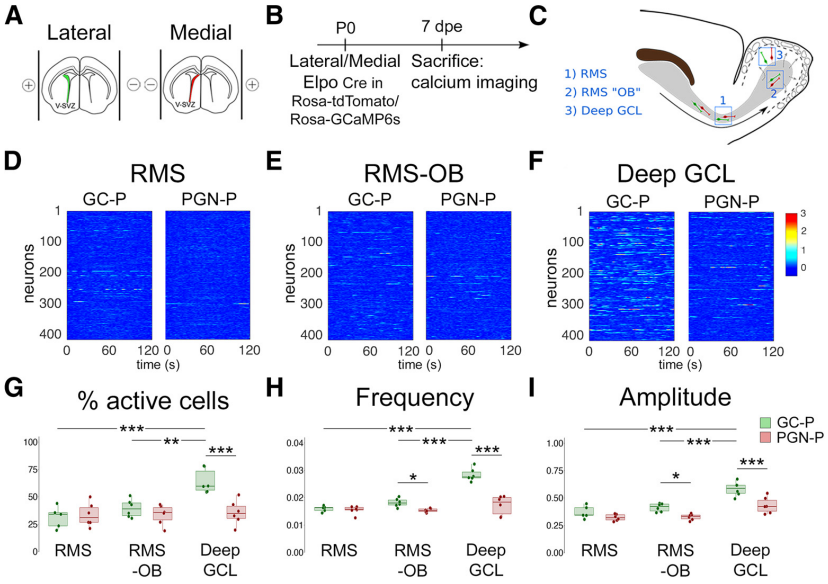

Figure 3. Spontaneous neuronal calcium activity in GC-P and PGN-P in the RMS, RMS-OB, and deep GCL. ***A***, Schematic representation of an OB sagittal slice. ***B***, Ai14/GCaMP6s P0 animals received lateral or medial electroporation of Cre mRNAs. ***C***, Calcium activity was recorded on acute brain slices at 7 dpe. Red and green cells represent medial and lateral cells migrating in the RMS, RMS-OB, or in the deep GCL. ***D–F***, Raster plot of calcium activity of GC-P (left) and PGN-P (right) recorded in the RMS (***D***), RMS-OB (***E***), and deep GCL (***F***). ***G–I***, Percentage of active cells (***G***), mean frequency (***H***), and mean amplitude (***I***) of calcium transients for GC-P and PGN-P in the RMS, RMS-OB, and in the deep GCL. Cells were defined as active if they showed at least one detectable calcium transient. The calcium activity of GC-P greatly increased on arrival in the RMS-OB and the deep GCL, in contrast with PGN-P activity. $N = 6$ slices from three animals per condition. ***G***, Percentage of active cells in each slice. Two-way ANOVA, interaction effect: $F(2) = 7.4$, $p = 0.0026$; Tukey's HSD test for *post hoc* multiple comparisons: RMS-GCp versus DeepGCL-GCp, $p = 0.00012$; RMS-GCp versus RMS-OB-GCp, $p = 0.0024$; DeepGCL-GCp versus DeepGCL-PGNp, $p = 0.00042$. ***H***, Mean frequency of calcium transients. $N = 624/1269/730$ versus $288/537/139$ (RMS/RMS-OB/Deep-GCL) cells. LMEM, $\chi^2(2) = 35.6$, $p < 0.0001$ (interaction effect); least-squares means and Tukey adjustment for *post hoc* multiple comparisons: RMS-GCp versus DeepGCL-GCp, $p < 0.0001$; RMS-GCp versus RMS-OB-GCp, $p < 0.0001$; RMS-OB-GCp versus RMS-OB-PGNp, $p = 0.049$; DeepGCL-GCp versus DeepGCL-PGNp, $p = 0.0001$. ***I***, Mean amplitude of calcium transients. $N = 624/1269/730$ versus $288/537/139$ (RMS/RMS-OB/Deep-GCL) cells. LMEM, $\chi^2(2) = 8.6$, $p = 0.014$ (interaction effect); least-squares means and Tukey adjustment for *post hoc* multiple comparisons: RMS-GCp versus DeepGCL-GCp, $p < 0.0001$; RMS-GCp versus RMS-OB-GCp, $p < 0.0001$; RMS-OB-GCp versus RMS-OB-PGNp, $p = 0.028$; DeepGCL-GCp versus DeepGCL-PGNp, $p = 0.0001$.

and settled in their terminal positions. For clarity, we use false-color representations, lateral electroporation in green and medial in red, throughout the manuscript. Introduction of a GFP-expression plasmid pCAG-GFP into the lateral ventricular wall labeled with high predominance (~80%) granule cells that remained in central positions within the GCL. Only few labeled neurons were found in the mitral cell layer (MCL) and the GL (Fig. 1*A*,*C*). In contrast, electroporation of pCAG-GFP into the medial wall labeled mainly cells that traversed the GCL to settle in the GL as PGN (~80%; Fig. 1*B*,*C*).

Thus, targeted electroporation of the lateral or the medial stem cell compartments labeled with high predominance the lineages that led to GCs and PGNs, respectively. We used this model to study their migratory behavior.

Migratory behavior of GC-P and PGN-P is indistinguishable

First, we compared GC-P and PGN-P during their tangential migration in the RMS using two-photon time-lapse imaging on acute brain slices at 5 d after lateral or medial electroporation (Fig. 1*D*,*E*). To increase the number of labeled cells for precise quantitative analyses, we used CRE-mRNA electroporation into R26 tdTomato transgenic mice. This approach allows specific targeting of the ventricular stem cell compartments at higher transfection efficiency (Bugeon et al., 2017).

Individual cells were manually tracked using Imaris software (Bitplane). The instantaneous speed and other migratory parameters of the cells were then derived based on their tracked position at each frame of the time lapse. Speed profiling of cell bodies (Fig. 1*F*), showed typical saltatory migration as reported before (Bellion et al., 2005; Nam et al., 2007; Inada et al., 2011), alternating short stationary phases and fast nuclear translocations, for both populations (Movie 1 for lateral electroporation; Movie 2 for medial electroporation). Speed of nuclear translocations, straightness of cell body progression, cell body displacement per hour and lengths of stationary phases were indistinguishable between both populations (Fig. 1*G*).

We then compared radial migration of both populations on acute brain slices at 7 dpe, a time point when large numbers of cells leave the RMS-OB and initiate radial migration to invade the OB target layers (Fig. 2*A*; Movie 3 for lateral electroporation; Movie 4 for medial electroporation). Quantification in the deeper half of the GCL during 5 h showed that ~60% of the GC-P and 80% of PGN-P had migrated during the recording period (Fig. 2*B*, left). The difference in migration between the two populations was even larger when we analyzed cells located in the superficial half of the GCL. Here, <30% of GC precursors, but still almost 80% of PGN-P, changed position during the recording period (Fig. 2*B*, right). For the migratory fractions of both populations, radial migration was still saltatory, like in the RMS, but with lower speed of nuclear translocation as compared with tangential migration (Fig. 2*C*; tangential: 75 µm/h; radial: 45 µm/h; Fig. 2*D*). Comparison of the different migratory parameters at

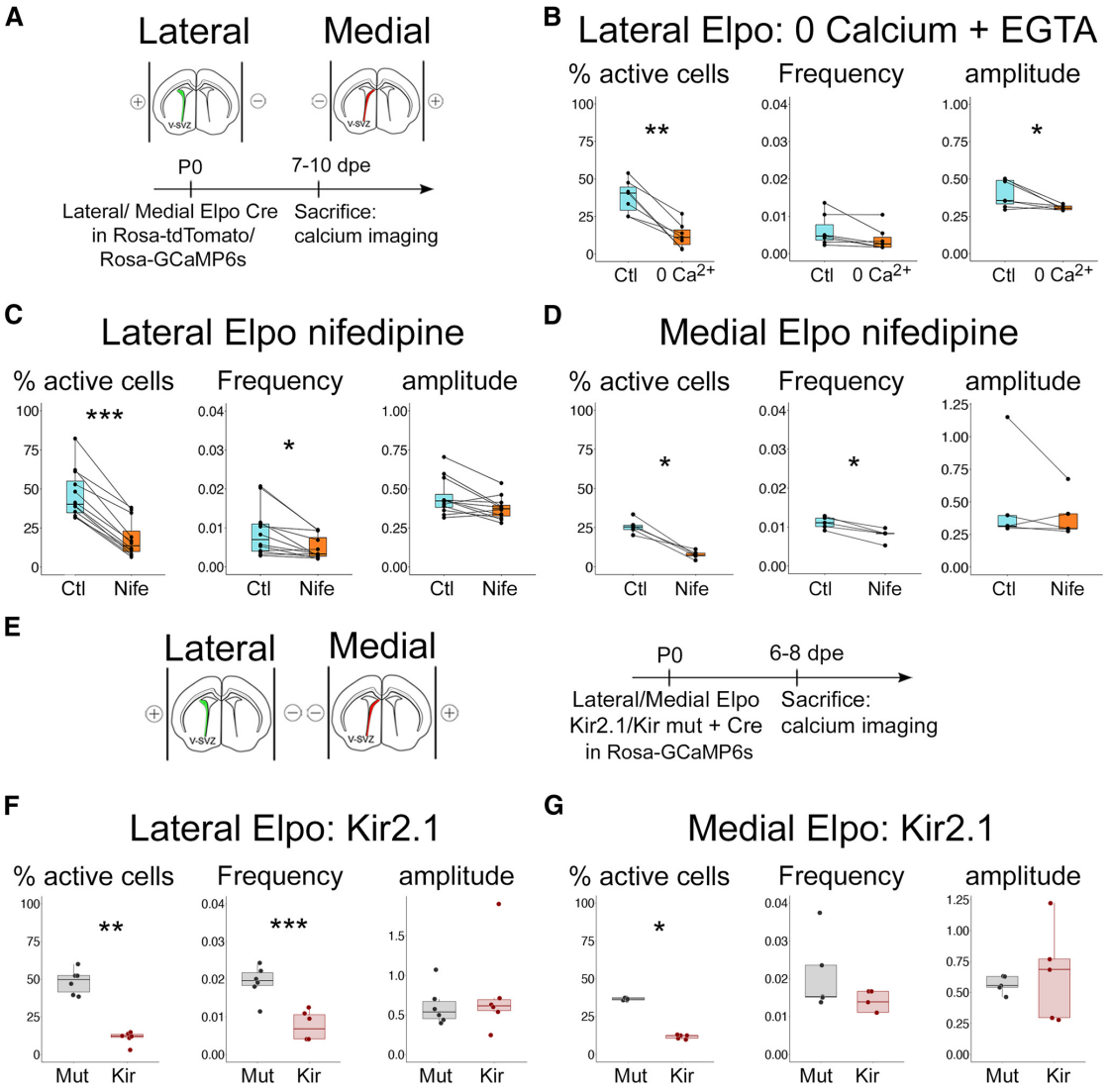

Figure 4. Spontaneous neuronal calcium activity in both GC-P and PGN-P can be partly blocked by L type-VGCC antagonist or KIR2.1 overexpression. ***A***, Rosa-tdTomato/Rosa-GCaMP6s P0 animals were electroporated with Cre recombinase, targeting either the lateral or medial wall of the V-SVZ. 7–10 d after electroporation the animals were killed, and acute brain slices were obtained and calcium activity was recorded in the deep GCL. ***B***, Percentage of active cells (left), mean frequency (middle), and mean amplitude (right) of calcium transients for GC-P, before and after incubation in calcium-free medium (no calcium + 2 mM EGTA). Both the percentage of active cells and amplitude of calcium transients were significantly reduced, suggesting that the observed calcium transients require an extracellular source for calcium. $N = 7$ animals. Percentage of active cells: Wilcoxon rank-sum test, $p = 0.005$. Mean frequency: Wilcoxon rank-sum test, $p = 0.16$. Mean amplitude: Wilcoxon rank-sum test, $p = 0.038$. ***C***, Percentage of active cells (left), mean frequency (middle), and mean amplitude (right) of calcium transients for GC-P, before and after incubation in a nifedipine (10 μM) supplemented medium. Both the percentage of active cells and frequency of calcium transients were significantly reduced, suggesting that the observed calcium transients depend at least partly on L-type voltage gated calcium channels. N = animals. Percentage of active cells: Wilcoxon rank-sum test, $p = 0.00014$. Mean frequency: Wilcoxon rank-sum test, $p = 0.04$. Mean amplitude: Wilcoxon rank-sum test, $p = 0.06$. ***D***, Percentage of active cells (left), mean frequency (middle), and mean amplitude (right) of calcium transients for PGN-P, before and after incubation in a nifedipine (10 μM) supplemented medium. Both the percentage of active cells and frequency of calcium transients were significantly reduced, suggesting that the observed calcium transients depend at least partly on L-type voltage gated calcium channels. $N = 5$ animals. Percentage of active cells: Wilcoxon rank-sum test, $p = 0.012$. Mean frequency: Wilcoxon rank-sum test, $p = 0.012$. Mean amplitude: Wilcoxon rank-sum test, $p = 0.42$. ***E***, Wild-type P0 animals were electroporated with either a KIR2.1 mutant form or the normal KIR2.1 channel, targeting either the lateral or medial wall of the V-SVZ; 6–8 d after electroporation, the animals were killed, and acute brain slices were obtained and imaged for calcium activity in the deep GCL. ***F***, Percentage of active cells (left), mean frequency (middle), and mean amplitude (right) of calcium transients for GC-P, with the mutant or normal KIR2.1 channel. Both the percentage of active cells and frequency of calcium transients were significantly reduced, showing that the overexpression of the KIR2.1 channel in GC-P significantly decreases calcium activity. $N = 6$ animals. Percentage of active cells: 48.3 ± 8.2 versus 11.2 ± 4.1, Mann–Whitney–Wilcoxon test, $p = 0.0022$, $W = 36$. Mean frequency: 0.019 ± 0.004 versus 0.0076 ± 0.0038, LMEM, $\chi^2(1) = 13$, $p = 0.0003$ (group effect). Mean amplitude: 0.61 ± 0.25 versus 0.77 ± 0.57, LMEM, $\chi^2(1) = 2.2$, $p = 0.14$ (group effect). ***G***, Percentage of active cells (left), mean frequency (middle), and mean amplitude (right) of calcium transients for PGN-P, with the

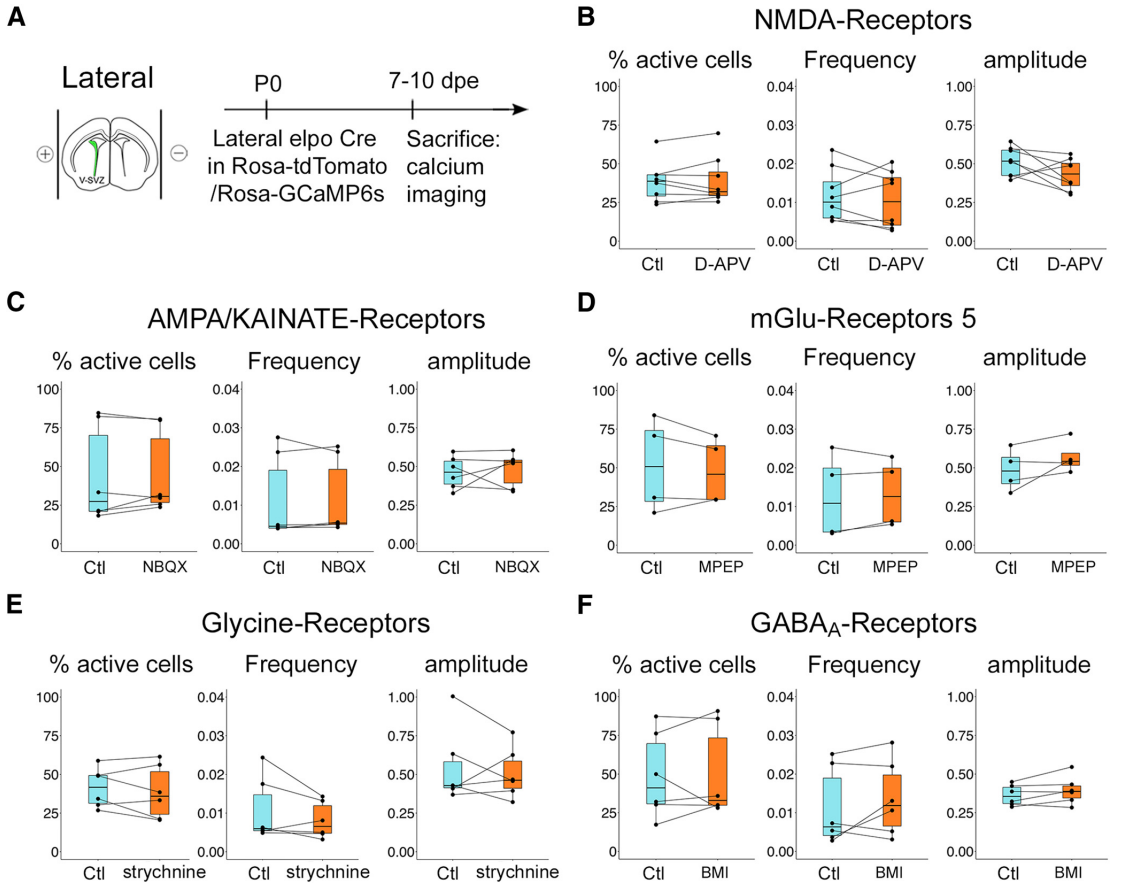

Figure 5. Spontaneous neuronal calcium activity in GC-P in the deep GCL is not affected by classical antagonists. ***A***, Rosa-tdTomato/Rosa-GCaMP6s P0 animals were electroporated with a Cre recombinase, targeting the lateral wall of the V-SVZ; 7–10 d after electroporation, the animals were killed, and acute brain slices were obtained and imaged for calcium activity in the deep GCL. ***B–F***, Spontaneous activity was recorded on each slice. The sections were then incubated with a given antagonist for 1 h, then calcium imaging was performed again to compare spontaneous activity with or without antagonist. ***B***, The NMDA receptors antagonist D-APV ($N = 8$ animals; percentage of active cells: Wilcoxon rank-sum test, $p = 1$; mean frequency: Wilcoxon rank-sum test, $p = 0.65$; mean amplitude: Wilcoxon rank-sum test, $p = 0.1$); (***C***) AMPA/kainate receptors antagonist NBQX ($N = 6$ animals; percentage of active cells: Wilcoxon rank-sum test, $p = 0.82$; mean frequency: Wilcoxon rank-sum test, $p = 0.3$; mean amplitude: Wilcoxon rank-sum test, $p = 0.82$); (***D***) metabotropic glutamate receptor 5 antagonist MPEP ($N = 4$ animals; percentage of active cells: Wilcoxon rank-sum test, $p = 0.69$; mean frequency: Wilcoxon rank-sum test, $p = 0.69$; mean amplitude: Wilcoxon rank-sum test, $p = 0.49$); (***E***) glycine receptor antagonist strychnine ($N = 6$ animals; percentage of active cells: Wilcoxon rank-sum test, $p = 0.82$; mean frequency: Wilcoxon rank-sum test, $p = 0.48$; mean amplitude: Wilcoxon rank-sum test, $p = 1$); and (***F***) GABA$_A$ receptors antagonist bicuculline ($N = 7$ animals; percentage of active cells: Wilcoxon rank-sum test, $p = 0.94$; mean frequency: Wilcoxon rank-sum test, $p = 0.7$; mean amplitude: Wilcoxon rank-sum test, $p = 0.7$) did not modify the percentage of active cells, frequency, or amplitude of calcium transient.

the population level showed no significant differences regarding the speed of nuclear translocation, displacement or percentage of time spent in stationary phases. Next, we compared migratory parameters in the OB of GC-P and PGN-P at the cellular level. The example presented in Figure 2*E* provides a high-resolution view of the sequence of events during which peaks in neurite length precede swelling formation and nuclear translocation (Fig. 2*F*; Movie 6 for lateral electroporation; Movie 7 for medial electroporation). Neurite length, frequency of neurite extension and frequency of swelling formation were similar between populations. There was a tendency toward a small but significant increase in swelling duration between GC-P and PGN-P (Fig. 2*G*). This result may indicate a different swelling formation mechanism between these two populations.

Overall, we conclude that GC-P and PGN-P share unique modes of tangential and radial migration toward and within the OB. The significantly lower mobility of GC-P in the GC likely reflects the fact that this population is rapidly recruited to the circuitry and stop migrating. In contrast, PGN-P do not stop migration as they traverse the GCL and integrate the PGL. A clear morphokinetic predictor of neuronal fate during tangential or radial migration was not detected.

←

mutant or normal KIR2.1 channel. The percentage of active cells was significantly reduced, showing that the overexpression of the KIR2.1 channel in PGN-P significantly decreases calcium activity. $N = 5$ animals. Percentage of active cells: 36.7 ± 0.75 versus 11.7 ± 1.3, Mann–Whitney–Wilcoxon test, $p = 0.0114$, $W = 25$. Mean frequency: 0.021 ± 0.0099 versus 0.014 ± 0.0027, LMEM, $\chi^2(1) = 1.6$, $p = 0.21$ (group effect). Mean amplitude: 0.56 ± 0.069 versus 0.65 ± 0.39, LMEM, $\chi^2(1) = 1.05$, $p = 0.3$ (group effect).

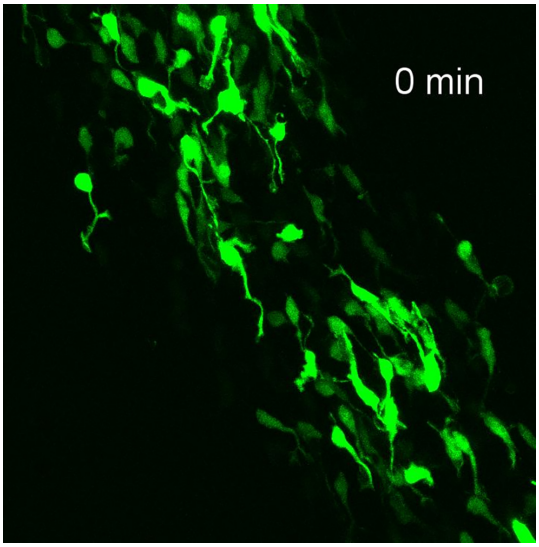

Movie 1. Example of a 70-min-long time lapse recording performed in the RMS 5 d after lateral electroporation. [View online]

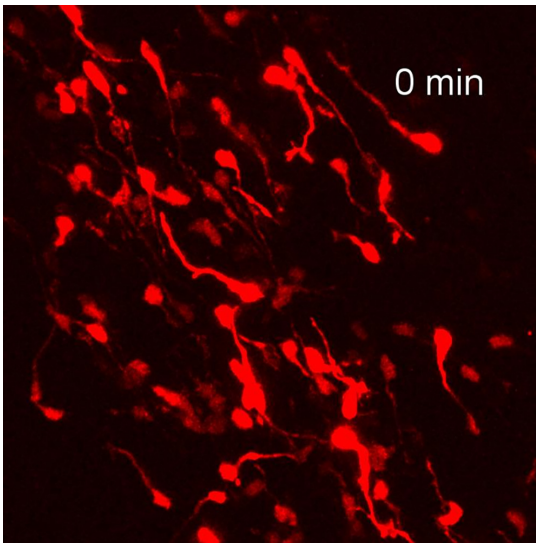

Movie 2. Example of a 70-min-long time lapse recording performed in the RMS 5 d after medial electroporation. [View online]

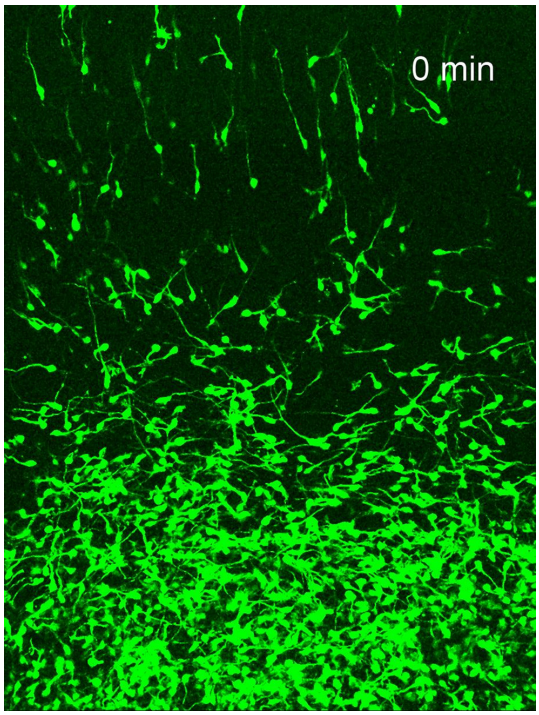

Movie 3. Example of a 160-min-long time lapse recording performed in the OB 7 d after lateral electroporation. [View online]

Neuronal activity increases in GC-P during recruitment in the OB

To investigate the impact of neuronal activity on migration and recruitment of GC-P and PGN-P in the OB neurogenic system, we quantified their spontaneous calcium activity. CRE-mRNA was targeted to either the lateral or the medial stem cell compartments of R26 tdTomato/GCaMP6s mice. Acute slices were prepared and imaged at 7 dpe by two-photon microscopy (Fig. 3*A*, *B*). Neuronal activity in GC-P and PGN-P was observed in three defined regions (Fig. 3*C*): first, in the RMS, before precursors enter the core of the OB; second, in the RMS-OB before the precursors enter in the OB; third, in the deep GCL. We observed an overall increase of calcium activity (% of active cells, frequency and amplitude, respectively Fig. 3*G–I*) between the RMS and the deep-GCL and between the RMS-OB and the deep-GCL for the GC-P.

In the RMS, about one third of the imaged cells were active during a 2-min recording (i.e., at least one detectable transient) with no significant differences between medial and lateral slices (Fig. 3*D*,*G*). Similarly, the amplitude and frequency of calcium transients were comparable for the two populations, with a mean of 35% dF/F0 at a frequency of 0.016 Hz (Fig. 3*H*,*I*). We then recorded spontaneous calcium activity in precursors located in the RMS-OB (Fig. 3*E*, Movie 8, Movie 9). While the percentage of active cells was similar between GC-P and PGN-P (Fig. 3*G*), we observed a significant increase of the frequency and amplitude of calcium transient in GC-P (Fig. 3*H*,*I*). When precursors migrated in the deep GCL (Fig. 3*F*), we observed an important increase of activity in GC-P compared with PGN-P. Indeed, the percentage of active cells was almost twice as large in GC-P (Fig. 3*G*), while there was respectively a 65% and 37% increase in amplitude and frequency of calcium transients in GC-P compared with PGN-P (Fig. 3*H*,*I*). Further statistical analysis revealed that for all parameters, there is a significant interaction between the type of electroporation (lateral vs medial) and the area where cells were recorded (RMS, RMS-OB, and deep GCL). This shows that the two subpopulations are different, and that this difference varies among layers. Indeed, while the activity of GC-Ps significantly increases in the GCL, this is not the case for PGN-Ps.

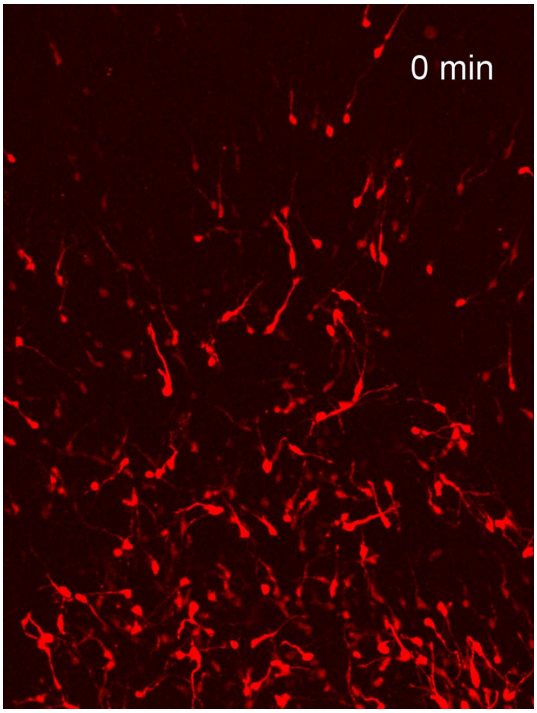

Movie 4. Example of a 160-min-long time lapse recording performed in the OB 7 d after medial electroporation. [View online]

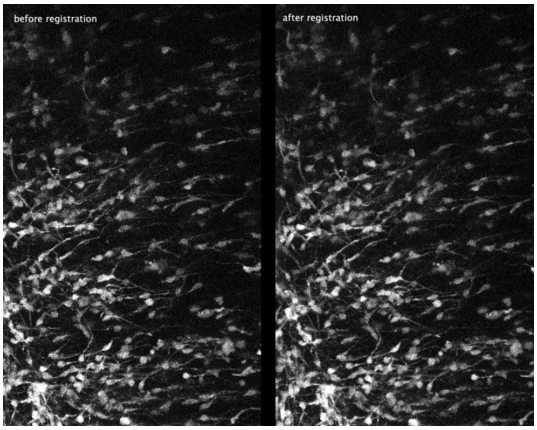

Movie 5. Example of time lapse recording before (left) and after image registration (right) to correct for horizontal drift. [View online]

We aimed at identifying the neurophysiological mechanisms underlying this increased activity of GC-P in the deep GCL (Fig. 4*A*). Perfusion of a calcium-free medium on OB slices led to a strong decrease in the percentage of active cells (41% vs 11%, $p = 0.004$; Fig. 4*B*) suggesting that the source of calcium was mainly extracellular. Moreover, blocking specifically L-type voltage gated calcium channels with nifedipine abolished most calcium activity in GC-P (Fig. 4*C*) indicating that a depolarization was responsible for the increase of

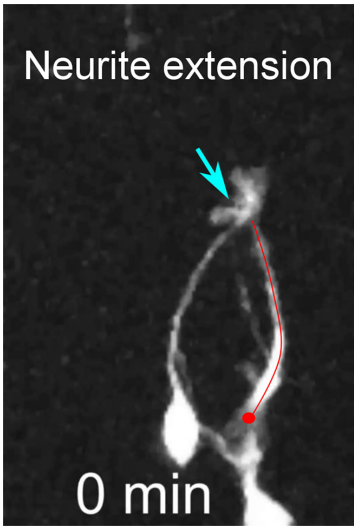

Movie 6. Example of a 110-min-long time lapse recording performed in the OB 7 d after lateral electroporation showing the different phases of neuronal migration: neurite extension, branch formation, swelling formation, and nuclear translocation. [View online]

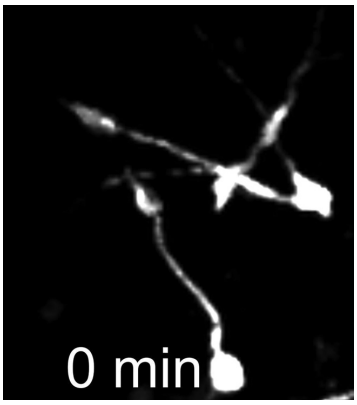

Movie 7. Example of a 110-min-long time lapse recording performed in the OB 7 d after medial electroporation showing the different phases of neuronal migration: neurite extension, branch formation, swelling formation, and nuclear translocation. [View online]

activity. While the level of activity was lower in PGN-P, activity could still be inhibited by nifedipine application (Fig. 4*D*). It was demonstrated that overexpression of the inward rectifying potassium channel Kir2.1 could highly affect neuronal activity by lowering the resting membrane potential, therefore altering neuronal excitability (De Marco García et al., 2011; Xue et al., 2014). We overexpressed Kir2.1 in GC-P and PGN-P and measured its effect on spontaneous calcium activity (Fig. 4*E*). We observed an important decrease of neuronal activity in GC-P (Fig. 4*F*). While neuronal activity was lower in PGN-P, it could still be inhibited by Kir expression (Fig. 4*G*).

We used a wide spectrum of pharmacological interventions to find the source of this depolarization, including the NMDA receptors antagonist D-APV, the AMPA receptors antagonist NBQX, the metabotropic glutamate receptor 5 antagonist MPEP,

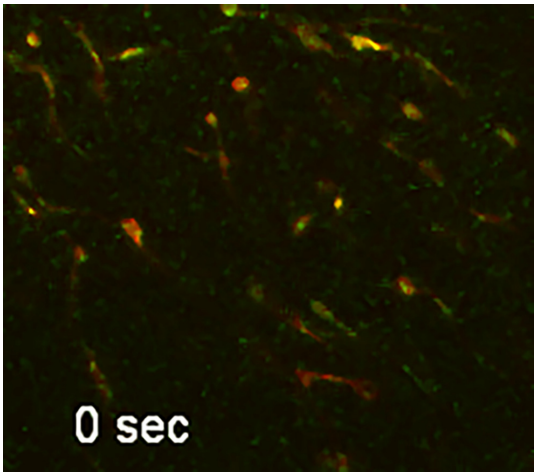

Movie 8. Example of a 2-min recording of calcium activity performed at the exit of the RMS-OB 7 d after lateral electroporation. GCaMP6s fluorescence is in green, tdTomato in red. [View online]

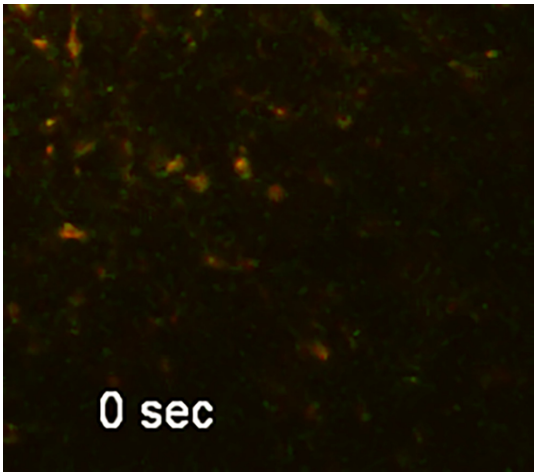

Movie 9. Example of a 2-min recording of calcium activity performed at the exit of the RMS-OB 7 d after medial electroporation. GCaMP6s fluorescence is in green, tdTomato in red. [View online]

the $GABA_A$ receptors antagonist bicuculline, the glycine receptor antagonist strychnine (Fig. 5*A–F*). None of these antagonists significantly modified the percentage of active cells, or the amplitude or frequency of calcium transients. Taken together, these results suggest that the calcium activity increase seen in GC-P was mainly due to a depolarization, leading to the opening of voltage-dependent L-type calcium channels and an entry of extracellular calcium.

Thus, after entering the RMS in the OB, and especially when they start exiting the RMS, GC-P, but not PGN-P, showed a large L-type calcium channel-dependent increase in neuronal activity. These results led us to hypothesize that the depolarization of GC-P during the transition from the RMS into the GCL is critical for their recruitment in the OB.

Neuronal activity is needed for recruitment and survival of GC-P

To test whether neuronal activity controls the migration and the recruitment of precursors from the RMS to the OB layers, we interfered with the activity of arriving GC-P.

First, we investigated whether blocking neuronal activity of GC-P with nifedipine could affect their migration. We recorded neuronal migration at 7–8 dpe in presence of nifedipine in the RMS-OB and in the deep-GCL (Fig. 6*A*). We did not find any significant change in the speed of nuclear translocations, straightness, cell displacement and stationary phases (Fig. 6*C,D*).

Then we overexpressed either Kir2.1 to block neuronal activity in GC-P or Kir2.1 mutant as a control and recorded migration at 7–8 dpe (Fig. 6*D*). In the RMS, expression of Kir2.1 compared with Kir2.1 mutant had no effect on the speed of nuclear translocations, straightness, cell displacement and stationary phases (Fig. 6*E*). Next, we analyzed migration in the RMS-OB, a region where neuronal activity is increased in GC-P compared with PGN-P (Fig. 3). In this region, expression of Kir2.1 slightly increased the percentage of cells in stationary phase (Fig. 6*F*). Finally, we analyzed GC-P in the deep GCL. Here, Kir2.1 expression had again no detectable effect on straightness, displacement and stationary phases but a small but significant increase in the speed of nuclear translocations (Fig. 6*G*). As an additional control, we compared the migration of cells electroporated with the Kir mutant plasmid (in CD1 mice) and cells electroporated with a Cre-RNA in Ai14 (C57bl6). We observed small differences, with a slight increase of the mean displacement (16.9 ± 8.9 vs 21.5 ± 10.6; LMEM, $\chi^2(1) = 4.2$, $p = 0.04$), and of the percentage of time spent in stationary phases (73.2 ± 17.2 vs 60.6 ± 19.5; LMEM, $\chi^2(1) = 6.6$, $p = 0.01$) nevertheless the speed of nuclear translocation was unchanged (43.9 ± 13.3 vs 42.5 ± 10.7; LMEM, $\chi^2(1) = 0.9$, $p = 0.3$). While this may indicate an effect of the Kir2.1 mutant form, the absence of effect of nifedipine incubation and the relative absence of effect of the Kir2.1 channel compared with the mutant form, overall suggest that blocking neuronal activity has very little effect on the migration of GC-P.

We then tested whether neuronal activity controls the recruitment of GC-P and PGN-P in the OB layers. To test this hypothesis, we overexpressed Kir2.1 in GC-P and PGN-P by lateral or medial electroporation and analyzed neuronal distribution in the OB at 8 dpe, when migratory precursors leave the RMS-OB and settle in the OB (Fig. 7*A,B*). Importantly, and as shown in our previous experiments (Fig. 4*F,G*), Kir2.1 overexpression significantly decreases intrinsic calcium activity in both populations. We also performed experiments at 12 dpe when more cells had reached the OB, to test for a potential cumulative effect.

At 8 dpe, the number of Kir2.1-expressing cells was significantly higher in the RMS-OB whereas less cells were present in the GCL (Fig. 7*C*). This effect was specific to GC-P, as distribution was unaffected in PGN-P after medial electroporation (Fig. 7*D*). At 12 dpe, when more cells entered the OB, this altered distribution in the GC population was slightly more pronounced (Fig. 7*C*) and, again, not detectable in PGN-P (Fig. 7*D*). At both time points, cell distribution in the GL was unaffected (Fig. 7*C,D*).

Finally, we asked whether blocking activity and/or the subsequent misdistribution of GCs had an impact on cell survival. To this end we overexpressed Kir2.1 and analyzed the expression of cleaved caspase 3 (c-caspase 3), a marker of apoptosis at 8 and 12 dpe in the RMS, the GCL and the GL (Fig. 8*A,B*). In agreement with previous studies, we found that the overall level of c-caspase

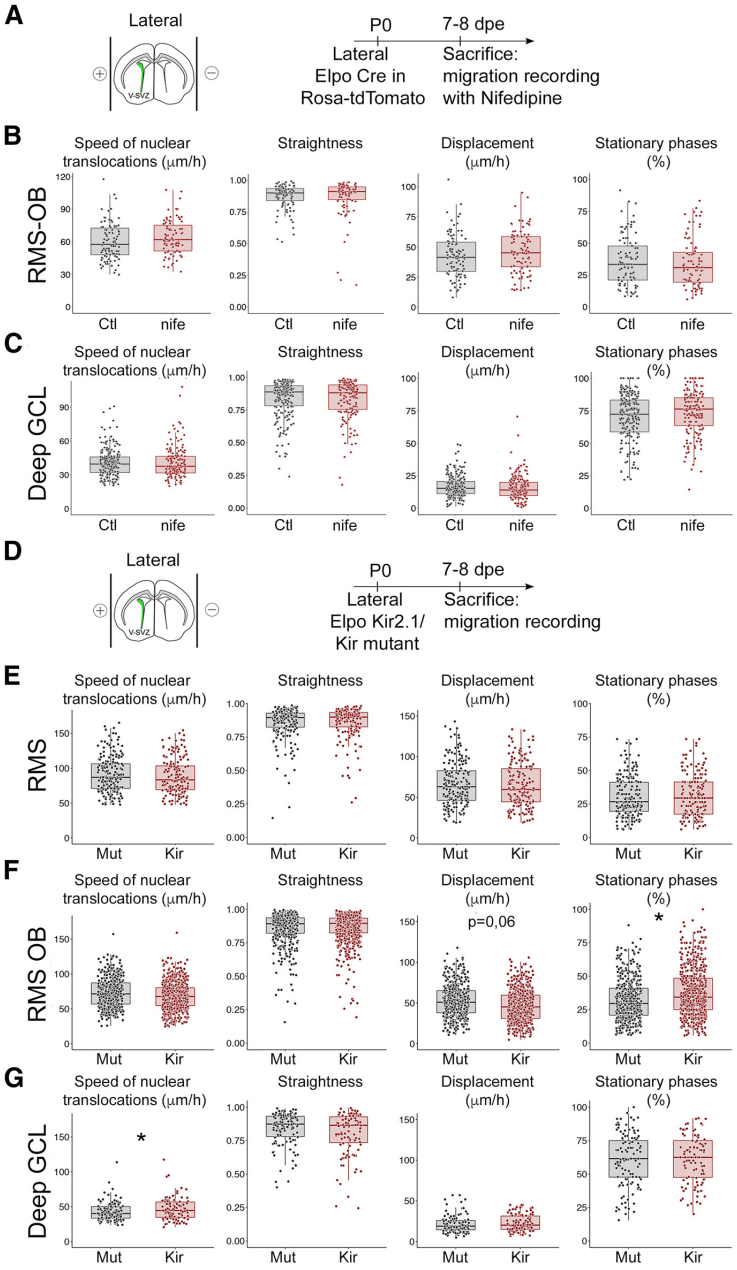

Figure 6. Effect of decreased neuronal activity on GC-P migration ***A***, P0 Rosa-tdTomato animals received lateral electroporation with Cre recombinase to label newborn cells. Mice were then killed at 7–8 dpe and the parameters of migration of GC-P were assessed on acute brain slices in the RMS-OB and deep GCL, with or without nifedipine (10 μM). ***B***, Quantification of migration parameters in the RMS-OB. $N = 102/91$ cells on four animals. Speed of nuclear translocation [60.15 $\pm$ 16.7 vs 64 $\pm$ 16; LMEM, $\chi^2(1) = 0.6$, $p = 0.44$ (group effect)], straightness [0.87 $\pm$ 0.10 vs 0.87 $\pm$ 0.15; LMEM, $\chi^2(1) = 0.3$, $p = 0.61$ (group effect)], mean displacement [42.4 $\pm$ 17.6 vs 46.1 $\pm$ 17.7; LMEM, $\chi^2(1) = 0.4$, $p = 0.54$ (group effect)], or percentage of time spent in stationary phases [35.9 $\pm$ 19.1 vs 33.9 $\pm$ 18.9; LMEM, $\chi^2(1) = 0.1$, $p = 0.75$ (group effect)] were similar between both conditions. ***C***, Quantification of migration parameters in the deep GCL. $N = 225/172$ cells on four animals. Speed of nuclear translocation [40.8 $\pm$ 12.4 vs 40.8 $\pm$ 13.7; LMEM, $\chi^2(1) = 0.05$, $p = 0.83$ (group effect)], straightness [0.84 $\pm$ 0.14 vs 0.83 $\pm$ 0.15; LMEM, $\chi^2(1) = 0.07$, $p = 0.79$ (group effect)], mean displacement [16.6 $\pm$ 8.1 vs 15.7 $\pm$ 9.4; LMEM, $\chi^2(1) = 0.4$, $p = 0.52$ (group effect)], or percentage of time spent in stationary phases [70.8 $\pm$ 17.5 vs 73.8 $\pm$ 16.8; LMEM, $\chi^2(1) = 0.81$, $p = 0.37$ (group effect)] were similar between both conditions. ***D***, P0 CD1 animals received lateral electroporation with either a Kir2.1 mutant or a functional Kir2.1 encoding plasmid. Mice were then killed at 7–8 dpe, and the parameters of migration of GC-P were assessed on acute brain slices in the RMS, RMS-OB, and deep GCL. ***E***, Quantification of migration parameters in the RMS. $N = 195/162$ cells on four animals. Speed of nuclear translocation [91.5 $\pm$ 26.7 vs 88.5 $\pm$ 25.6; LMEM, $\chi^2(1) = 0.05$, $p = 0.8142$ (group effect)], straightness [0.86 $\pm$ 0.124 vs 0.86 $\pm$ 0.122; LMEM, $\chi^2(1) = 0.005$, $p = 0.94$ (group effect)], mean displacement [67.2 $\pm$ 27.8 vs 64.6 $\pm$ 27.5; LMEM,

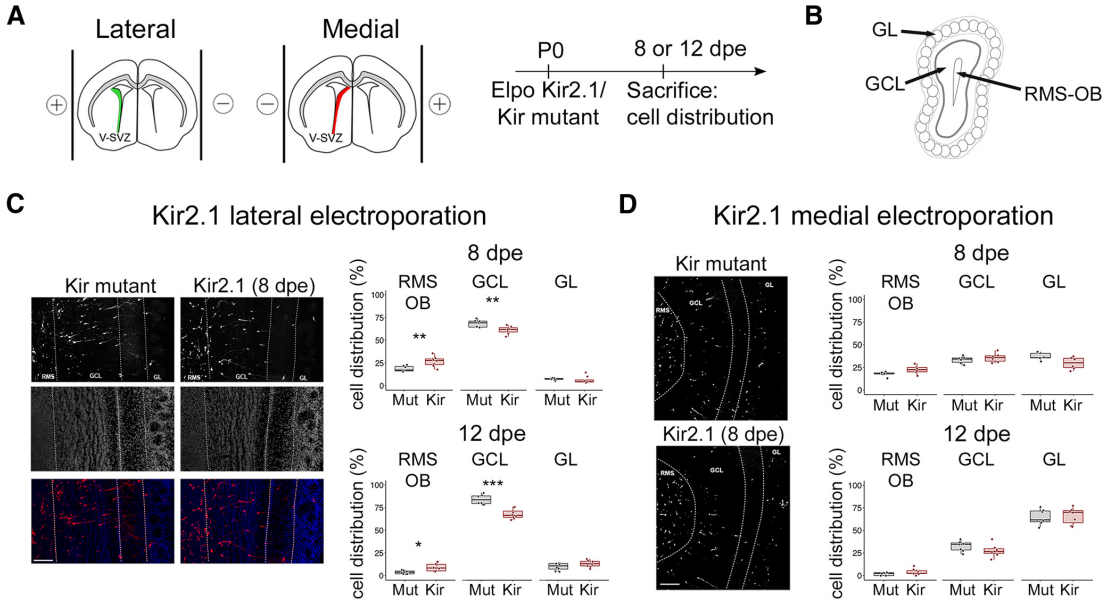

Figure 7. Effect of Kir2.1 expression on cellular distribution. ***A***, P0 CD1 animals received lateral or medial electroporation with either a Kir2.1 mutant or a functional Kir2.1 encoding plasmid. Mice were then killed either at 8 or 12 dpe. and the cellular distribution of tdTomato cells was assessed. ***B***, Cellular distribution was observed on fixed coronal brain slices and cells attributed to the RMS, GCL, or GL. ***C***, left, OB coronal sections of Kir2.1 mutant (Mut) and Kir2.1 (Kir) laterally electroporated animals at 8 dpe. Dotted lines separate OB layers. DAPI stains cell nuclei. Scale bar: 100 µm. Right, Quantification of the cellular distribution at 8 dpe ($N = 7$ animals) and 12 dpe ($N = 8$ animals) in each OB layer showing an increased percentage of Kir2.1 cells in the RMS (8 dpe: 18.5 ± 3.1 vs 26.7 ± 5.5, Mann–Whitney–Wilcoxon test, $p = 0.006$, 12 dpe: 9 ± 4.1 vs 3.8 ± 1.9, Mann–Whitney–Wilcoxon test, $p = 0.007$) and a decrease in the GCL (8 dpe: 68.2 ± 4 vs 61.2 ± 4.2, Mann–Whitney–Wilcoxon test, $p = 0.009$; 12 dpe: 84 ± 5.2 vs 68 ± 5.3, Mann–Whitney–Wilcoxon test, $p = 0.00015$). Cellular distribution in the GL were similar for both conditions at 8 dpe (7.2 ± 1.2 vs 6.13 ± 4, Mann–Whitney–Wilcoxon test, $p = 0.12$) and 12 dpe (9.9 ± 3.9 vs 13.2 ± 3.7, Mann–Whitney–Wilcoxon test, $p = 0.13$). ***D***, left, OB coronal sections of Kir2.1 mutant and Kir2.1 medially electroporated animals at 8 dpe. Dotted lines separate OB layers. Scale bar: 100 µm. Right, Quantification of the cellular distribution at 8 dpe ($N = 6$ animals) and 12 dpe ($N = 7$ animals) in each OB layer. No significant effect on cellular distribution was observed in this condition, neither in the RMS (8 dpe: 17.8 ± 2.5 vs 22.5 ± 4.7, Mann–Whitney–Wilcoxon test, $p = 0.07$, 12 dpe: 1.9 ± 1.8 vs 4.1 ± 3.6, Mann–Whitney–Wilcoxon test, $p = 0.33$), GCL (8 dpe: 33.3 ± 4 vs 35.87 ± 5.5, Mann–Whitney–Wilcoxon test, $p = 0.48$, 12 dpe: 32.6 ± 5.9 vs 27.7 ± 7, Mann–Whitney–Wilcoxon test, $p = 0.16$ nor GL (8 dpe: 37.2 ± 4.2 vs 29.7 ± 6.7, Mann–Whitney–Wilcoxon test, $p = 0.132$, 12 dpe: 64.8 ± 8.4 vs 3.8 ± 1.9, Mann–Whitney–Wilcoxon test, $p = 0.71$).

3 expressing cells was very low (Petreanu and Alvarez-Buylla, 2002; Yamaguchi and Mori, 2005; Platel et al., 2010). However, 8 d after lateral electroporation, we detected a slight but significant increase of c-caspase 3 immunoreactive cells among GC-P-expressing Kir2.1 in the GCL. At 12 dpe, this effect was even more pronounced in the GCL (Fig. 8*C*) and we observed a strong but not significant tendency in the RMS-OB. Importantly, we did not observe any increase in apoptosis after expression of Kir2.1 in PGN-P at 8 or 12 dpe (Fig. 8*D*).

Overall, we conclude that activity in GC-P has very little effect on neuronal migration, but is important for their recruitment and survival in the GCL. PGN-P are not affected by the inhibition of activity. Taken together, these results suggest that activity in GC-P at the exit of the RMS is a controlling factor in the recruitment and positioning process in the OB.

Discussion

Combining targeted electroporation and time-lapse two-photon imaging, we were able for the first time to compare and analyze migrating precursors of the two main OB interneuron subtypes. Our deep characterization of the tangential and radial migration of these two cell types did not show any obvious morphologic or kinetic parameter that allows to differentiate them, suggesting that GC-P and PGN-P share the same mode of migration to reach the OB. However, we identified a dramatic increase of calcium activity in GC-P at the time of switching between tangential to radial migration. This calcium activity was found to be mostly mediated by a voltage-dependent extracellular calcium entry through L-type calcium channels, meaning that precursors were depolarized. Blocking this activity by dampening neuronal excitability with nifedipine or by overexpressing Kir channels did not strongly alter GC-P migration. Interestingly, blocking activity led

←

$\chi^2(1) = 0.03$, $p = 0.86$ (group effect)], or percentage of time spent in stationary phases [30.5 ± 14.9 vs 31.3 ± 16; LMEM, $\chi^2(1) = 0.013$, $p = 0.91$ (group effect)] were similar between both populations. ***F***, Quantification of migration parameters in the RMS-OB. $N = 472/602$ cells on 13 animals. Speed of nuclear translocation [73 ± 20.7 vs 68.2 ± 19.8; LMEM, $\chi^2(1) = 2.5$, $p = 0.1138$ (group effect)], straightness [0.86 ± 0.11 vs 0.862 ± 0.12; LMEM, $\chi^2(1) = 0.08$, $p = 0.78$ (group effect)], or mean displacement [52.5 ± 19.8 vs 46.4 ± 19.5; LMEM, $\chi^2(1) = 3.5$, $p = 0.061$ (group effect)] were not significantly different between the two groups. However, GC precursors expressing Kir2.1 in the RMS-OB slightly increased their time spent in stationary phases [32.2 ± 15.2 vs 37.7 ± 17.6; LMEM, $\chi^2(1) = 4.1$, $p = 0.043$ (group effect)]. ***G***, Quantification of migration parameters in the deep GCL. $N = 119/103$ cells on 5 animals. Straightness [0.84 ± 0.13 vs 0.80 ± 0.16; LMEM, $\chi^2(1) = 1.9$, $p = 0.17$ (group effect)], mean displacement [21.5 ± 10.6 vs 22.8 ± 10.4; LMEM, $\chi^2(1) = 0.02$, $p = 0.88$ (group effect)], or percentage of time spent in stationary phases [60.6 ± 19.5 vs 61.7 ± 17.6; LMEM, $\chi^2(1) = 0.12$, $p = 0.73$ (group effect)] were similar between both populations. A slight increase of the speed of nuclear translocation is observed in the deep GCL for KIR2.1-expressing cells [42.6 ± 13.4 vs 46.9 ± 16.3, LMEM, $\chi^2(1) = 4.7$, $p = 0.031$ (group effect)].

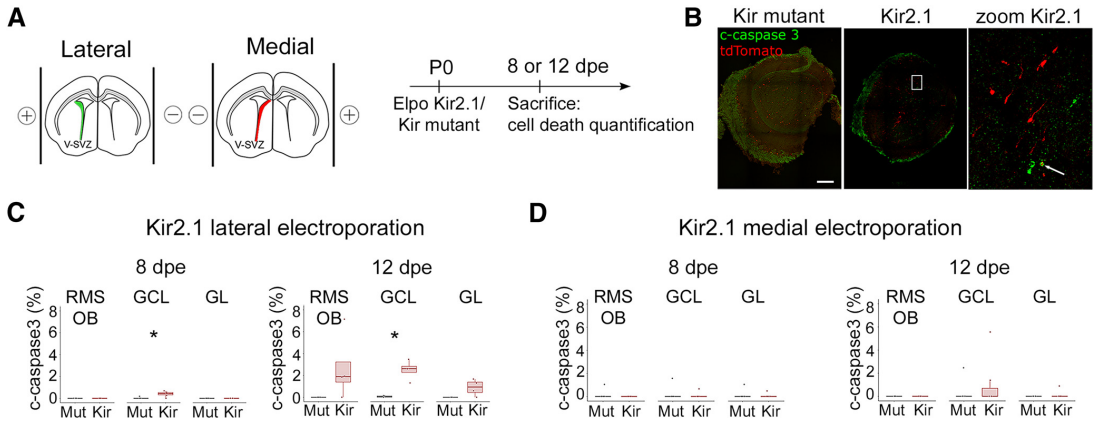

Figure 8. Effect of Kir2.1 expression on neuronal cell death. ***A***, P0 CD1 animals received lateral or medial electroporation with either a Kir2.1 mutant or a functional Kir2.1 encoding plasmid. Mice were then killed at 8 or 12 dpe and the level of apoptotic cell death in tdTomato cells was quantified. ***B***, OB coronal sections of Kir mutant and Kir2.1 labeled with c-caspase 3 at 12 dpe. Note the presence of a double-labeled cell in the Kir condition. ***C***, ***D***, Quantification of the percentage of c-caspase 3-positive cells among lateral (***C***) or medial (***D***) electroporation of Kir2.1 (Kir) or Kir2.1 mutant (Mut) cells per OB region at 8 dpe (lateral: $N = 6$ animals; medial: $N = 6$ animals) or 12 dpe (lateral: $N = 7$ animals; medial: $N = 4$ animals). There is an increase of c-caspase 3-positive cells after lateral electroporation of Kir2.1 in the GCL at 8 dpe (0.03 ± 0.07 vs 0.4 ± 0.24, Mann–Whitney–Wilcoxon test, $p = 0.017$) and 12 dpe (0.07 ± 0.08 vs 2.5 ± 0.9, Mann–Whitney–Wilcoxon test, $p = 0.029$) but not after medial electroporation.

to a progressive accumulation of GC-P in the RMS OB at the expanse of the GCL and to a increase in cell death in radially migrating GC-P. In contrast, blocking neuronal activity in PGN precursors did not affect their cellular distribution or cell death. Overall, these experiments suggest that neuronal activity in GC precursors is necessary for their recruitment in the OB, while this is not the case for PGN-P.

It was shown in the OB that olfactory training (Mouret et al., 2008) or overexpression of NaChBac (Lin et al., 2010) could increase recruitment during synaptic integration. In sharp contrast, it was recently demonstrated that in physiological condition, selection during synaptic integration is nearly absent (Platel et al., 2019) pointing to a first selection step occurring before integration (Biebl et al., 2000; Platel et al., 2010). In agreement with these latter studies, our results suggest that survival of neuroblasts during radial migration is dependent on neuronal activity. Importantly, this phenomenon seems to be subpopulation specific. While it is known that layer positioning of different cortical interneurons depends on neuronal activity (De Marco García et al., 2011; Lodato et al., 2011), it is unclear to which extent this is a result of altered recruitment or differential cell death.

Our study also show a subtype-specific effect of neuronal activity during the switch between tangential to radial migration. It should be noted that the expression of the calcium indicator (GCaMP6s) could have disturbed Ca^{2+} currents in our subpopulations, and in particular L-type VGCCs mediated calcium currents (Bellion et al., 2005; Steinmetz et al., 2017; Yang et al., 2018). However, we believe that the simplest hypothesis is that this would affect our two subpopulations similarly, therefore not impacting our conclusions. Also, we found that the expression of the mutant form of Kir2.1 had a mild effect on migration compared with other experiments using Cre electroporation in Rosa tdTomato mice. This suggests that overexpressing even a non functional channel could affect the cells. It is thus important to compare the effect of the normal Kir2.1 to the mutant form, to make sure that the effects are because of increased excitability rather than because of the overexpression itself. It should also be noted that the comparison between the mutant and the wildtype forms was performed in two independent experiments and in in different mouse lines, making the comparison more difficult.

Despite our efforts, we could not identify a specific signal explaining the large increase in neuronal activity at the RMS exit for the GC-P. It was found for migrating glutamatergic cortical neurons that transient synaptic connections occur during migration and that these connections were impacting migration (Ohtaka-Maruyama et al., 2018). In our pharmacological screen, neither glutamate nor GABA nor glycine receptors' antagonists were able to block the large rise in calcium activity. A tempting hypothesis would be that rather than being dependent on extracellular signals (such as neurotransmitter), this activity could be the consequence of neuroblast maturation. Interestingly, our observations suggest that cells can migrate for a significant time (at least 8 h) in the RMS of the OB before exiting in the GCL. In this hypothesis, migrating cells in the RMS would need to reach a certain threshold of maturation, allowing proper intrinsic activity, which would in turn favor their switch to radial migration.

Contrary to GC precursors, PGN precursors were not affected by Kir2.1 mediated hyperpolarization suggesting that the recruitment of future PGNs is not activity dependent. This is in line with findings showing that knocking out serotonin receptors did no affect cell density in the GL (García-González et al., 2017) and results showing that the migration of PGN precursors in the GL does not depend on sensory activity (Liang et al., 2016). Of note, this later study also showed that PGN neurons migrate for an extended period in the GL while most GCs had settled. This is coherent with the hypothesis that the maturation of GCs and PGNs during migration follows a different time course.

To our knowledge, there is no candidate factor known to regulate the addressing of PGN to their specific layer. New advances in single cell transcriptomics coupled to our specific targeting of the two subpopulations might allow to decipher which molecular pathways differ between PGN and GC precursors during their radial migration.

In conclusion, we show that intrinsic neuronal activity early during neuronal development, when neurons are still migrating, can control the recruitment of specific interneuron subtypes to their target layer.

References

Bellion A, Baudoin JP, Alvarez C, Bornens M, Métin C (2005) Nucleokinesis in tangentially migrating neurons comprises two alternating phases: forward migration of the Golgi/centrosome associated with centrosome splitting and myosin contraction at the rear. J Neurosci 25:5691–5699.

Biebl M, Cooper CM, Winkler J, Kuhn HG (2000) Analysis of neurogenesis and programmed cell death reveals a self-renewing capacity in the adult rat brain. Neurosci Lett 291:17–20.

Boutin C, Diestel S, Desoeuvre A, Tiveron MC, Cremer H (2008) Efficient in vivo electroporation of the postnatal rodent forebrain. PLoS One 3:e1883.

Bugeon S, de Chevigny A, Boutin C, Coré N, Wild S, Bosio A, Cremer H, Beclin C (2017) Direct and efficient transfection of mouse neural stem cells and mature neurons by in vivo mRNA electroporation. Development 144:3968–3977.

De Marco García NV, Karayannis T, Fishell G (2011) Neuronal activity is required for the development of specific cortical interneuron subtypes. Nature 472:351–355.

Fernández ME, Croce S, Boutin C, Cremer H, Raineteau O (2011) Targeted electroporation of defined lateral ventricular walls: a novel and rapid method to study fate specification during postnatal forebrain neurogenesis. Neural Dev 6:13.

García-González D, Khodosevich K, Watanabe Y, Rollenhagen A, Lübke JHR, Monyer H (2017) Serotonergic projections govern postnatal neuroblast migration. Neuron 94:534–549.e9.

Inada H, Watanabe M, Uchida T, Ishibashi H, Wake H, Nemoto T, Yanagawa Y, Fukuda A, Nabekura J (2011) GABA regulates the multidirectional tangential migration of GABAergic interneurons in living neonatal mice. PLoS One 6:e27048.

Liang Y, Li K, Riecken K, Maslyukov A, Gomez-Nicola D, Kovalchuk Y, Fehse B, Garaschuk O (2016) Long-term in vivo single-cell tracking reveals the switch of migration patterns in adult-born juxtaglomerular cells of the mouse olfactory bulb. Cell Res 26:805–821.

Lin CW, Sim S, Ainsworth A, Okada M, Kelsch W, Lois C (2010) Genetically increased cell-intrinsic excitability enhances neuronal integration into adult brain circuits. Neuron 65:32–39.

Lodato S, Rouaux C, Quast KB, Jantrachotechatchawan C, Studer M, Hensch TK, Arlotta P (2011) Excitatory projection neuron subtypes control the distribution of local inhibitory interneurons in the cerebral cortex. Neuron 69:763–779.

Lois C, Alvarez-Buylla A (1994) Long-distance neuronal migration in the adult mammalian brain. Science 264:1145–1148.

Merkle FT, Mirzadeh Z, Alvarez-Buylla A (2007) Mosaic organization of neural stem cells in the adult brain. Science 317:381–384.

Morin X, Jaouen F, Durbec P (2007) Control of planar divisions by the G-protein regulator LGN maintains progenitors in the chick neuroepithelium. Nat Neurosci 10:1440–1448.

Mouret A, Gheusi G, Gabellec MM, de Chaumont F, Olivo-Marin JC, Lledo PM (2008) Learning and survival of newly generated neurons: when time matters. J Neurosci 28:11511–11516.

Nam SC, Kim Y, Dryanovski D, Walker A, Goings G, Woolfrey K, Kang SS, Chu C, Chenn A, Erdelyi F, Szabo G, Hockberger P, Szele FG (2007) Dynamic features of postnatal subventricular zone cell motility: a two-photon time-lapse study. J Comp Neurol 505:190–208.

Ohtaka-Maruyama C, Okamoto M, Endo K, Oshima M, Kaneko N, Yura K, Okado H, Miyata T, Maeda N (2018) Synaptic transmission from subplate neurons controls radial migration of neocortical neurons. Science 360:313–317.

Petreanu L, Alvarez-Buylla A (2002) Maturation and death of adult-born olfactory bulb granule neurons: role of olfaction. J Neurosci 22:6106–6113.

Platel JC, Dave KA, Gordon V, Lacar B, Rubio ME, Bordey A (2010) NMDA receptors activated by subventricular zone astrocytic glutamate are critical for neuroblast survival prior to entering a synaptic network. Neuron 65:859–872.

Platel JC, Angelova A, Bugeon S, Wallace J, Ganay T, Chudotvorova I, Deloulme JC, Béclin C, Tiveron MC, Coré N, Murthy VN, Cremer H (2019) Neuronal integration in the adult mouse olfactory bulb is a non-selective addition process. Elife 8:e44830.

Saghatelyan A, Roux P, Migliore M, Rochefort C, Desmaisons D, Charneau P, Shepherd GM, Lledo PM (2005) Activity-dependent adjustments of the inhibitory network in the olfactory bulb following early postnatal deprivation. Neuron 46:103–116.

Steinmetz NA, Buetfering C, Lecoq J, Lee CR, Peters AJ, Jacobs EAK, Coen P, Ollerenshaw DR, Valley MT, de Vries SEJ, Garrett M, Zhuang J, Groblewski PA, Manavi S, Miles J, White C, Lee E, Griffin F, Larkin JD, Roll K, et al. (2017) Aberrant cortical activity in multiple GCaMP6-expressing transgenic mouse lines. eNeuro 4:ENEURO.0207-17.2017.

Wong FK, Bercsenyi K, Sreenivasan V, Portalés A, Fernández-Otero M, Marín O (2018) Pyramidal cell regulation of interneuron survival sculpts cortical networks. Nature 557:668–673.

Xue M, Atallah BV, Scanziani M (2014) Equalizing excitation-inhibition ratios across visual cortical neurons. Nature 511:596–600.

Yamaguchi M, Mori K (2005) Critical period for sensory experience-dependent survival of newly generated granule cells in the adult mouse olfactory bulb. Proc Natl Acad Sci USA 102:9697–9702.

Yang Y, Liu N, He Y, Liu Y, Ge L, Zou L, Song S, Xiong W, Liu X (2018) Improved calcium sensor GCaMP-X overcomes the calcium channel perturbations induced by the calmodulin in GCaMP. Nat Commun 9:1504.

DECLARATION / ERKLÄRUNGEN
über frühere Promotionsversuche und Selbständigkeit

(1) Ich erkläre, dass ich mich an keiner anderen Hochschule einem Promotionsverfahren unterzogen bzw. eine Promotion begonnen habe.

(2) Ich erkläre, die Angaben wahrheitsgemäß gemacht und die wissenschaftliche Arbeit an keiner anderen wissenschaftlichen Einrichtung zur Erlangung eines akademischen Grades eingereicht zu haben.

(3) Ich erkläre an Eides statt, dass ich die Arbeit selbstständig und ohne fremde Hilfe verfasst habe. Alle Regeln der guten wissenschaftlichen Praxis wurden eingehalten; es wurden keine anderen als die von mir angegebenen Quellen und Hilfsmittel benutzt und die den benutzten Werken wörtlich oder inhaltlich entnommenen Stellen als solche kenntlich gemacht.

26.01.2022,

ACKNOWLEDGMENTS

Especially, I want to thank my supervisor Prof. Dr. Horstkorte for his support, advice and administrative help from the very beginning all the way to the end of the my MD PhD work. I am very grateful that he was open for the idea of an international cooperation and introduced me to his research partner in Marseille.

At the same time, I thank Dr. Cremer for the opportunity to work in France and learn the basics of fundamental research in his ambitious team. His trust and constructive criticism have always pushed me further - scientifically as well as on a personal level.

I thank JC Platel for his practical guidance and numerous theoretical discussions. Due to his great enthusiasm, I felt always motivated to start new experiments and look at problems from a different angle. During the time we worked and climbed together, I learned to take confidence in his great experience - despite (or because) of some passionate debates. Thanks for all explanations, corrections and inspiration.

I would like to underline the outstanding role that Stéphane Burgeon played in initiating the project and instructing me upon my arrival in the institute. Without him it would have never been possible for me to work as independently within such a short time period. I want to thank him for his incredible patience while answering every single of my questions and assuring me that mistakes are normal after I had messed up something.

A big thank you also to Alexandra Angelova and Christophe Béclin who were the best “office mates” I could wish for. With their good humor, biological/statistical/oenological knowledge and social networking skills every problem could be solved at once. After this year, they were rather friends than colleges to me.

Overall, the atmosphere in the Cremer lab was not only scientifically ambitious and challenging but also welcoming and cordially from a personal point of view. I would like to thank Andrea Erni for critically reading my manuscript and encouraging words. Thanks also to Nathalie Core-Polo and Marie-Catherine Tiveron for all their support and help throughout the entire year.
I want to express my gratitude for everyone who contributed to this work: former members and interns in our team, the animal and imaging facility of the IBDM as well as the ERASMUS and Konrad-Adenauer foundation for their funding.

Finally, I would like to thank my family and friends who accompanied me on this journey and gave me strength with their understanding and criticism. A special thank to Naomi for bringing light into administrative darkness and Sebastian for being the light at the end of the tunnel.